The influence of underhood flow on bluff road vehicles in a platooning configuration

A numerical study

M.M. van Rijsingen

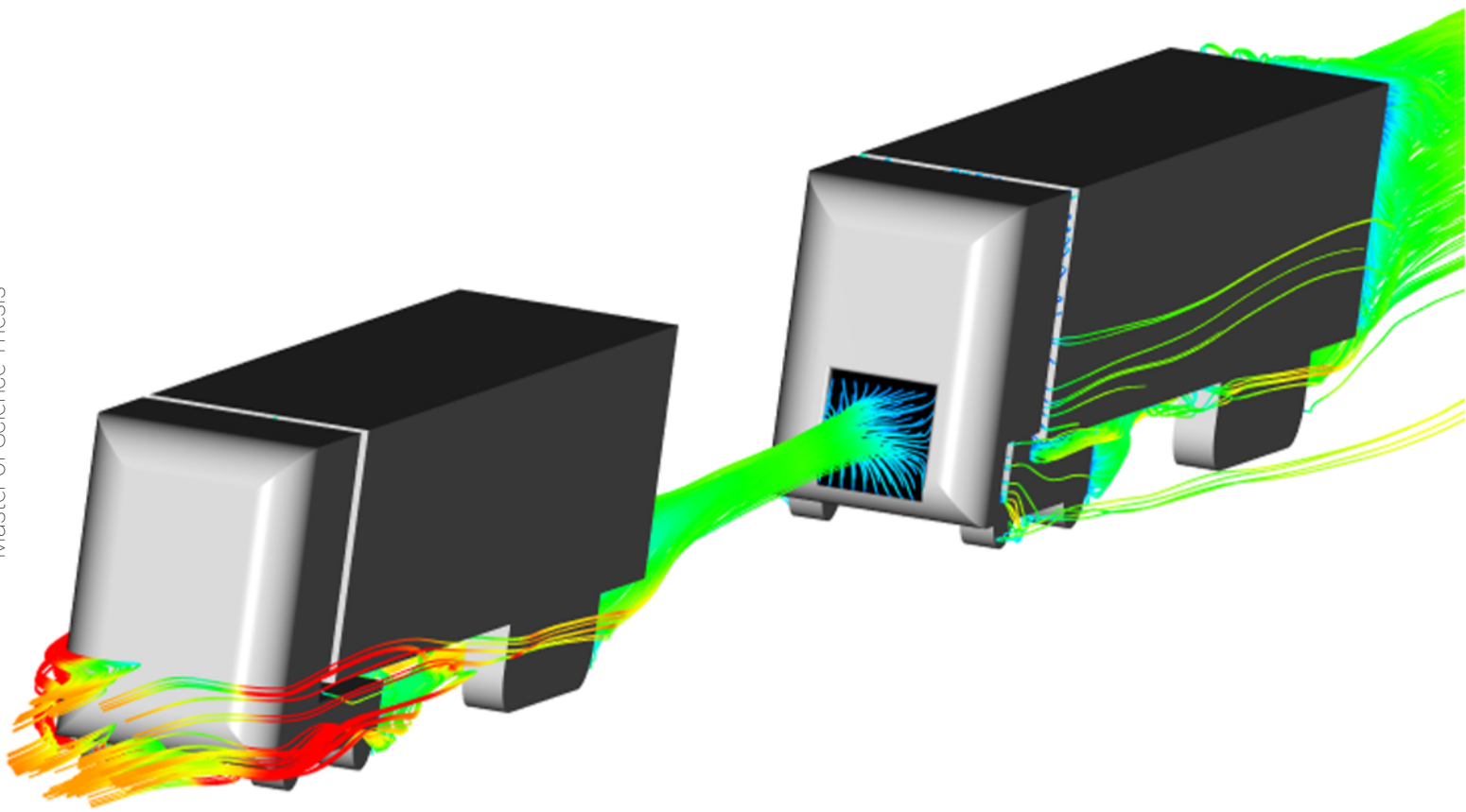

Master of Science Thesis

TU Delft

The influence of underhood flow on bluff road vehicles in a platooning configuration

A numerical study

by

M.M. van Rijsingen

to obtain the degree of Master of Science
at the Delft University of Technology,
to be defended publicly on Thursday December 20, 2018 at 1:00 PM.

Student number: 4078357

Thesis committee:	Prof. Dr. ing. G. Eitelberg,	TU Delft, chair
	Dr. ir. G.M.R. van Raemdonck,	TU Delft & WABCO OptiFlow, supervisor
	Dr. ir. R. Vos,	TU Delft
	Dr. ir. A.H. van Zuijlen,	TU Delft

An electronic version of this thesis is available at `http://repository.tudelft.nl/`.

TU Delft

Preface

This thesis marks the end of my long journey to become an aerospace engineer. After quite some delays, both intentional and unintentional ones, I am proud, happy and somewhat relieved that I can close my time as a student. My interest in road vehicle aerodynamics was one of the reasons to come to Delft and this project has proven that it still fascinates me till this day.

First of all, I would like to thank my supervisor Gandert van Raemdonck for giving me the opportunity to work on this topic. His enthusiasm and guidance helped me a lot. Some problems that caused me headaches for multiple days he managed to solve in minutes during our meetings. He, and his company WABCO, also provided me with excellent computational resources that made my life a lot easier during this project. I also want to thank Damiano Casalino for making this possible from the side of Exa and acting as 'costumer support' for me. Exa is also the company where I did my internship. Everything the people of the Stuttgart office taught me during this period helped me a lot in this project. Therefore I want to thank them again for that. Francesco Avallone and Roy Veldhuizen gave me the last bits of guidance on the simulation setup and post-processing during my thesis, so a thank you to them as well.

During my thesis I was working in the infamous basement of the TU Delft High Speed Laboratory. Working day in day out by yourself on a thesis project from a basement can be quite depressing. Luckily my days were vastly improved by the colleagues I met there. I want to thank Anna, Derek, Ventsislav, Javier, Jaime, Dorian, Arent, Joel, Christophe, Jorge, Niels, David, Francesco, Jordi, Arun, Luigi, Corrado, Sumedh, Carlos, Martin, Joris, Lucas and all others for all the lunches and coffee breaks we had together.

Last but not least I have to thank my parents for supporting in all kinds of ways throughout the course of my studies. Without them I would never have been able to finish this study.

Mart van Rijsingen
Delft, December 2018

Summary

The transport sector is making a significant contribution to the global CO_2 emissions causing Global Warming. A large portion of this is caused by heavy-duty vehicles like tractor semi-trailer combinations. Since tractor semi-trailer combinations are often operated at relatively high speeds for long periods of time their fuel consumption, and with that their emissions, can be strongly reduced by reducing the aerodynamic drag. This can be done by improving the aerodynamics of individual vehicles, by carefully rounding their leading edges or application of drag reduction devices, like boat tails and side skirts. Another option is to use the benefits of drafting by operating two or more vehicles closely together in a platoon. The benefits of this have already been proven in multiple studies and real world experiments.

When platooning will be implemented on a large scale, it will be beneficial to optimise the platoons for maximum drag reduction. To be able to do this, the effect of different truck design parameters have to be investigated. This study focuses on the influence of underhood flow on the drag of a tractor semi-trailer in isolation and in a platoon. This is done by using simplified models adapted to have a underhood model consisting of one porous medium and four ducts to replicate the mass flow, pressure drop and flow field of a real underhood area. Simulations were performed on full-size and highway speeds using the commercially available PowerFLOW solver, based on the Lattice Boltzmann Method.

For an isolated vehicle it was found that an increased underhood mass flow gives a higher total drag, mainly because of the drag contribution of the porous medium. Due to the mass flow entering the underhood, the suction over the leading edges is slightly reduced. On the other hand, smaller leading edge radii with higher suction give less mass flow through the underhood. Besides this the underhood flow actually has beneficial effects on the parts surrounding the tractor-trailer gap and in the trailer underbody area. The highest total drag was found for the models with the most underhood flow and the smallest leading edge radius.

Platoons of two vehicles were tested with three different inter vehicle distances, 3.75, 7.5 and 15 meters. The leading vehicle, which did not have underhood flow in all cases, has the strongest drag reduction for the shortest distance. The trailing vehicle has the lowest drag at the largest tested distance, while it is highest for the middle distance. This can be explained by the reduction in pressure in front of the vehicle. This reduces the drag contribution of the front surface, but also reduces the suction over the leading edges. The models with underhood flow experienced a stronger drag reduction, meaning that the absolute drag values were closer than for the isolated vehicle. This is caused by the reduced underhood mass flow in a platoon. At the shortest inter vehicle distance only 35% of the mass flow of an isolated vehicle is available, while this is 50 and 70% when the distance is increased. The beneficial effects of underhood flow on an isolated vehicle are still present in a platoon, although they are reduced in strength.

When a boat tail is mounted on the back of the trailer of the leading vehicle the drag of this vehicle is strongly reduced due to the increased back pressure. However, this might not be beneficial for the trailing vehicle. The increased stagnation pressure indeed increases the total drag of the trailing vehicle at an inter vehicle distance of 3.75 m. As discussed before, an increased stagnation pressure also gives increased leading edge suction. Therefore the drag is actually reduced for the two larger inter vehicle distances. It was also found that the tail gives higher flow speeds over the top of the trailing vehicle, and lower flow speeds around the bottom. This reduces the drag for the underbody parts like the wheels and slightly decreases the underhood mass flow.

When the platoon is placed at a yaw angle, the total drag of the leading vehicle is increased. The contribution of the front part is decreased, but this is more than compensated for by the drag increase for the rear and all other parts, which are no longer perfectly aligned with the flow. The drag increase of the trailing vehicle is stronger, due to an increased contribution of the front part. The underhood mass flow is also increased compared to the platoons without yaw, this effect is strongest at small inter vehicle distances. The leading vehicle causes the flow to be more aligned for the trailing vehicle, therefore the drag increase for most other parts is less strong. The same effect can be seen for the side force, which is way lower for the trailing vehicle and increases for increasing inter vehicle distance.

Nomenclature

δP	Pressure drop	$[Pa]$
δx	Porous medium thickness	$[m]$
η	Engine efficiency	[-]
ρ	Air density	$[kg/m^3]$
C_D	Drag coefficient	[-]
C_P	Pressure coefficient	[-]
C_S	Side force coefficient	[-]
e_a	Approximate relative error	[-]
F	Drag force reduction	$[N]$
H	Vehicle height	$[m]$
I	Inertial resistance coefficient	$[1/m]$
L	Vehicle length	$[m]$
P	Engine power	$[W]$
p	Apparent order	[-]
r_{ij}	Grid refinement factor/ratio between grids i and j	[-]
Re	Reynolds number	[-]
u	Air velocity	$[m/s]$
V	Viscous resistance coefficient	$[1/s]$
v	Vehicle speed	$[m/s$
W	Vehicle width	$[m]$
y^+	Non-dimensional wall distance	[-]

Contents

1 Introduction

In this chapter the relevance and motivation for this study will be introduced. First some background will be given on the environmental impact of heavy duty vehicles in section 1.1. Sections 1.2 and 1.3 will focus on previous research done on the aerodynamics of individual trucks and platoons respectively.

1.1. Background

The emission of greenhouse gasses like CO_2 into the atmosphere is causing major climate change around the world, more commonly known as Global Warming. Figure 1.1 shows that the transport sector is making a significant contribution to this. Almost three quarters of the emissions are coming from road transport. Therefore the main challenge of the road transport sector today is to reduce emissions of greenhouse gasses. Almost 50 percent of the CO_2 emitted on roads worldwide is produced by Heavy-Duty Vehicles (HDVs), while this is 30 percent within the European Union (EU) [1]. HDVs include pickup trucks, vans and busses, but most of them are tractor semi-trailer combinations. This kind of trucks is often used for long-haul freight transport. Therefore they are operated for long distances on relatively high speeds.

The amount of CO_2 emitted by a vehicle is a direct consequence of the amount of fuel it uses. So to reduce

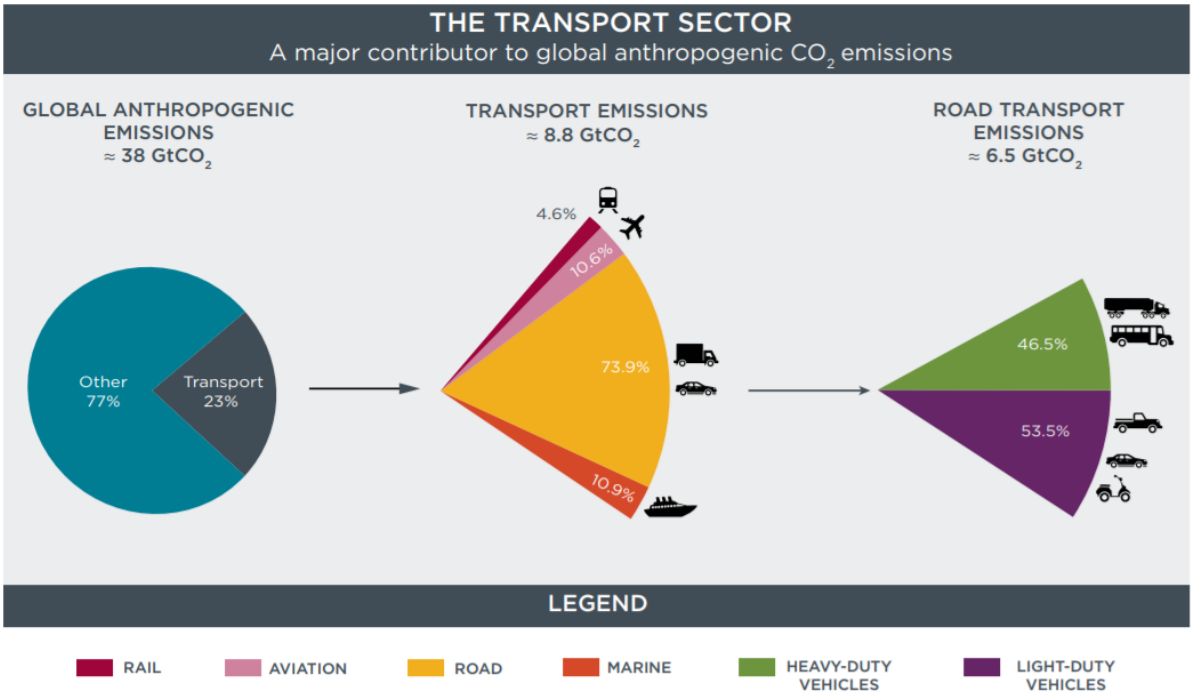

Figure 1.1: Overview of global CO_2 emissions by the transportation sector [2]

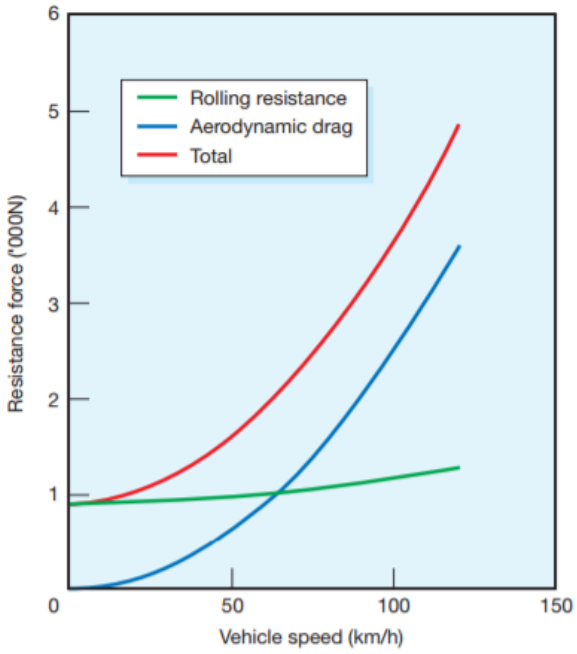

Figure 1.2: Resistance forces experienced by a typical 10 tonne rigid truck at various speeds [3]

the emissions the fuel consumption should be reduced. This can be done by increasing the efficiency of the vehicle powertrain or by reducing the resistance the vehicle experiences during driving. Figure 1.2 shows that aerodynamic drag plays a dominant role at highway speeds. Therefore reducing the aerodynamic drag of tractor semi-trailer combinations can be an important method to reduce the amount of CO_2 emitted in road transport.

The drag of individual trucks can be reduced by careful design of the tractor or by applying aerodynamic features to reduce drag at the gap between the tractor and trailer or at the rear end of the trailer. Another way to reduce aerodynamic drag is to have multiple vehicles drive close together using each others wake. This is called drafting. In recent years a lot of research has been done into the possibility to use this in an organised way, called platooning. In a platoon the lead vehicle determines the speed and direction and the following vehicles automatically respond to that [4]. The aerodynamic benefits of truck platooning have already been proven in many experiments [5] [6] [7] [8] [9] [10]. On top of that, truck platooning can have benefits in terms of efficiency and road safety [4]. Previous research performed on both isolated vehicles and platoons will be discussed in the following sections.

1.2. Bluff body aerodynamics

The aerodynamics of isolated tractor-trailers has already been researched extensively. The main findings will be discussed in this section. First the important flow features will be discussed in section 1.2.1. Multiple devices have been developed to decrease the drag, these devices are treated in section 1.2.2. Finally the influence of underhood flow is discussed in section 1.2.3.

1.2.1. Basic bluff body

Aerodynamics is not the main criterion when deciding on the overall shape of road vehicles. Practical, economical and aesthetic considerations are usually more important. Therefore road vehicles do not have a smooth shape with little separation, like an aircraft [11]. The shape of road vehicles can be described as a bluff body. The main characteristic of a bluff body is that pressure drag is more important than friction drag.

In figure 1.3 the regions where drag is typically generated are identified. It can be seen that the tractor-trailer gap and the underbody generate a large part of the drag. This is because high momentum flow from the outside flows inside these areas of low momentum flow with non aerodynamically shaped parts. The other large contributor is the large pressure difference between the stagnation area at the nose of the vehicle and the wake behind the vehicle. The wake is the most complex part of the flow around a heavy duty vehicle.

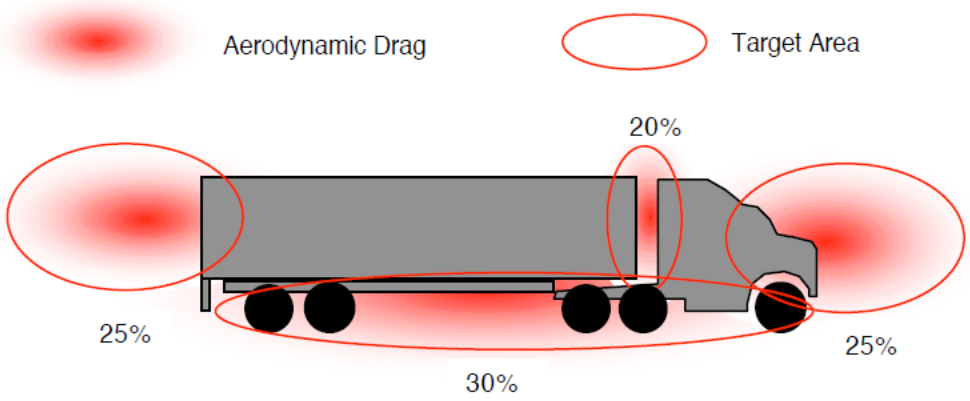

Figure 1.3: Aerodynamic drag distribution of a typical tractor-trailer [12]

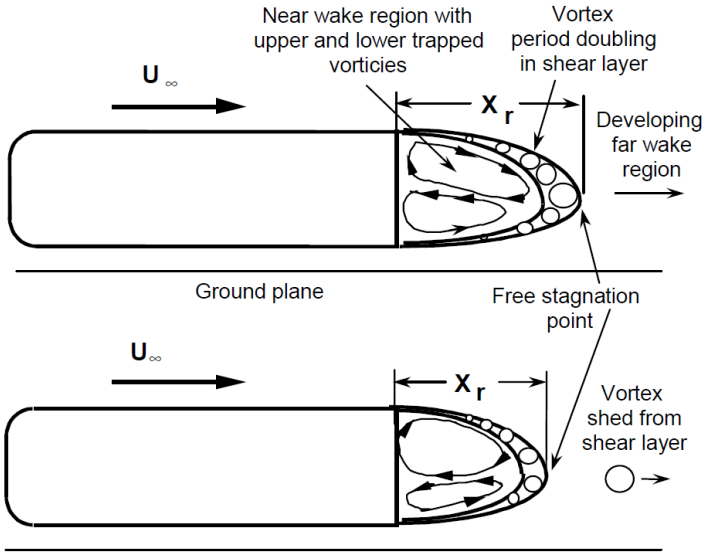

Figure 1.4: Schematic representation of the side view of the wake behind a bluff body [13]

A schematic representation of the wake in side view is given in figure 1.4. It can be seen that two vortices are present in the wake region, which are not completely symmetric because of the ground plane. Roughly the same is happening with the flow separating from the vehicle sides. This means that the full wake can be described as a ring type vortex. Wrapped around the vortices a shear layer is present, which is the result of the separation of the thick boundary layers.

The friction drag over a vehicle shape is largely dependent on the boundary layer. Aircraft, which have a smooth shape and are usually operated in laminar flow conditions, have a laminar boundary layer for a significant part of the vehicle length. Trucks on the other hand are often operated in turbulent air flow, due to other traffic and are not as smoothly shaped. Trucks often have separation bubbles on the leading edges, after a separation bubble the boundary layer is always turbulent. Also the tractor-trailer gap gives a region of separated flow after which the boundary layer thickness increases [14]. On top of that a detailed truck has small edges where panels meet which can cause the boundary layer to trip. Therefore it can be assumed that by far the largest part of the boundary layer over a tractor-trailer is turbulent.

The behaviour of the boundary layer and wake is different for different Reynolds number regimes [15]. Figure 1.5 shows the typical behaviour of the drag coefficient for increasing Reynolds number for a sphere and a bluff vehicle. A complete vehicle consists of multiple components which are probably not all at the same point of these curves at the main operation condition of the vehicle. Therefore they will respond differently when the Reynolds number is altered. Wood [15] recommends to use a width-based Reynolds number of at least 2 million for testing full vehicles. However, it is best to test or simulate at the same Reynolds number as the vehicle will encounter in operation.

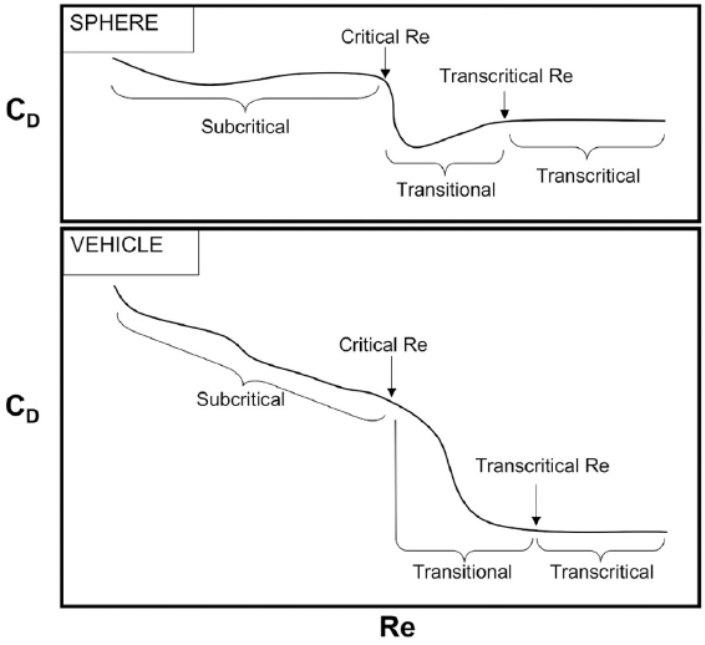

Figure 1.5: Typical variation of the drag coefficient with Reynolds number for a sphere and a bluff vehicle [15]

In practice, road vehicles rarely operate in conditions were the flow is perfectly aligned with the vehicle body. This is due to the ambient air speed that is usually present. These cross winds can be taken into account by placing the vehicle under a certain yaw angle with the flow. Doing this is important because the yaw angle gives a side force and it generally increases the drag.

A road vehicle in cross wind conditions behaves very similar to an airfoil under an angle of attack. A higher angle gives a force due to the pressure difference between the windward and leeward side. In case of an airfoil this lift force is favourable, but a side force on road vehicles negatively influences the driving characteristics. This is inconvenient at low cross wind angles and speeds and can be dangerous in more extreme conditions. The side force is reduced when the flow separates at the leeward side, like stall on an airfoil. However, this increases the drag. Therefore a compromise should be found at which angle the flow is separating to give good drag characteristics, but dangerous effects of side force are prevented [14]. In general it was found that more aerodynamically shaped vehicles are less sensitive to cross winds [16] [17].

1.2.2. Drag reduction devices

European Cabin over Engine (CoE) trucks have little possibilities to change the overall shape for aerodynamic benefits. As a result, most changes in aerodynamic design for tractor-trailers are done using add-on features which are later incorporated in the initial design of new trucks. A clear example is the flow deflector on top of the cabin used to make sure the air is deflected over the vertical part of the trailer. First this was done with a simple plate, in modern tractors it is an integrated part of the design and houses room for storage or sleeping.

Solutions for all areas identified in figure 1.3 have been investigated. The gap between the tractor and the trailer should be as small as possible, this can be done by adding aerodynamic fairings on either the back of the cabin or the front of the trailer. The drag of the underbody can be reduced by making sure less air is going there. This can be done by adding an air dam in front of the front wheels and by shielding the sides with sideskirts [3]. In a platooning configuration, the devices influencing the area in front and behind the vehicle are most important. Therefore the influence of the leading edge radius and boat tails will treated here in more detail.

Multiple studies were already performed on the influence of the leading edge radius. All of them used simplified vehicle models, since changing the front edge radius on a detailed truck is more complicated and expensive. Cooper [18] used a generic box shape to study the behaviour of different leading edges at various Reynolds numbers. The reason to round the edges is to make sure the flow does not separate. Cooper found that the Reynolds number has a big influence on the radius at which separation does not occur anymore. Figure 1.6 shows the plots of the drag coefficient versus the Reynolds number for different dimensionless

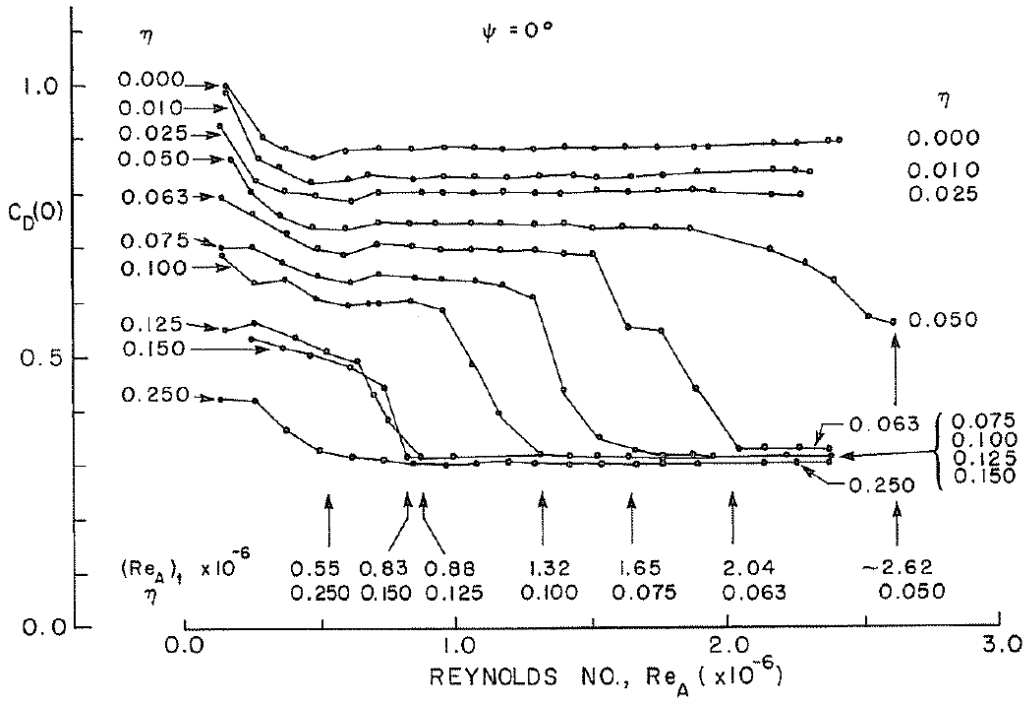

Figure 1.6: Drag coefficient versus Reynolds number for a generic box shape with different leading edge radii [18]

radii. It can be seen that small radii give approximately the same drag coefficient for all Reynolds numbers. However for larger radii the drag coefficient drops rapidly after a certain Reynolds number. Beyond a critical Reynolds number the drag coefficient becomes constant again at almost the same value for all radii. The same was found by Hammache and Browand [19], who tested a simplified tractor-trailer combination with two leading edge radii. These two studies show that increasing the radius beyond a certain level does not reduce the drag anymore. However, to find that point it is important that the correct Reynolds number is taken into account.

Gheyssens [16] used the General European Transportation System model (GETS) and halved the standard leading edge radius twice. He found that the leading edges experience suction reducing the drag of the total frontal part. When the leading edge radius was halved once, the suction increased. However, due to the smaller radius, the size of the edges decreased, while the frontal surface increased. Therefore the total drag of the front part still increased. When the radius was halved again, the suction on three edges decreased due to separation.

Multiple add-on devices have been developed and tested to increase the base pressure behind the vehicle, like guide vanes [20], a stepped tail [12] [20] [21], vortex generators [12] [21] and base flaps [12]. In this study the most common add-on device will be used, the boat tail. By a boat tail, plates mounted flush to the edges of the trailer with a taper angle are meant. Such a device moves the separation point rearwards, giving a portion of almost stagnated air at the rear end of the trailer. The taper also reduces the size of the wake, as shown in figure 1.7.

In general it was found that a longer boat tail gives more drag reduction [20]. This can be explained by the size of the wake, which can be reduced further for a longer tail with the same angle. However, in the European Union the length of a boat tail is restricted to 0.5 m [22].

The most efficient and therefore most tested boat tails have four straight panels, are open in the back and have a taper ratio. Multiple studies focused on finding the optimal angle for these type of boat tails. The optimum angle is the largest angle the boat tail can have before separation occurs. Kruijssen [23] who used the General European Model (GEM), found that the optimum angle changes for different yaw angles. For zero yaw Kruijssen found an optimum angle of 14 deg, but for larger angles the optimum was a bit lower at 12 deg. Van Raemdonck [20] found that a 15 degree angle performed worse than a 10 degree one with a drag reduction of 12%. Applying this angle to a prototype with a length of two meters in road tests gave a reduction of fuel consumption of 2 $l/100km$ a fuel saving of 7.5%. Storms et al. [21] found the optimum to be between 12 and 16 degrees in a scaled wind tunnel test.

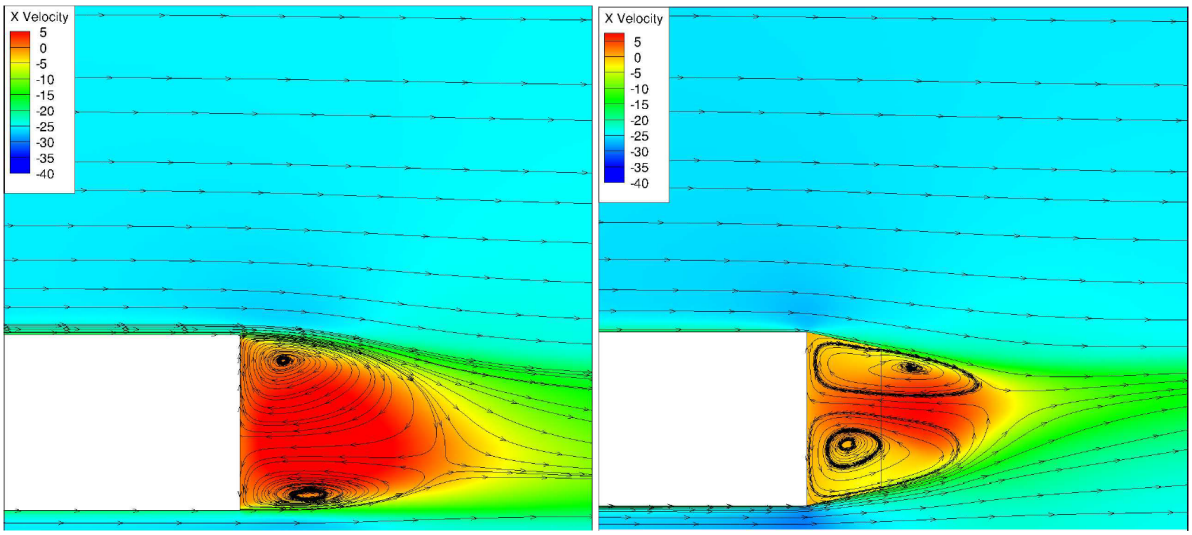

(a) No tail (b) 12 deg tail

Figure 1.7: Flow field behind a trailer without tail and with tail [16]

1.2.3. Effect of underhood flow

Cooling performance is a major point of concern for vehicle manufacturers. It is essential that their products have sufficient cooling at all times. The cooling drag is usually measured by comparing the drag of a model with cooling to one where the complete grill is closed. For heavy duty vehicles the cooling drag can be up to 8% of the total vehicle drag [24].

Modern trucks have multiple heat exchangers mounted close together in a cooling package. The cooling package is typically mounted in the very front of the vehicle. The benefit of this position is that the ram air effect is used. Simply because the vehicle is moving, air will be forced through the heat exchangers. For situations when there is insufficient air flow a fan is mounted behind the cooling package to suck more air through it.

Since drag reduction is becoming more and more important for vehicle manufacturers, the cooling system should generate as little drag as possible as well. The drag can be reduced by placing the heat exchangers in a cooling duct. Such a smooth channel makes sure all air entering actually flows through the cooling package and no additional drag is generated by flow passing over other components. This can halve the cooling drag [25]. However, due to practical and space limitations, these kind of fully ducted systems is almost exclusively found on racing cars. On trucks a short inlet duct can be mounted to make sure all air entering the grille also passes through the heat exchangers. This rather simple modification already reduces the drag significantly, as was found by Martini [24]. It also makes sure that hot air that already passed through the cooling package is not recirculated at low driving speeds.

Behind the cooling package the cooling flow is usually simply flowing over the underhood components towards an exit. Where the flow can leave the underhood area depends on the specific design of the vehicle, but typically part of the flow leaves through the rear encapsulation, through the wheel arches and to the bottom, as shown by Hallqvist [26] in figure 1.8. Drag reductions could be achieved by guiding the flow in the most favourable direction. Martini [24] found that even in the relatively small space created by using a Soft Nose concept an outlet duct that gives lower drag could be fitted.

For the normal configuration, without ducts, Hallqvist [26] concluded that the whole underhood system should be optimised to improve its performance. Changing only one aspect does not work. This means that the cooling system should be optimised for each detailed vehicle geometry. Therefore this is done in the development process of each manufacturer, but not on a more fundamental level.

A couple of more fundamental studies on cooling system aerodynamics inside bluff bodies are available, like the ones done by Barnard [27] and Bäder et al. [28]. Cooling airflow always increases the total drag of a vehicle, due to the pressure drop over the heat exchanger. It was found that a higher mass flow through the heat exchanger gives a linear cooling drag increase [28]. Bäder et al. also found that a body with cooling flow has a higher pressure round its inlet and lower pressure round its outlet, compared to the same body without cooling flow. Since the outlet is always located downstream of the inlet this increases the drag. This effect

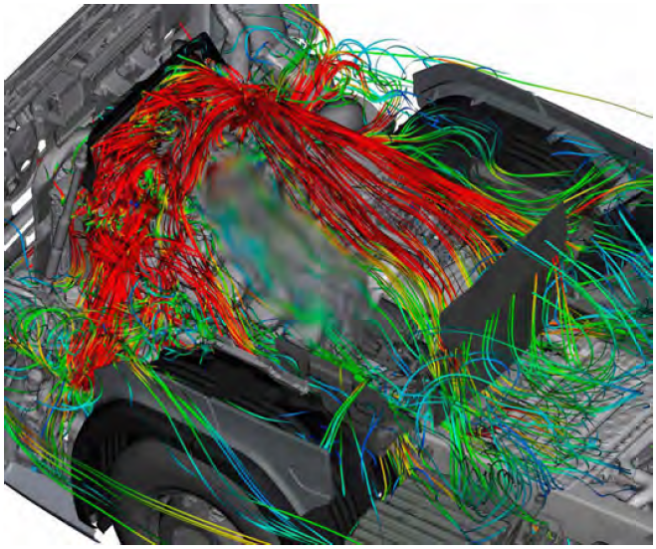

Figure 1.8: Streamlines through a detailed underhood geometry. When the streamlines are red the velocity is high, when they are blue the velocity is low [26].

was increased for higher mass flows [29]. Both studies looked at the interaction between underhood flow and the external flow around the body. Barnard used the Ahmed body, while Bäder et al. used the SAE Body. An important difference between these models and a tractor-trailer combination is the location of the outlet of the cooling flow. In the referenced studies the cooling air is either guided towards the bottom of the model or towards the rear end. In a tractor-trailer combination on the other hand a large portion of the cooling air leaves the tractor at the rear side of the cabin, after which it is free to flow around the trailer. No studies resembling a tractor-trailer including cooling flow were found.

Cooling systems are sized to provide sufficient cooling in a certain critical condition. However, this means that in most conditions the system is oversized. For example, during highway driving, when the truck has a constant high speed. There is a lot of airflow, but the engine does not need to deliver full power. This means that more air is flowing through the cooling package and the underhood than required, generating unnecessary drag. This can be prevented by using Active Grille Shutters (AGS). Such a system consist of a number of aerodynamic flaps placed in the grille which can be adjusted to cover different portions of the cooling inlet. Pfeifer [30] states that for a heavy truck the drag coefficient can be reduced by 8% by using an AGS. This makes sense, since as was stated before the total cooling drag can be up to 8%. So closing the grille completely can save the same amount. However, it that case no cooling will be available at all. Martini [24] investigated how much of the grille could be covered while maintaining sufficient cooling for highway conditions. It was found that for the tested Volvo FH-series truck only 17.5% of the grille needed to be open. This gave a drag reduction of 26.5 drag counts, which means the cooling drag was reduced by 60%.

1.3. Drafting aerodynamics

When two vehicles are driving close together in a platoon the second vehicle is positioned in the wake of the first vehicle. This means that the second vehicle is experiencing a lower air velocity than it would do in free stream conditions and therefore it generates less drag. The presence of that vehicle in the wake increases the pressure in that region and therefore at the base of the first vehicle. As discussed in section 1.2.2, an increased base pressure reduces the drag. Therefore both vehicles benefit from driving in a platoon. The resulting flow field can be seen in figure 1.9. This drafting effect is widely used in sports, cyclist use it to work together while racing drivers use it to make overtakes. In general, it was found that for shapes representing tractor-trailers operation in a platoon always decreases the drag [19] and that it is best to position the most aerodynamically clean vehicle in the lead of the platoon [31].

In this section the influence of the inter vehicle distance, leading edge radius, a boat tail, the yaw angle and underhood flow on the aerodynamic performance of a platoon will be discussed. In the last section the results of real world testing will be shown.

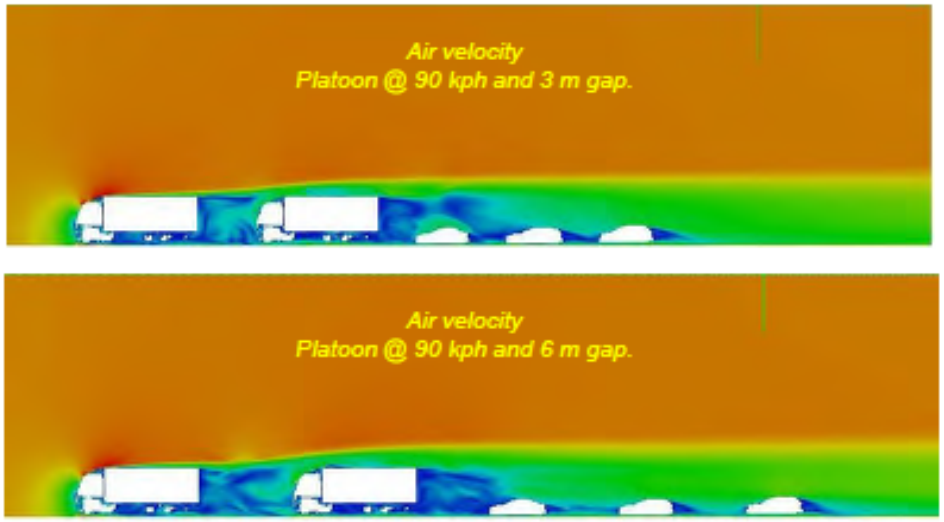

Figure 1.9: Numerical results of the air velocity around a platoon with 3 and 6 m gaps [32]

1.3.1. Effect of inter vehicle spacing

The distance between the vehicles in a platoon is the most important parameter in any study about platooning. It can be changed all the time and has a large influence on the drag reduction. Figure 1.10 shows the drag coefficient of the lead and following vehicle divided by the drag coefficient for a vehicle in isolation plotted against the spacing between the vehicles. It can be seen that the lead vehicle has a strong drag reduction for small distances after which it asymptotically grows to the value of the isolated vehicle. For a spacing of more than one vehicle length there is barely any drag reduction left. The trailing vehicle keeps on benefiting from the platoon for distances larger than plotted in the figure. This might be the case up to ten vehicle lengths [33]. The same was found in CFD simulations with detailed truck geometries [34].

It can also be seen in figure 1.10 that for distances below half a vehicle distance the drag of the trailing vehicle is higher than for larger distances. This result is counterintuitive, but was also found by Smith et al. [34], Gheyssens [16] and Van Tilborg [35].

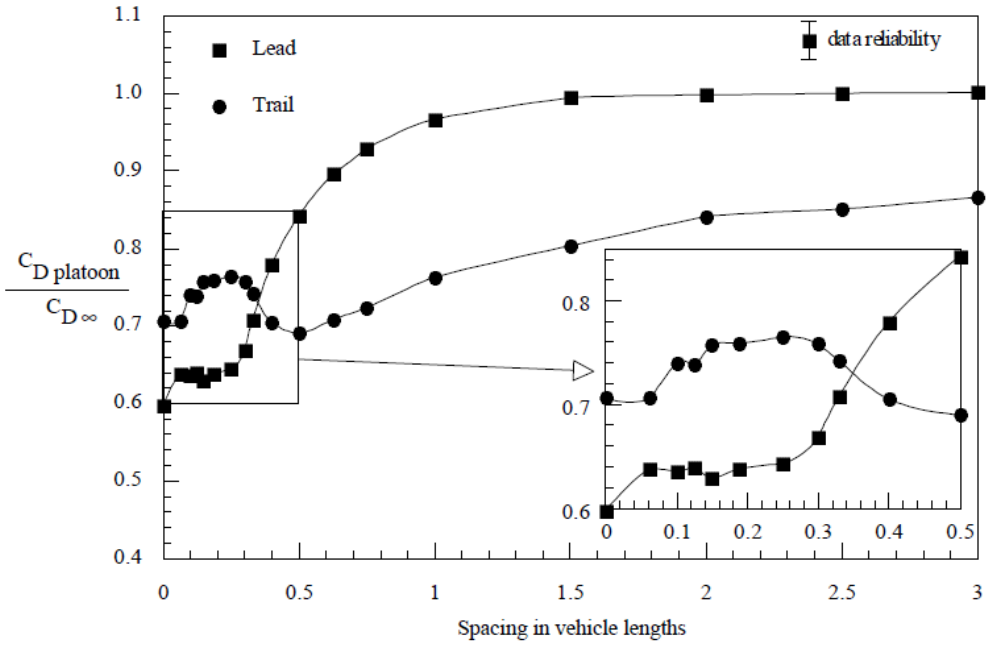

Figure 1.10: Drag ratio vs vehicle spacing for a two vehicle platoon [33]

Van Tilborg [35] also had a closer look at the flow field in between the two vehicles. The X-velocity in between the vehicles is plotted for separation distances of 0.1, 0.45 and 0.91 times the vehicle length in figure 1.11. For the smallest gap it was found that most air in the gap entered from the bottom and follows an S-shaped path. For larger distances the air enters from all sides and a wake very similar to that of a isolated vehicle can form. For a separation distance of 0.45 vehicle length it can be seen that the wake still has a strong influence on the velocity near the front of the trailing vehicle, for the largest gap this influence is smaller. For both the 0.45 and the 0.91 gap the reduced velocity over the leading edges of the trailing vehicle is clearly visible.

This shows that the behaviour of the drag for small vehicle distances is strongly dependent on the vehicle geometry. Therefore the following sections will focus on the influence of the different design parameters in this area.

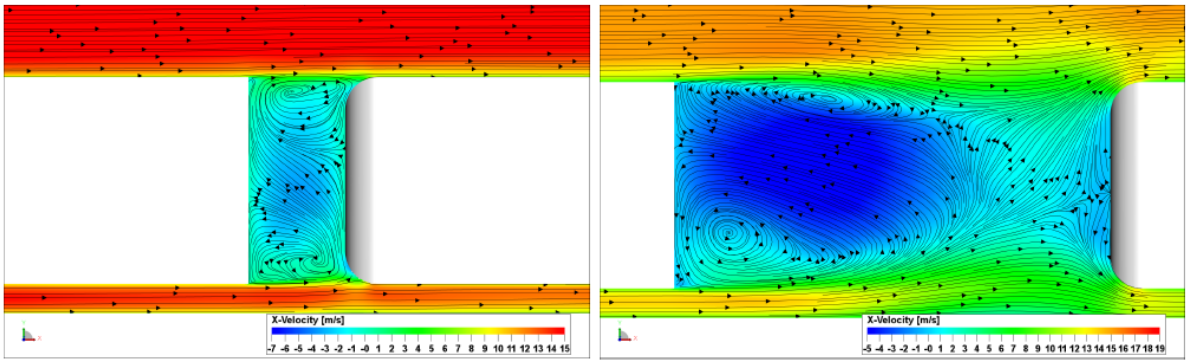

(a) 0.1 vehicle length

(b) 0.45 vehicle length

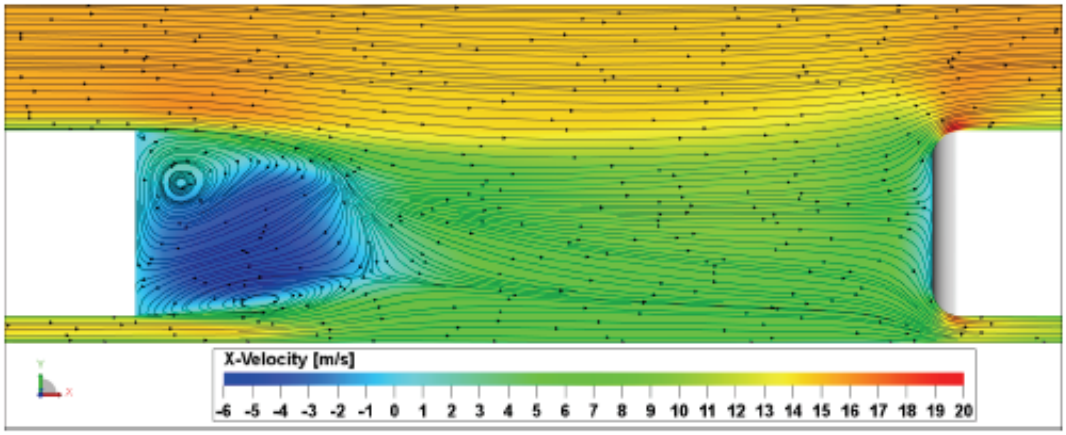

(c) 0.91 vehicle length

Figure 1.11: X-velocity in the vertical centre plane between two vehicles at different separation distances [35]

1.3.2. Effect of the leading edge radius

Hammache and Browand [19] tested the aerodynamic drag of two box like shapes, either with or without rounded leading edges, in tandem. This gave four different combinations of blunt and rounded models. It was found that all combinations had lower drag than two vehicles in isolation. The lowest drag was not found for the combination of two bodies with rounded edges, but for the platoon with a rounded body in the front and a blunt body behind it. Gheyssens [16] had similar results. He concluded that due to the reduced speed the stagnation pressure is lower, reducing the drag, but also the suction on the edges is lower, increasing the drag. As discussed in section 1.2.2 a smaller radius gives more suction, until the peak is too large and the flow separates. In a platoon the flow is less likely to separate, so therefore it is beneficial to have a smaller leading edge radius. Van Tilborg [35] found that when a vehicle had a smaller leading edge radius a platoon gave a higher drag reduction, but the absolute drag was still lower for a vehicle with a larger radius.

1.3.3. Effect of boat tails

Gheyssens [16] found that when a tail is deflected more inward, the stagnation pressure on the following vehicle is increased and the suction on the leading edges is reduced. Both effects increase the drag of the following vehicle. It was concluded that increasing the angle of the boat tail had a similar effect as increasing the inter vehicle distance. However, the boat tail still does decrease the drag of the leading vehicle. Therefore it might still have a beneficial effect on the overall drag of the platoon. In this study it was found that the models with the highest drag in isolation experienced the highest drag decrease in a platoon, but the lowest absolute drag was still obtained by a platoon of vehicles with the lowest drag in isolation.

1.3.4. Effect of cross wind

Marcu and Browand [36] performed an experimental study on a platoon of three 1/8 scale models of the Chevrolet Lumina minivan in a wind tunnel with a yaw angle of 10 degrees. It was found that the side force experienced by the leading vehicle is always close to the value of an isolated vehicle in yaw. The middle and trailing vehicle on the other hand experience a strongly reduced side force. This is explained by the fact that each body aligns the flow more with the vehicle direction. An effect that is comparable to the behaviour seen on a multi-element airfoil.

The same effect was found by Gheyssens [16] in his CFD study using a platoon of GETS models. However, it was also found that the leading vehicle is redirecting the flow in such a way that the stagnation pressure is increased. Resulting in higher drag for the following vehicle.

1.3.5. Effect of underhood flow

Smith et al. [34] simulated a platoon of two detailed American style trucks with underhood flow and studied the effect of vehicle separation on the mass flow through the heat exchangers. It was found that the mass flow is strongly reduced when the separation distance is decreased. Already when driving at a distance of 49 m without yaw the mass flow is reduced by 20%. For the smallest separation distance of 9 m the mass flow is down by 44%. As mentioned before, in highway conditions a truck normally does not use all its power, while a lot of mass flow is available. This means that a reduction in cooling flow does not need to be a problem in highway conditions. All simulations were done without yaw angle and with a yaw angle of 6 degrees. It was found that at a yaw angle the mass flow is around 5% higher compared to the zero yaw case. This can be explained by the increase inflow from the side into the gap between the two trucks in yaw conditions.

The same study investigated the cooling flow on the trailing vehicle in a real world test on the highway by measuring the windmilling rpm of the fan behind the cooling package. The data obtained shows a clear trend. For distances below 10 m the mass flow is at a steady low value, between 10 and 20 m there is a steep increase in mass flow after which it starts increasing more gradually towards the value of an isolated vehicle.

Salari and Ortega [37] measured the static pressure in the grille of 1:50 scaled American truck models in a platoon. The results can be seen in figure 1.12. It can be seen that for the leading vehicle the pressure coefficient, C_P is always around 1. For small inter vehicle distances, the trailing vehicle experiences a very low static pressure, which rapidly increases when the distance is increased. When the distance becomes more than a vehicle length the increase in pressure is not as steep anymore. It also never seems to approach the values found for the leading vehicle. When a boat tail is applied the pressure is slightly lower over the entire range.

Ellis et al. [38] simulated a three vehicle platoon of American tractor-trailers. Four variants of the same vehicle were tested. The first one without aerodynamic devices, the second one with small trailer skirts, the third had small trailer skirts and a boat tail and the last variant featured a boat tail and full trailer skirts. They were tested at separation distances of 5 and 9 m. The resulting normalised radiator mass flow for all vehicles in all variants can be seen in figure 1.13.

In figure 1.13 it can be seen that the mass flow is strongly reduced for all vehicles in second and third position. It can also be seen that when boat tails are applied the mass flow reduction is even stronger. This reduction in mass flow is translated in a reduction in heat rejection. However the exact heat rejection does not only depend on mass flow but also on the conditions, like air temperature and density. In the article it is mentioned that there is the risk of fan engagement when the heat rejection falls below a certain threshold, but it is not mentioned what this threshold is. As mentioned before in section 1.2.3, Martini [24] found that only 17.5% of the grille of a Volvo FH-series truck had to be opened to have sufficient cooling in highway conditions. In that condition an air mass flow of 1.3 kg/s through the radiator was found, while the same truck in normal conditions had a mass flow of 2.95 kg/s [24] [39]. This would mean that a reduction of up to 56% could be dealt with without the need to use a fan.

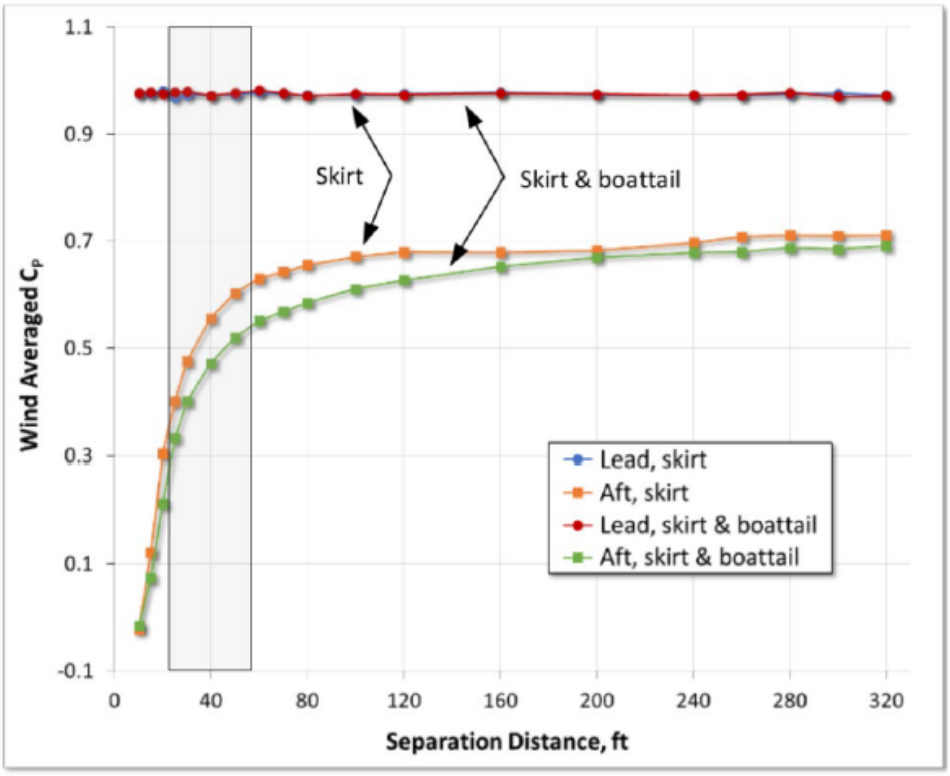

Figure 1.12: Wind averaged C_P measured in the grille of the vehicles in a two-vehicle platoon with and without boat tails

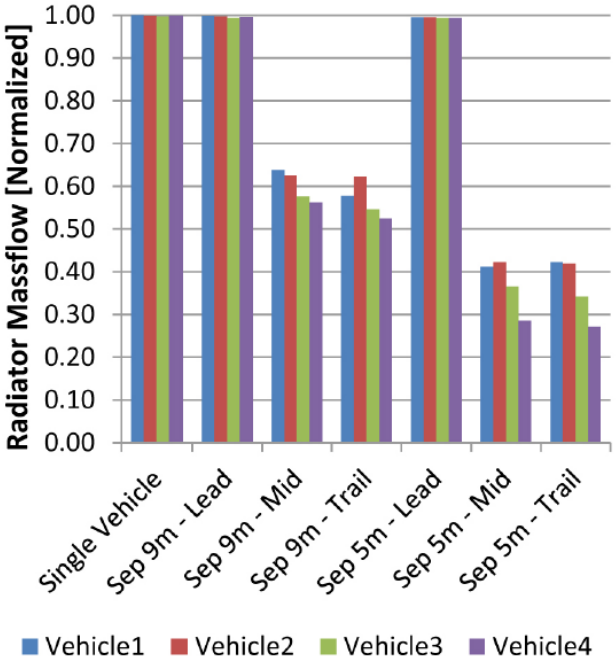

Figure 1.13: Normalised radiator mass flow for a single vehicle and 3 vehicle platoons using different vehicles: vehicle 1: no add-on features, vehicle 2: small trailer skirts, vehicle 3: small trailer skirts and boat tail, vehicle 4: full trailer skirts and boat tail [38]

That operating the fan can have a large influence on the fuel consumption was found in track testing conducted by Lammert et al. [6]. In general the trailing vehicle in a two truck platoon of American tractor-trailers had a fuel saving between 2.8 and 9.7%. For the runs without fan-on time this was between 8.4 and 9.7%.

It is clear that the mass flow through the radiator of a trailing vehicle in a platoon is strongly influenced by the distance to and the geometry of the leading vehicle. A reduced underhood mass flow also reduces the drag. However, it is important that the trailing vehicle always has sufficient cooling flow. A fan could increase the mass flow, but this takes energy and the drag of the truck increases again due to the increased mass flow, which makes it questionable if this is an economical solution.

1.3.6. Real world testing

Numerous studies have been done to find the potential of platooning in reducing the fuel consumption of real life trucks. Some studies still use a sort of experimental setup by doing track testing, others actually investigated platoons on open roads.

The results of a number of these studies was summarised by the NACFE [5]. The results for lead and trailing vehicle are shown in figure 1.14 and 1.15 respectively. For the lead vehicle it can be seen that there is a clear trend towards more fuel saving for lower separation distances. Where the maximum is found at around 9% for a separation distance between 3 and 6 meters (10 to 20 ft). However, the exact reduction in fuel consumption is rather spread. For the trailing vehicles the differences between studies is even bigger, as can be seen in figure 1.15. This is caused by a large spread in conditions and vehicles used in these studies. Between American and European tests, you have the difference in vehicles. Since in this study European CoE tractor-trailers will be used, the studies using these kind of vehicles will be discussed in more detail.

Bonnet and Fritz [40] performed an experimental study for DaimlerChrysler with a leading truck of 14.5 tonnes and a following truck of 28 tonnes on a level test track. For a speed of 80 km/h a maximum reduction in fuel consumption of 21% was found for the following vehicle at a spacing of 8 meters. The fuel consumption of the lead vehicle was reduced by 8% in the same conditions. Further reducing the spacing increased the reduction for the lead vehicle, but had an adverse effect on the following vehicle. Alam [41] reported a maximum fuel reduction of 4.7 to 7.7% using two Scania trucks with a weight of 39 tonnes. The tests were conducted with a speed of 90 km/h on a Swedish highway. As a part of the European SARTRE project two rigid Volvo trucks were tested on a oval test track at 90 km/h. It was found that both vehicles had increasing fuel saving when reducing the gap from 25 to 5 meters. The maximal savings were 12% for the following vehicle and 8% for the leading vehicle.

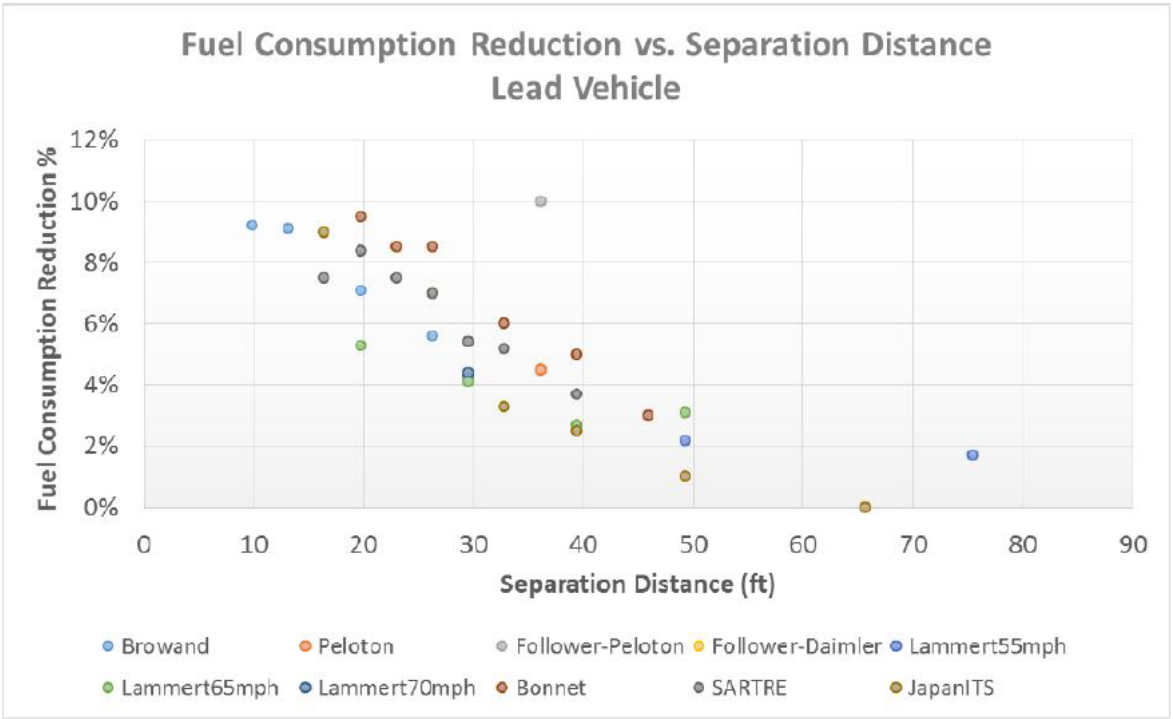

Figure 1.14: Summary of fuel consumption reduction found for the leading vehicle in platooning tests around the world [5]

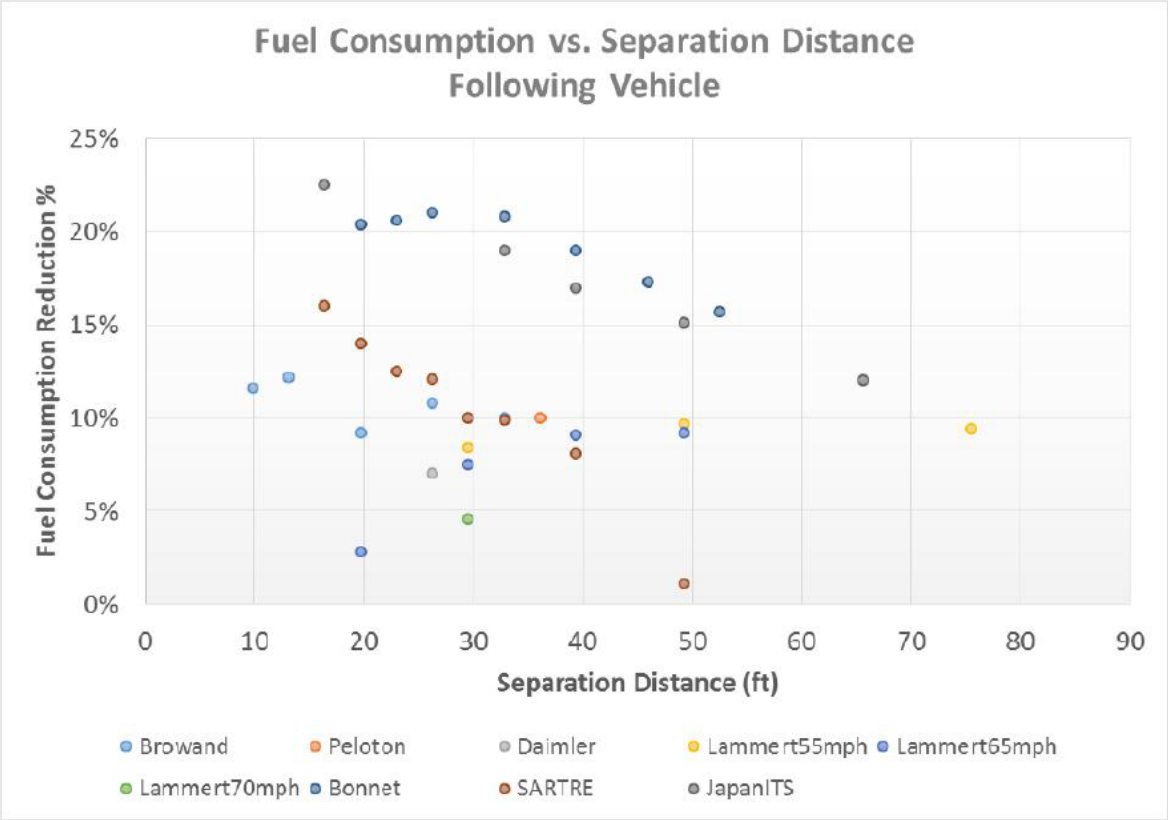

Figure 1.15: Summary of fuel consumption reduction found for the trailing vehicle in platooning tests around the world [5]

1.4. Present study

Based on the literature discussed above, it can be concluded that both bluff body and drafting aerodynamics have already been studied extensively. However, underhood flow is often not taken into account, while it might have a big influence on the aerodynamic performance of the corresponding vehicles when the distance between two vehicles is small. Therefore, in this study it will be attempted to answer the following research question:

What is the influence of underhood flow on the aerodynamic drag of a platoon of tractor semi-trailer combinations?

To answer this main question the following sub-questions should be answered:

- *What is the effect of underhood flow on the aerodynamic drag of an isolated tractor semi-trailer combination?*
- *What is the relation between aerodynamic drag and inter vehicle distance when underhood flow is taken into account?*
  - *How does this relation change when the radius of the leading edges of the second vehicle changes?*
  - *How does this relation change when the first vehicle is equipped with a boat tail?*
  - *How does this relation change when the platoon experiences a cross wind?*

It was decided to do the study using numerical simulations with the aid of CFD. Due to the inherent unsteady nature of the flow in the near wake of bluff bodies, a commercially available software package based on the Lattice-Boltzmann Method, Exa PowerFLOW, will be used. The characteristics of this software and the simulation setup used will be discussed in chapter 2. Since no new experiments were performed, the simulation method was validated using data from previous TU Delft projects. The results of this are shown in chapter 3. The simulation results for an isolated vehicle and the platoon are discussed in chapter 4 and 5 respectively. Finally the conclusions and recommendations are drawn in chapter 7.

2

Numerical setup

The study will be performed using Exa PowerFLOW, a commercially available CFD software package based on the Lattice-Boltzmann Method (LBM). In this chapter the numerical methods to be used will treated. First the model is discussed in section 2.1. After that the theoretical background of the software and the specific settings used in this study are shown in section 2.2 and 2.3 respectively. To finalise the numerical setup a mesh study was performed to find an appropriate resolution and simulation time, the results of this study are discussed in section 2.4. In section 2.5 the uncertainty of this simulation method will be discussed.

2.1. GEM model

The General European Model (GEM) will be used in this study. What this model looks like and why it is chosen will be discussed in section 2.1.1. The basic model will be modified to have underhood flow. How the underhood is modelled is shown in section 2.1.2. The design alterations that will be done during this study are discussed in section 2.1.3.

2.1.1. Basic model

The basic GEM model is shown in figure 2.1. It is based on the maximum dimensions of a European tractor-trailer with a length of 16.5 m and a height of 4 m. Figure 2.1 shows that the model is slightly higher than this. This is because the wheels are completely round. In the simulation the roof of the model will be 4 m above the ground, resulting in an intersection between the floor and the wheels and thus effectively a contact patch. This is the recommended way of doing it in PowerFLOW, since perfectly abutting surfaces can cause problems [42].

The GEM model was chosen because it is a simplified representation of a tractor-trailer combination, which makes it suitable to investigate fundamental effects without interference of detailed, manufacturer specific, geometry. This also reduces the simulation costs. Although the model is simplified, it has a clear distinction between the tractor and the trailer. This means that a underhood model can be implemented rather easily. The GEM model was designed by Mulkens [43] and used by Mulkens and Kruijssen [23]. In both studies the model was evaluated using CFD and in a wind tunnel, which gives data for validation.

2.1.2. Underhood modelling

As discussed in section 1.2.3, the underhood area of a truck is filled with many different components with different, non-aerodynamic, shapes and differs per truck model. Therefore it was decided to use a simplified model of the underhood in this study. The model will consist of a porous medium which is placed inside a duct in the lower cabin area. The inlet is placed in the frontal area of the truck while the outlets will guide the air towards the regions the air would exit on real trucks as well. The parameters of the porous medium will be chosen such that the mass flow and pressure drop of a realistic underhood are approximated.

To determine the desired mass flow, pressure drop and flow field the results of multiple other simulations performed on realistic truck models were studied. Based on the studies performed by Scheeve [44], Larsson and Martini [39] and two simulations performed at WABCO it was decided that the mass flow through the underhood should be 5 kg/s, while having a total pressure drop of 450 Pa.

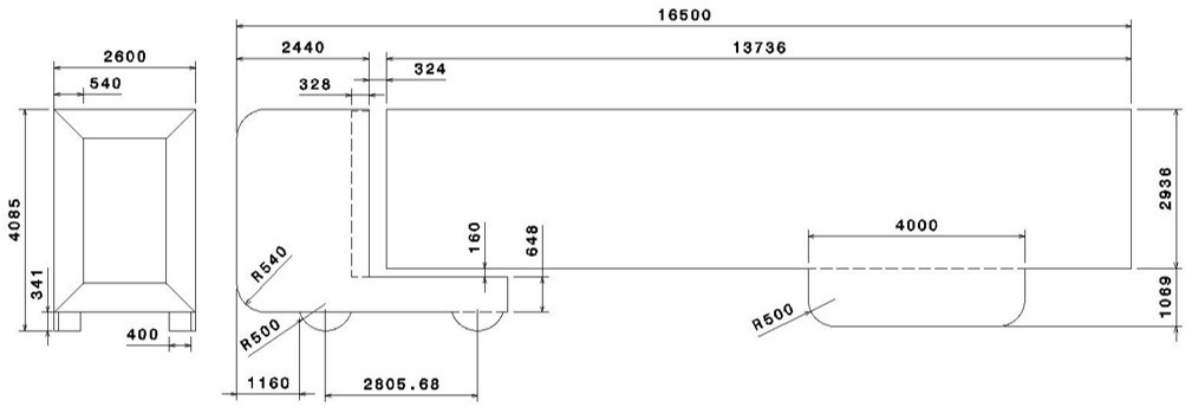

Figure 2.1: Drawing of the basic GEM model, dimensions are in mm

Two underhood models will be made. One is designed to have the mass flow and pressure drop stated above, the other one to have halve the mass flow. To achieve this the area of the inlet and porous medium will be halved for the second version. By having three versions, a trend can be spotted. Besides that, each version represents a different type of truck. The version with full underhood model represents a current tractor-trailer powered by a diesel engine. The version with reduced underhood mass flow represents a future truck with a smaller or more efficient combustion engine. This might be achieved by multiple innovations, like improved engine technology, improved aerodynamics, reduced weight or hybridisation. It can also represent a current truck using grille shutters. Finally, the basic GEM model can be seen as a future electric truck, since battery electric vehicles require way less forced cooling. This is shown for example by the absence of a large cooling inlet in the front of the Tesla Semi electric truck [45]. In the future these three types of vehicles might end up in the same platoon, the results in this study can help to determine the optimal platoon in that case. For the remainder of this thesis the model without underhood flow will be referred to as UH0, the model with halve the mass flow as UH1 and the one with the full underhood mass flow as UH2.

The size and position of the inlet for the UH2 model is based on the grille area of existing tractors and is shown in figure 2.2b. It has a width of 125 cm and a height of 135 cm for the UH2 model. It is positioned in the middle front face of the tractor at 50 cm above the road and 24.4 cm above the bottom of the front face, leaving room for a bumper with license plate. The edges of the inlet are given a fillet with a radius of 50 mm to avoid separation. For the UH1 model it was decided to keep the bottom of the inlet at same location and halve the height, as shown in figure 2.2a. It has to be noted that on real trucks the grill area is not the only inlet. Because the cabin can be tilted forwards to reach the engine, a splitline is present in the front face of the cabin. After the inlet a simple straight duct is placed to house the porous medium.

The porous medium is modelled as a simple block with a thickness of 20 cm, close to the thickness of a typical cooling package. The height and width of the block are slightly larger than those of the duct in order to avoid abutting surfaces, for the same reason discussed for the wheels. The porous medium is placed 15 cm behind the leading edge of the cabin, equal to the position of the cooling package found in [26].

The resistance of a porous medium is defined in PowerFLOW using the following equation [46]:

$$\frac{\delta P}{\delta x} = -\rho(Vu \cdot Iu^2) \tag{2.1}$$

Where δP is the pressure drop, δx the thickness of the porous medium, ρ the air density and u the air velocity. V and I are the coefficients for viscous and inertial resistance respectively. Normally they are determined by the manufacturer of the heat exchanger, by testing it in a wind tunnel. However, in this case the porous medium has to represent a full underhood, with multiple heat exchangers and all components mounted behind it. Therefore no coefficients are available. As mentioned before, the desired mass flow and pressure drop are known. Using the mass flow and size of the porous medium the flow velocity can be determined, which only leaves V and I as unknowns in the equation. To make sure the behaviour of the underhood flow is also realistic at higher or lower mass flows, the coefficients of multiple types of heat exchangers were used [1]. It was found that V is approximately four times higher than I in most cases. Using this and the desired mass

[1] Values supplied by Roy Veldhuizen of WABCO OptiFlow in personal correspondence

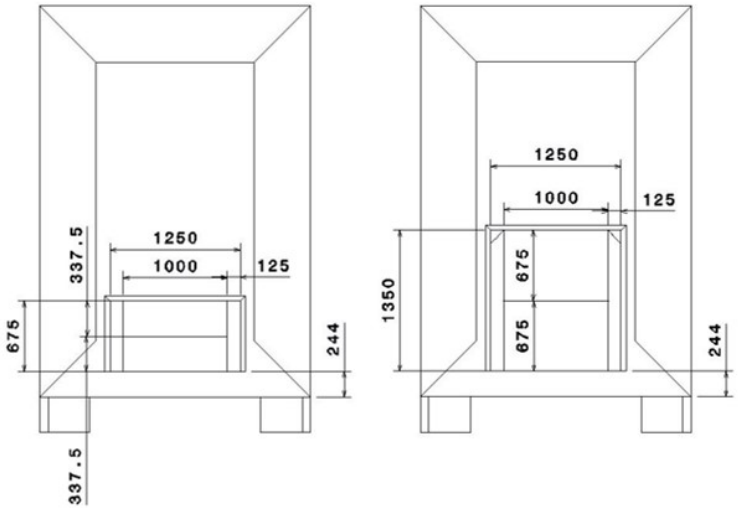

(a) UH1 (b) UH2

Figure 2.2: Front view of the models with underhood showing the size and position of the inlets, dimensions are in mm

flow and pressure drop, the values for V and I are found to be 473 and 118 respectively. These values were used for the first iteration. Later they were fine tuned to 404 and 101.

Behind the porous medium the duct is split to guide air in different directions. Based on the references mentioned before, it was decided to guide 40% of the air to the bottom of the tractor, 40% to rear of the cabin, 10% to the left and 10% to the right. The division was made by placing the duct inlets directly behind the porous medium and use the desired mass flow ratios as the area ratios. In figure 2.2 the inlet size and position of each duct can be seen. Initial simulations showed that the resulting mass flow distribution was very close to the desired one.

The air that is deflected towards the left and right side of the cabin is meant to represent the air leaving through the wheel arches. Due to the absence of rotating wheels, accurately modelling this is not possible. Therefore simple rectangular outlets positioned above the front wheels were chosen. The size and position are the same for both models and are shown in figure 2.3b. The air is flowing towards these exits through simple curved ducts as shown in figure 2.3a. The height of the ducts differs per model, due to the difference in inlet height.

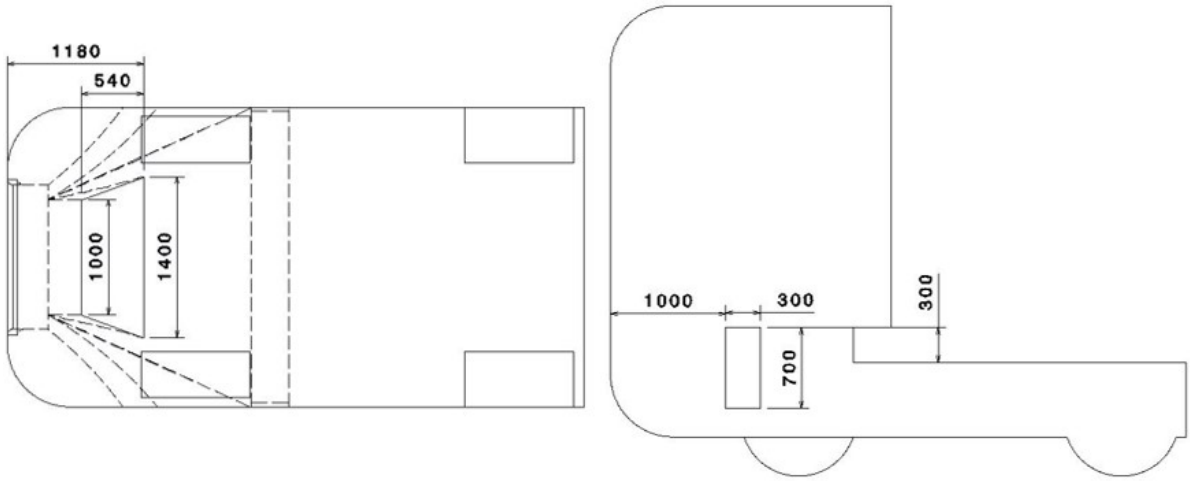

(a) Bottom view (b) Side view

Figure 2.3: Drawings with dimensions for both underhood models, dimensions in mm

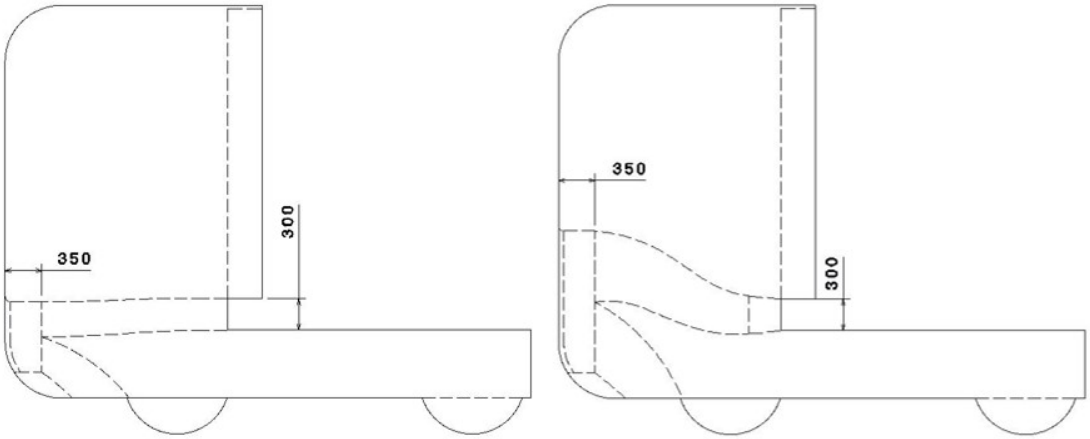

(a) UH1 (b) UH2

Figure 2.4: Side view of the models with underhood showing the outlines of the top and bottom ducts, dimensions in mm

The bottom duct represents the air that goes down immediately after the cooling package and passes underneath the engine block. Therefore the outlet is placed in front of the front wheels and only a short curved duct is used. The outlet is the same for both models and is shown in figure 2.3a. Due to the difference in inlet size the curvature of the duct differs per model as can be seen in figure 2.4.

The outlet at the rear of the cabin is placed at the bottom of the tractor-trailer gap, with a cutout in the cabin side extenders next to the outlet to allow flow to leave towards the sides as well. To make a fair comparison, these cutouts will be present on the UH0 models as well. Figure 2.4 shows that the duct going towards this exit differs quite a bit between UH1 and UH2. Due to the difference in inlet position having a duct straight to the end of the cabin would result in different outflow directions. Therefore it was decided to give both ducts a horizontal part at the end, resulting in an S-shaped duct for UH2.

Trial runs with this configuration showed a large mass flow through the horizontal gap between the tractor and trailer and no flow going up through the tractor-trailer gap. While in the reference simulations flow is going up over the trailer, as shown in figure 2.7a, while in the horizontal tractor-trailer gap two large circulating areas can be seen, with little effective mass flow towards the rear, shown in figure 2.6a. It was found that this difference could be explained by the angle of the cabin roof. Giving the GEM model a similar 12.5 degree angle (see figure 2.5) as the roof deflector of the reference model give a very similar flow field, as shown in figures 2.6b and 2.7b. A more in-depth analysis of the model with angled roof can be found in Appendix A. It was decided to keep using the model with a straight roof for this study, to not deviate too much from the basic model that was already used in other studies.

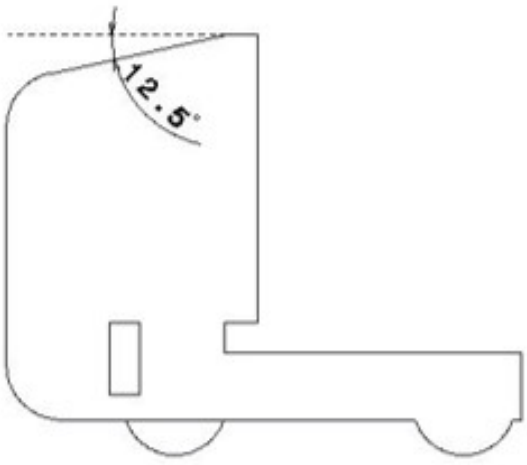

Figure 2.5: Side view of the GEM tractor with an angled roof to replicate the effect of a roof deflector

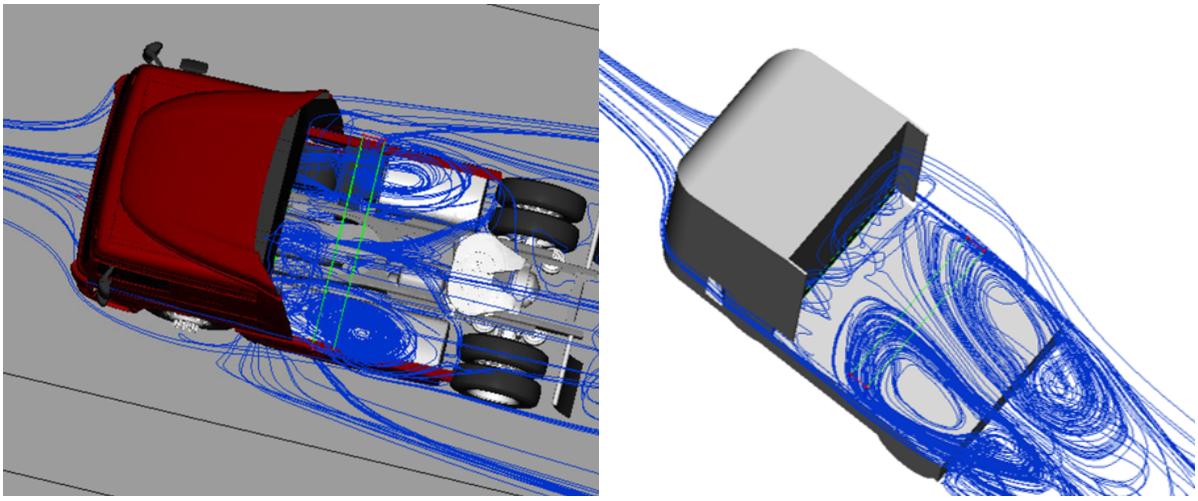

(a) DAF model (b) GEM model with angled roof

Figure 2.6: Streamlines passing through the horizontal tractor-trailer gap

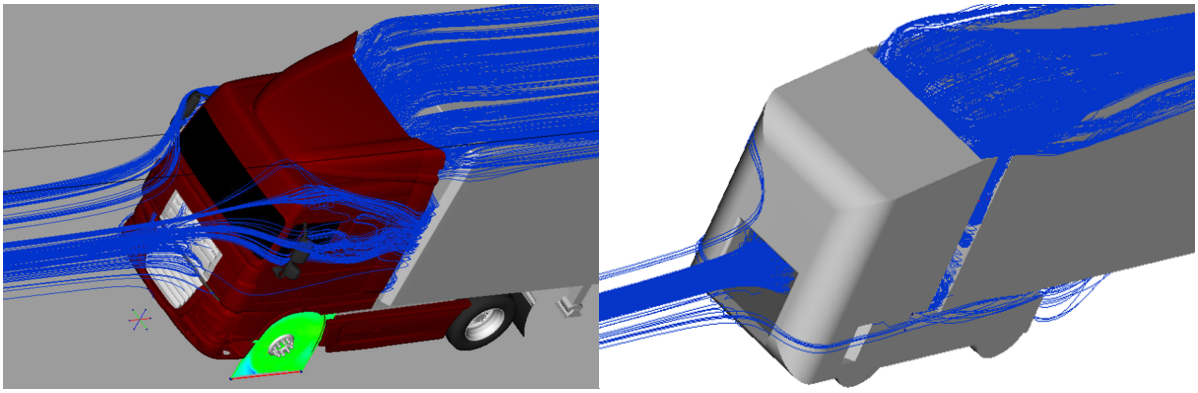

(a) DAF model (b) GEM model with angled roof

Figure 2.7: Streamlines passing through the vertical tractor-trailer gap

2.1.3. Design alterations

To investigate the influence of design aspects, they should be altered multiple times to see a trend. Besides the underhood models discussed above, two drag reduction devices directly influencing the area between two trucks in a platoon will be investigated, the leading edge radius and the boat tail. The standard leading edge radius of 540 mm will be halved twice to 270 and 135 mm. As described in section 1.2.2, the design of boat tails has already been studied extensively. Therefore only one design will be tested here. A proven design with a length of 0.5 m and an angle of 12 degrees, shown in figure 2.8. For the platoon runs the distance between the vehicles will be altered. Three distances will be used: 3.75, 7.5 and 15 meters, equivalent to 0.23, 0.45 and 0.91 vehicle lengths respectively. Finally the effect of cross-winds will be tested by simulating platoons at a yaw angle of 6 degrees.

Throughout this study a large number of simulations will be performed. To distinguish them easily a simple coding system is used. It starts with 'IV' when an isolated vehicle is simulated and 'PL' for a platooning run. After that, comes 'UH' with a number as discussed before, to indicate the used underhood model. This is followed by the leading edge radius in mm with an 'R' before it. For platooning runs the inter vehicle distance will be noted as D23, D45 or D91 corresponding to the decimals of the distance measured in vehicle lengths.

So for example in simulation IV_UH2_R540 an isolated vehicle with the full underhood model and a leading edge radius of 540 mm is used and in PL_UH0_R135_D91 a platoon with a inter vehicle distance of 0.91 vehicle lengths and a trailing vehicle without underhood mass flow and a leading edge radius of 135 mm.

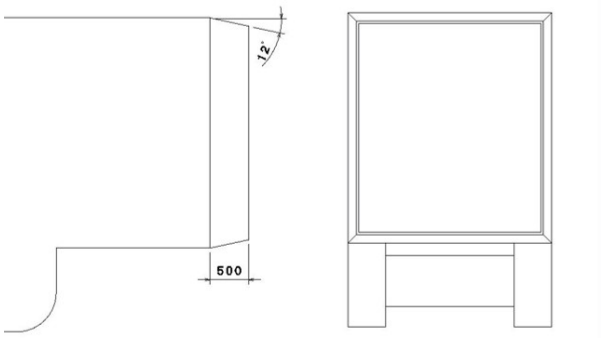

Figure 2.8: Side and rear view of the boat tail used in this study

One of the advantages of using CFD simulations is that the drag coefficient of different parts can easily be extracted from the results, so the origin of differences in drag for the whole vehicle can be located. To do this both the tractor and the trailer have been subdivided in a number of parts, the division can be found in Appendix B.

2.2. Lattice-Boltzmann Method

The CFD software to be used in this study, PowerFLOW, is based on the Lattice-Boltzmann Method (LBM), while most commercially available software packages are based on the Navier-Stokes equations. Therefore, in this section the theoretical background of PowerFLOW and how this differs from the Navier-Stokes method will be discussed.

Both methods start with defining a large number of discrete particles moving around in a space. The locations and speeds of all these particles describe the behaviour of the fluid. Using kinetic theory and statistical physics, along with some assumptions about the nature of the collision process, the non-linear Navier-Stokes equations can be derived from this. To solve these equations computationally, the representation should be discretised. This means splitting the space in a computational grid. By introducing this grid, errors are introduced as well. When the resolution of the grid is too coarse, this can lead to unstable or diverging solutions. Usually Navier-Stokes solvers are steady state, to reduce the simulations costs and avoid numerical instability [47].

In LBM the discretisation step is done on a lower level. The particles have a discrete speed at a discrete location at a discrete moment in time. In PowerFLOW the particles can move in 19 directions in three dimensions, the so-called D3Q19 model [49], shown in figure 2.9. How many particles with what speed are present at a certain location is used determine the behaviour of the flow. This means that a Lattice-Boltzmann solver is always transient. In practice this means that to do a steady state simulation, a simulation has to be run for a certain time with the same boundary conditions, until the flow has converged to a steady state. Using this method also means that the volume mesh is less critical. Refining the mesh will improve the results because the flow is captured in more detail, so the small effects are not averaged out. However, a coarse grid

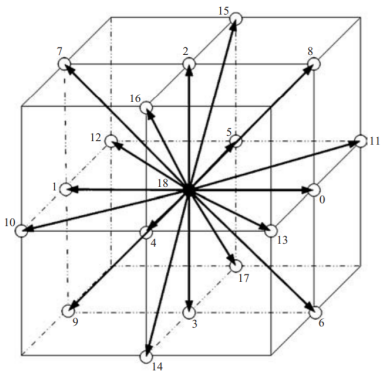

Figure 2.9: The D3Q19 model [48]

will never make the simulation unstable or divergent [47]. To show that this method gives valid results, it was proven that using the Chapman-Enskog expansion the Navier-Stokes equations can be recovered for low Mach numbers [49].

For the high Reynolds numbers that will be encountered in this study, turbulence and boundary layer modelling is required to make sure the computational costs stay within boundaries. PowerFLOW uses a Very Large Eddy Simulation (VLES) to model turbulence with a $\kappa-\epsilon$ Renormalization Group (RNG) [50]. To model the boundary layer PowerFLOW assumes that the cell closest to a surface is a non-geometry-dependent part of the turbulent boundary layer. The flow inside these cells is modelled using the Law of the Wall, as shown in figure 2.10 [50].

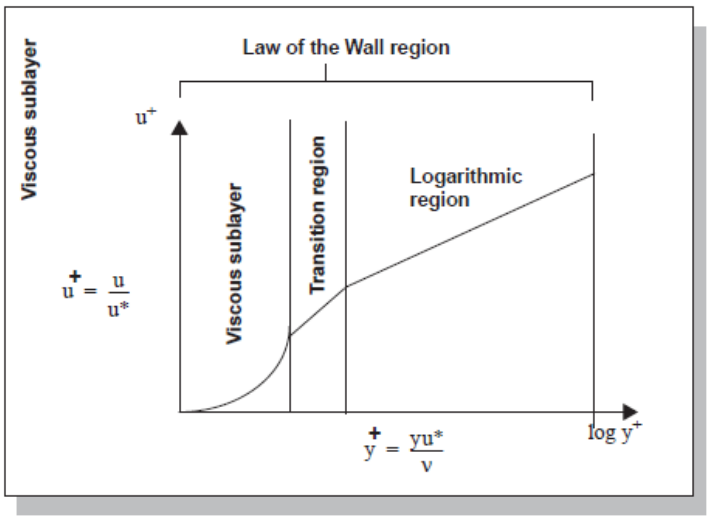

Figure 2.10: Turbulent boundary layer profile [50]

2.3. Simulation setup

After discussing the theoretical side of PowerFLOW in the previous section, in this section the more practical side will be discussed by looking at the settings used for the simulations.

When creating a new case, a number of settings have to be chosen immediately. Those settings are displayed in figure 2.11. Most choices are rather obvious, but the last two might need some explanation. First, no vehicle simulation is used, although vehicle models will be used. The vehicle simulation option enables options to determine the forces on different axles for example. However, the simplified GEM model does not have rotating wheels, so no axles. Enabling this option would result in features that cannot be applied to this model. Finally the 'Boundary Layer Transition Model' option is not enabled, this means that the boundary layer is fully turbulent at all locations. This is close to real life as was discussed in section 1.2.1.

After this, the simulated conditions should be specified in the 'Globals' tab, shown in figure 2.12. The characteristic pressure, temperature and viscosity are based on the standard atmospheric conditions at sea level, while the characteristic velocity is set at 85 km/h, representing highway conditions. The square root of the frontal area and the frontal area of the vehicle are used for the characteristic length and area respectively. The value supplied at resolution determines the number of cells size of the cells in the highest refinement level. This will be discussed further in the next section, as will be the maximum simulation duration. The simulated Mach number is set to be chosen by PowerFLOW. This means that the simulation will be ran with a Mach number that is higher than would normally be the case. In the low subsonic regime, the flow results are independent of the Mach number. However, for higher Mach numbers the amount of timesteps required for the same amount of physical time reduces. Therefore the simulation costs reduce for higher Mach numbers. PowerFLOW uses the highest possible Mach number, around 0.4 [46]. In this case a maximum expected velocity has to be supplied, this velocity will be mapped into a value that will not exceed the maximum Mach number. When the flow speed in the simulation exceed this value, the results will become unreliable. The value is set to 153 km/h, which is 1.8 times the characteristic velocity. This is recommended for particularly bluff bodies, initial simulations showed that this is approximately correct. For the Gas Molecular Weight and all parameters below that default values are used.

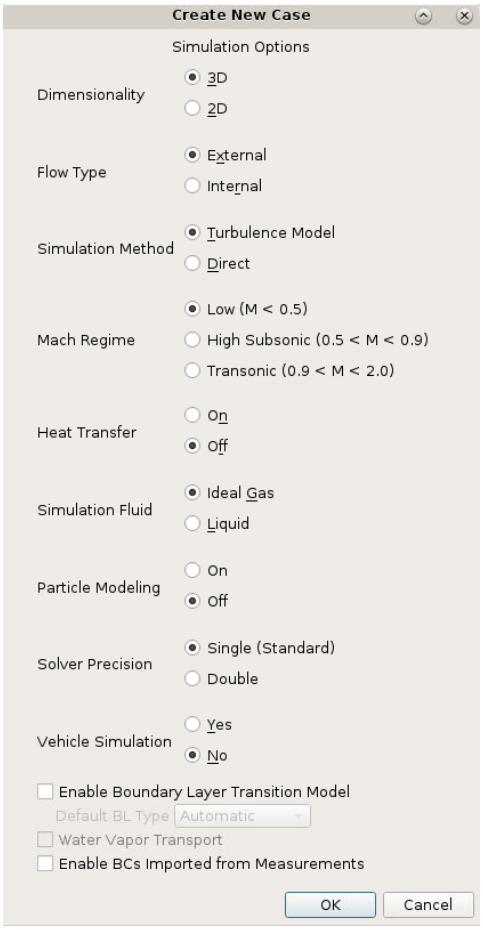

Figure 2.11: PowerCASE simulation settings selected for the simulations in this study

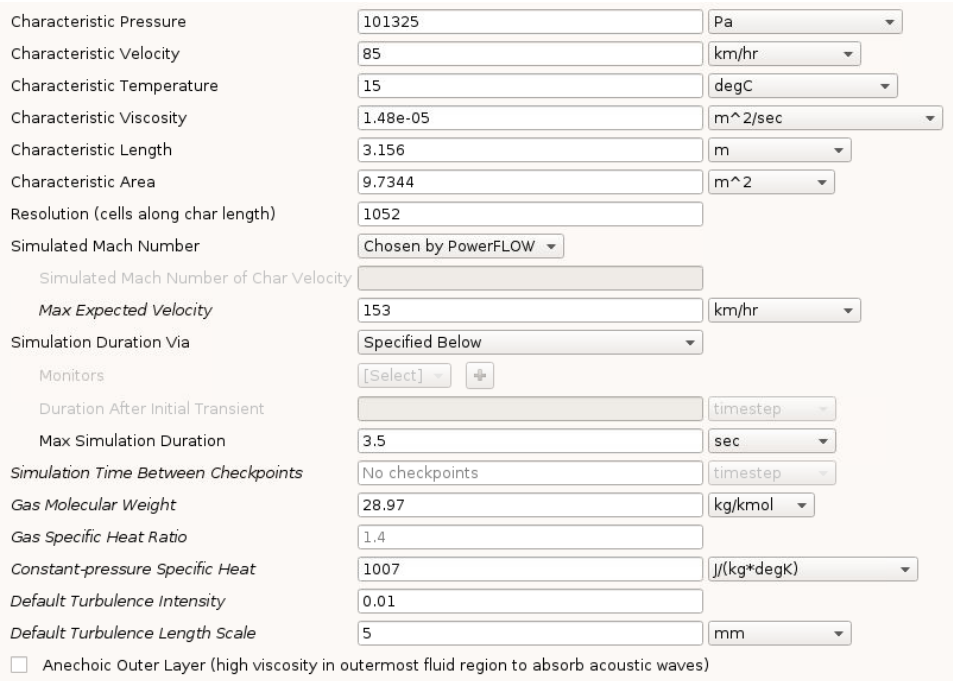

Figure 2.12: 'Globals' tab from PowerCASE

The size of the simulation volume around the model is based on the recommendations found in the SAE J2966 standard [51]. The volume stretches from three vehicle lengths in front of the vehicle to seven vehicles lengths behind it. The width is ten times the width of the model and the height is six times the vehicle height. The simulation volume with dimensions is shown in figure 2.13. For platooning simulations the length of the second vehicle and the distance between the models will be added. Unfortunately, this did not happen in all instances which had some influence on the results. This is discussed in section 5.1.1.

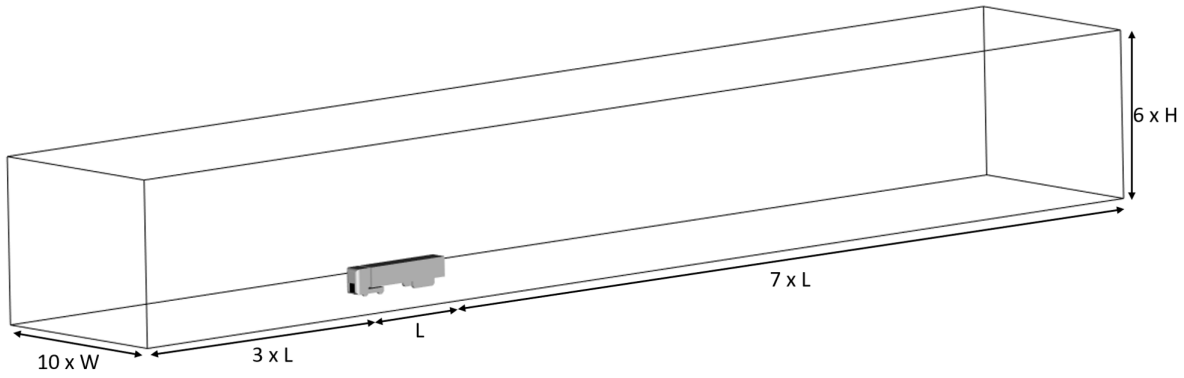

Figure 2.13: Simulation volume with dimensions, where L, W and H are the length width and height of the model respectively

The inlet is defined as a velocity inlet, with the characteristic velocity defined earlier. The outlet is a zero-gradient outlet. The sides and top of the simulation volume are defined as frictionless walls, this means no flow is passing through it, but no boundary layer is forming either. Finally the floor uses the moving wall boundary condition, therefore it moves at the same speed as the inlet air. These boundary conditions are in compliance with the SAE J2966 standard [51]. All surfaces of the vehicle model are simple walls, except for the walls of the ducts in the underhood. Since these do not represent a physical part of the vehicle they are defined as frictionless walls.

For the simulations with a yaw angle the vehicles will be placed in a separate reference frame which is rotated by 6 degrees compared to the default reference frame. This means that the flow is still passing straight through the simulation volume, but the vehicles are placed at an angle. This means that the boundary conditions remain the same except for the moving wall condition of the floor. The direction of this boundary condition has to be rotated as well. As stated in the SAE J2966 standard [51] the size of the simulation volume should be based on the size of the model in flow direction. Because the models are rotated the width in flow direction is increased and the simulation volume width should be increased accordingly.

To determine which data is recorded during the simulations, measurements have to be defined in PowerCASE. To save storage space, the data of the complete simulation volume will not be saved, but just that from an area around the model. For the same reason, a period is defined after which the flow data is stored, because saving every timestep would create a lot of unnecessary data. Van Tilborg [35] found that the highest frequency of unsteady forces around a truck model is 10 Hz. To capture those it was decided to use a sampling time of 0.03 s. This means that the data over a period of 0.03 s is averaged and saved as a frame. In the end the results are averaged over 47 frames, equal to 1.4 s or 2 flow passes, to find the steady forces.

2.4. Mesh study

After decisions on all settings discussed above have been made, two important questions remain: What should the mesh look like and for how long should the simulation run? To answer these questions a mesh study was carried out.

PowerFLOW requires a surface mesh of the model, composed of triangles. The most important requirement for the size of these triangles is that they accurately represent the curvature of the model. The SAE J2966 standards [51] state that the chordal deviation should be less than 0.1 mm for a full scale vehicle and less than 0.05 mm in flow-critical areas. Since a simplified model is used here, basically every curvature is flow critical. For flat surfaces chordal deviation does not make a difference. Therefore a upper limit of 0.05 mm was used everywhere.

In PowerFLOW the volume mesh is composed of cubical elements called voxels. This mesh is automatically generated by PowerFLOW based on a few user inputs. The resolution is divided in different levels,

so-called Variable Resolution (VR) levels. The user has to specify the resolution in the 'Globals' tab shown in the previous section. This value represents the amount of cells along the characteristic length in the highest specified VR level. One VR level higher, the cell size is doubled. Same for the next level, etc..

Having a underhood model in place will probably influence the results of the mesh study. However, since these are the first simulations to be performed, it was unknown what the underhood model had to be exactly. It was decided to use a first version of the underhood throughout the mesh study and optimise it after that. The initial model featured two outlets, one at the bottom of the tractor, in front of the front wheels, and one in the rear of the cabin. Flow from the lower 40% of the porous medium was guided to the bottom, the other 60% to the rear of the cabin.

The first meshes used the same strategy as was used by Van Tilborg [35]. Which means that a box is drawn around the complete model and its wake region. Therefore this is referred to as the 'wake box'. The dimensions of the wake box are shown in figure 2.14. The wake box defines the boundary of the second finest VR level. The only finer level is defined by an offset from the model. Four meshes were created using this strategy. The first was rather coarse. Each mesh that followed halved the cell size of the finest level and therefore also of the wake box. The VR distribution is shown in table 2.1.

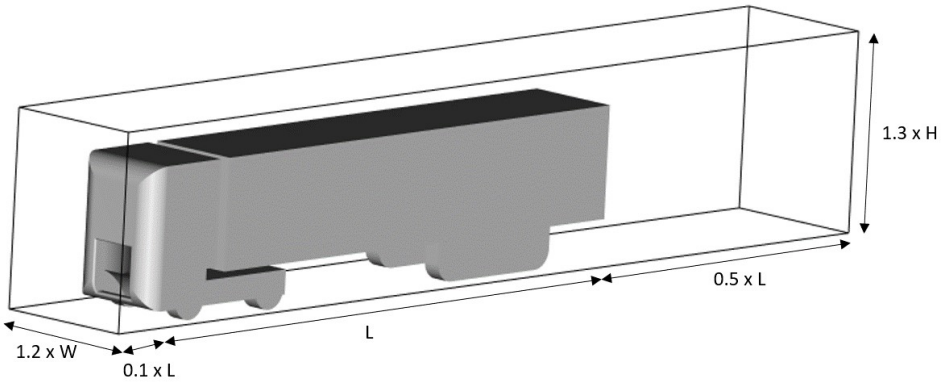

Figure 2.14: Dimensions of the wake box, where L, W and H are the length width and height of the model respectively

Table 2.1: VR distribution of Mesh 1 to 4

Mesh	Wake box VR level and cell size	Offset VR level and cell size
Mesh 1	VR5, 92 mm	VR6, 48 mm
Mesh 2	VR6, 48 mm	VR7, 24 mm
Mesh 3	VR7, 24 mm	VR8, 12 mm
Mesh 4	VR8, 12 mm	VR9, 6 mm

Increasing the resolution increases the amount of voxels in a mesh and increases the amount timesteps required to simulate the same physical time. Therefore computational costs increase exponentially when the resolution is increased. However, when a transient simulation is started an initial transient will be seen in which the results are not usable. This initial transient is reduced when the simulation starts with a realistic flow field, instead of the initial conditions. This can be achieved by first performing a coarse run, with low simulation costs, and using its results as starting point for the fine run. This method is called coarse-to-fine seeding [42] and will be used throughout this study.

First mesh 1 was ran for 5.6 *s*, equal to 8 flow passes. Where a flow pass is the time it takes for the ambient flow to travel one vehicle length. The results of this simulation were used to seed the runs for meshes 2, 3 and 4. Mesh 2 and 3 were again ran for 5.6 *s*, but the run of mesh 4 was terminated before that. This was done since it would take a large amount of the available resources for this study to complete it. Therefore it would be too expensive to use for further simulations anyway.

As mentioned before, a boundary layer is used by PowerFLOW. For this model to be accurate, the y^+ values around the model should be below 300 [42]. The results of mesh 3 showed that large parts of the tractor had a y^+ value above 300, while this was still the case for the leading edges in the premature mesh 4 results. This meant that the mesh has to be refined while the computational costs have to come down. Therefore another strategy was chosen.

The new mesh still features the wake box, but multiple refinements are made inside this box. This means that more refined cells are present near the surface, but the resolution in the wake box is decreased. In mesh 5 the wake box is defined as VR6. VR7 consists of a 6 voxel offset from the complete vehicle. Another 10 voxel offset is used for a VR8 region around the cabin area of the tractor, see figure 2.15a. VR9 is defined as an 6 voxel offset around only the front part of the cabin, see figure 2.15b. The finest level, VR10, uses a 6 voxel offset around the leading edges of the tractor, see figure 2.15c.

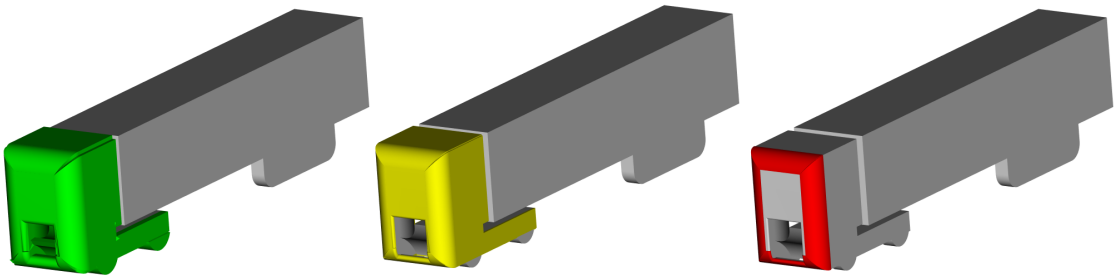

(a) Cabin offset (b) Cabin front offset (c) Leading edges offset

Figure 2.15: Offsets used for mesh refinement in Mesh 5, 6 and 7

The computational costs were reduced significantly by using this method. The results also showed y^+ levels between 100 and 200 for most of the tractor surfaces. However, large parts of the trailer now had y^+ values above 300. Therefore two additional meshes were created. For mesh 6 the exact same strategy was used as for mesh 5, but with an increased resolution. This means that the cell size of each level was halved. The final mesh, mesh 7, has the same resolution as mesh 5. However, the VR8 offset is put around the complete vehicle. Therefore only the resolution around the trailer is increased. An overview of the VR distribution used in meshes 5, 6 and 7 is shown in table 2.2.

Table 2.2: VR distribution of Mesh 5, 6 and 7

Mesh	VR6 (48 mm)	VR7 (24 mm)	VR8 (12 mm)	VR9 (6 mm)	VR10 (3 mm)	VR11 (1.5 mm)
Mesh 5	Wake box	Complete vehicle offset	Cabin offset	Cabin front offset	Leading edges offset	-
Mesh 6		Wake box	Complete vehicle offset	Cabin offset	Cabin front offset	Leading edges offset
Mesh 7	Wake box	Complete vehicle offset	Complete vehicle offset	Cabin front offset	Leading edges offset	-

Meshes 5 and 7 were ran for 4.2 s or 6 flow passes, while using the results of mesh 3 as seeding. Due to its large amount of voxels, mesh 6 was only ran for 2.1 s while also being seeded from mesh 3. The results of all meshes are summarised in figure 2.16. It can be seen that the drag coefficient does not differ a lot, except for mesh 6 which gives a lower value. The underhood mass flow seems to converge to a steady value when the amount of voxels is increased. Based on these results, the y^+ distribution, shown in figure 2.17, and the computational costs, it was decided to use mesh 7 for the rest of the study.

The meshes described above are all applied on a isolated vehicle. For simulations of a platoon the mesh has to be altered slightly. For the platoons with a zero yaw angle not a lot is changed. Both vehicles have the same offsets as applied to the isolated vehicle. The VR6 wake box is extended to contain both vehicles and the distance in between them. For the simulations with a yaw angle the VR6 to VR3 regions are rotated with the models. On top of that the width of the wake box is extended on the leeward side of the vehicles to captured the wake.

As mentioned above, the results of earlier runs were used as seeding during the mesh study. However, when the geometry is changed, a new coarse run should be performed. Therefore the results of the mesh study do not give a definitive answer on the physical time required to be simulated. This was further investigated during iterations on the underhood flow. The drag coefficient development over time for both the

coarse and the fine run of the final iteration is shown in figure 2.18. It was decided to use the physical simulation time used here, 5.6 *s* for the coarse run and 3.5 *s* for the fine run, for the rest of the study. The results will be averaged over the last two flow passes of the fine run. This means that averaging starts at 2.1 *s* and ends at the end of the simulation.

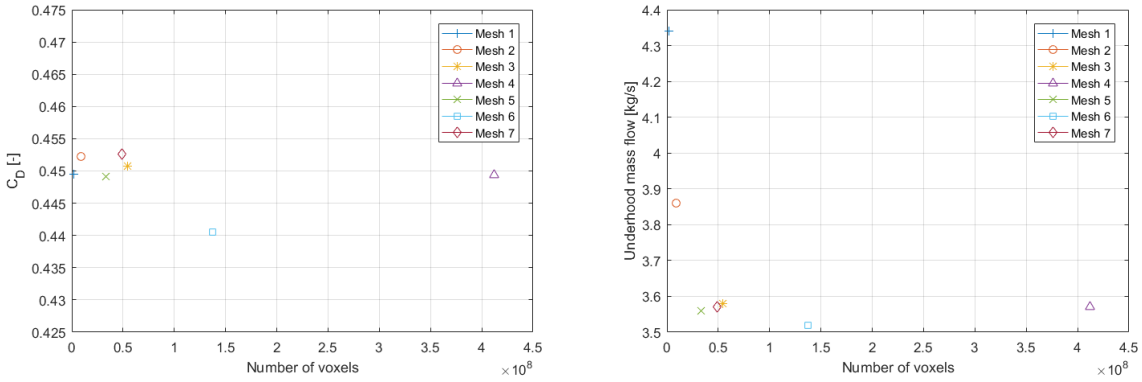

Figure 2.16: The drag coefficient and underhood mass flow found for each mesh plotted against the number of voxels

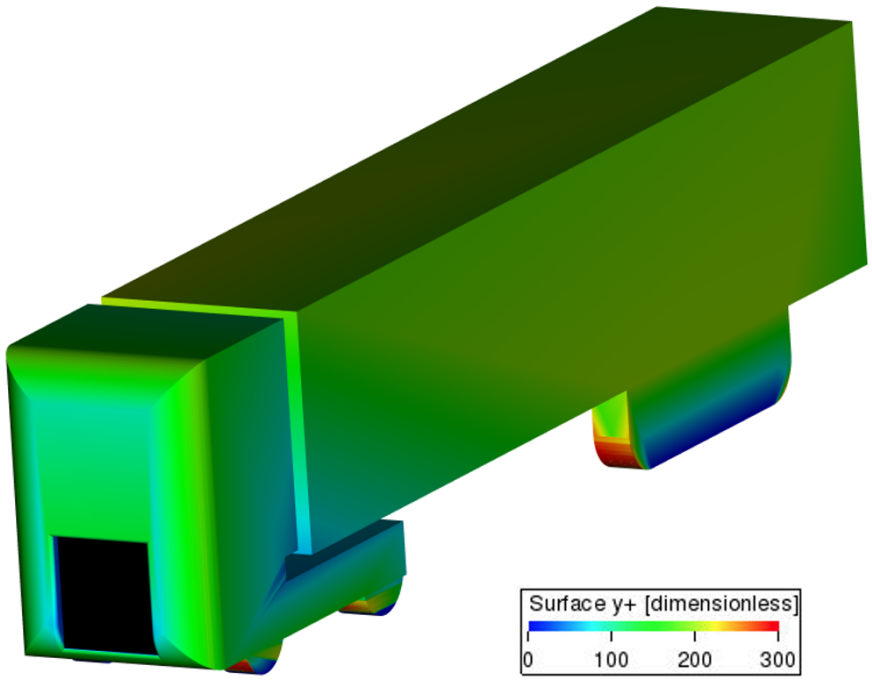

Figure 2.17: y^+ distribution over the model in mesh 7

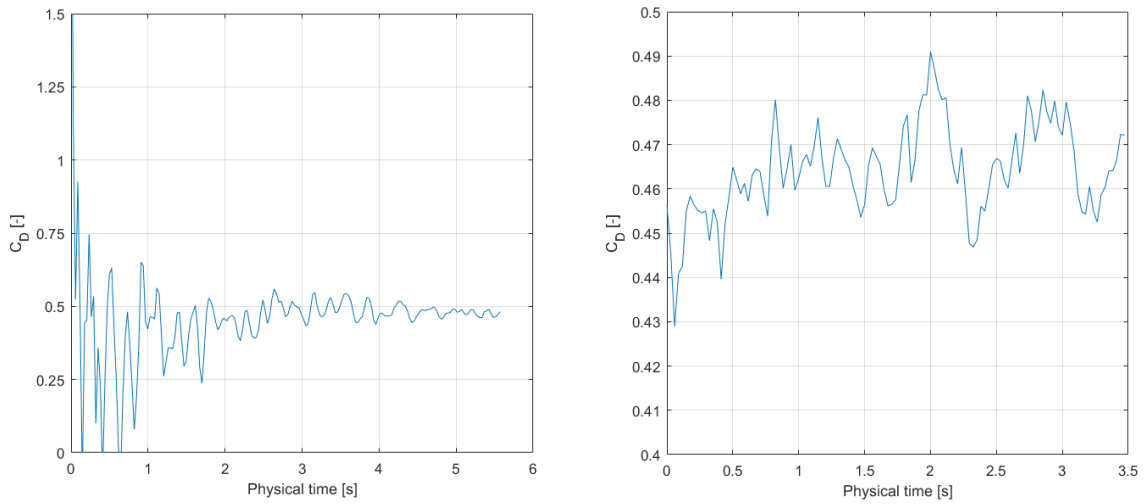

(a) Coarse run

(b) Fine run

Figure 2.18: The drag coefficient development of the final iteration of the underhood model

2.5. Uncertainty

Since not the finest mesh has been chosen, some uncertainty is introduced into the results. An attempt has been made to quantify this uncertainty. The first method to do this is recommended by the SAE [51]. The method uses three grids, where number 1 is the finest and number 3 is the coarsest. Using the ratio between the representative grid sizes, r_{21} and r_{32} and an iterative process the apparent order p can be found using two equations:

$$p = \frac{1}{ln(r_{21})}\left|ln\left|\frac{\epsilon_{32}}{\epsilon_{21}}\right| + q(p)\right| \tag{2.2}$$

$$q(p) = ln\left(\frac{r_{21}^p - s}{r_{32}^p - s}\right) \tag{2.3}$$

Where ϵ_{32} is the drag coefficient found for grid 3 subtracted by the drag coefficient of grid 2. The same is done for ϵ_{21} with grids 2 and 1. Finally, s is the sign of ϵ_{32} divided by ϵ_{21} multiplied by one. The approximate relative error is defined as:

$$e_a^{21} = \left|\frac{C_{D,1} - C_{D,2}}{C_{D,1}}\right| \tag{2.4}$$

Finally, the Grid Convergence Index (GCI), a percentage that the found value might be off the actual value, can be found using:

$$GCI_{finest}^{21} = \frac{1.25e_a^{21}}{r_{21}^p - 1} \tag{2.5}$$

Figure 2.16 shows that in this case refining the mesh does not give a relation asymptotically converging to a final value. Therefore the three meshes that are being chosen have a big influence on the resulting GCI value. For example using meshes 1, 2 and 7 gives a GCI of 0.02% and using meshes 1, 3 and 7 gives a GCI of 0.00001%. Both very small numbers, which seem to be unrealistic. On top of that mesh 1, 2 and 3 use a different meshing strategy and have different physical runtimes. The most realistic option would be use mesh 5, 7 and 6, since almost the same meshing strategy was used on all of them. Doing this gives a GCI of 2.42%. However, it still has to be noted that mesh 6 was ran for a shorter time due to its high computational costs.

Another way to look at uncertainty is to look at the transient behaviour of the drag force. This has been done for the isolated vehicle runs, which will be discussed in chapter 4. Since different geometries were used in this run, it does not makes sense to look at the absolute drag values. Therefore the transient values were normalised by the average drag value over the measurement window. The minimum and maximum drag

values found inside the averaging window were determined. It was found that on average the minimum and maximum value were separated by 6.8% of the average value. This could be interpreted as a uncertainty of 3.4%. Figure 2.19 shows the normalised transient plots of the nine isolate vehicle runs inside the averaging window. The two horizontal lines indicate an uncertainty level of 3.4% in both directions. It can be seen that all simulations are fluctuating over roughly the same bandwidth and that only few peaks are outside the indicated uncertainty margins. This could indicate that 3.4% is a reasonable uncertainty margin. However, it can be seen that only peaks are approaching this margin. Having a few peaks with this difference from the average does not mean that the average can be off by 3.4%. Therefore the uncertainty will probably be smaller than this value, but by how much is hard to say.

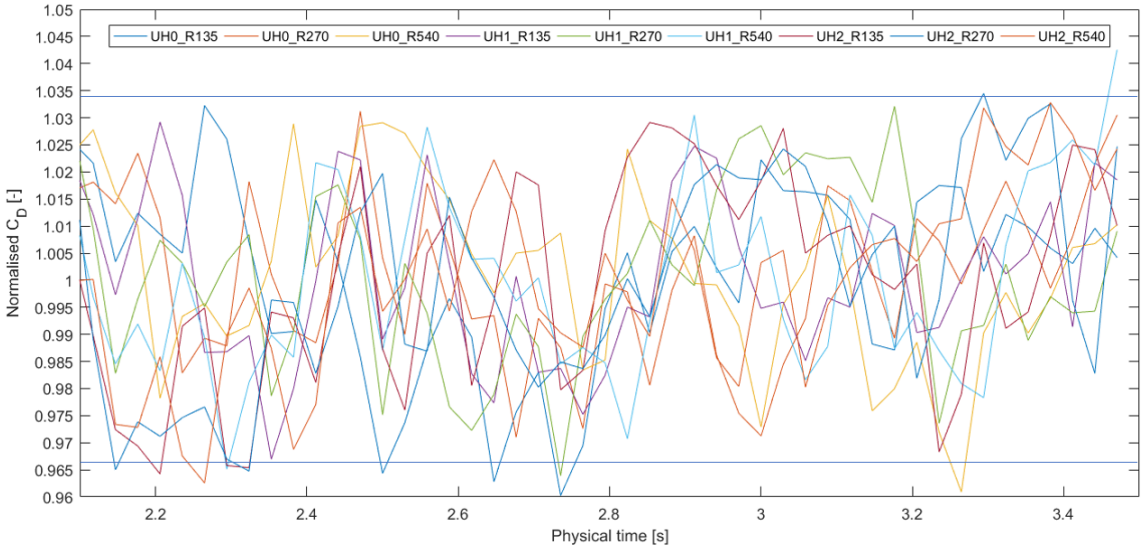

Figure 2.19: Normalised transient behaviour of the total drag coefficient inside the averaging window for the isolated vehicle runs, the horizontal lines indicate a uncertainty of 3.4%

It can be concluded that based on the available data it is difficult to quantify the uncertainty encountered in these simulations. The GCI-method does not seem to be suitable for the current situation, while looking at the variations does not give a a lot of information about the uncertainty of the average value.

3

Verification and validation

To validate the simulation method described in chapter 2 it will be applied to a case reproducing the experiments and simulations performed by Kruijssen [23] and Mulkens [43]. Both of them investigated the influence of add-on aerodynamic features on the basic GEM model. The model was tested in a wind tunnel and simulated using the Reynolds Averaged Navier-Stokes (RANS) method in ANSYS Fluent. First the setup used will be discussed in section 3.1. After that the results will be shown in section 3.2.

3.1. Simulation setup

The GEM model was originally designed by Mulkens [43], who also built a 1:8 scale model of it. This model was used by both Mulkens and Kruijssen to perform experiments in the Open Jet Facility (OJF) wind tunnel at TU Delft. Both used the wind tunnel setup shown in Appendix C. The model was placed on a static, elevated, floor plate inside a larger open jet tunnel. Mulkens ran the tunnel at a velocity of 27.2 m/s, while this was 25 m/s for Kruijssens experiments. The turbulence intensity of the OJF was determined to be 0.3%. In both studies CFD simulations were performed as well. In both cases steady RANS was used with a $k-\omega$ Shear Stress Transport (SST) turbulence model. The meshes used were not the same. The mesh used by Mulkens had around 10 million cells, the one used by Kruijssen only 6.4 million.

To mimic the circumstances in the wind tunnel test in the boundary conditions of the CFD simulation for this study an approach similar to the one used by Mulkens was used. The original floor was moved down a bit, but kept its original moving wall condition. A panel with approximately the same dimensions as the one in the wind tunnel setup, see figure 3.1, was added as a simple wall on top of the floor. All other boundary conditions remained the same. An air velocity of 25 m/s was used here.

The same meshing strategy was used as in mesh 7 of the mesh study. The cell sizes were kept the same, since the model is scaled the offsets are relatively big compared to the full size case. However, using smaller offsets would reduce the amount of cells in the VR layer, which is not recommended.

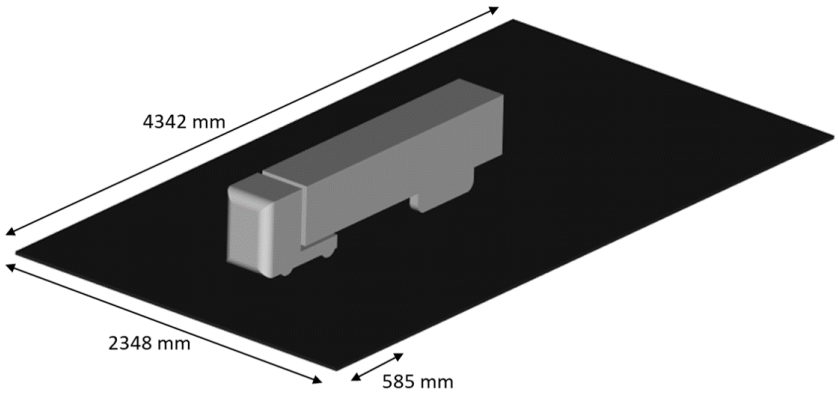

Figure 3.1: Dimensions of the static floor plate used in the validation case

3.2. Results

First a coarse run was performed for 5.6 *s* physical time, after that another 5.6 *s* was simulated in the fine simulation. The results were averaged over the last 1.8 seconds. Figure 3.2 shows that the results taken into account were converged.

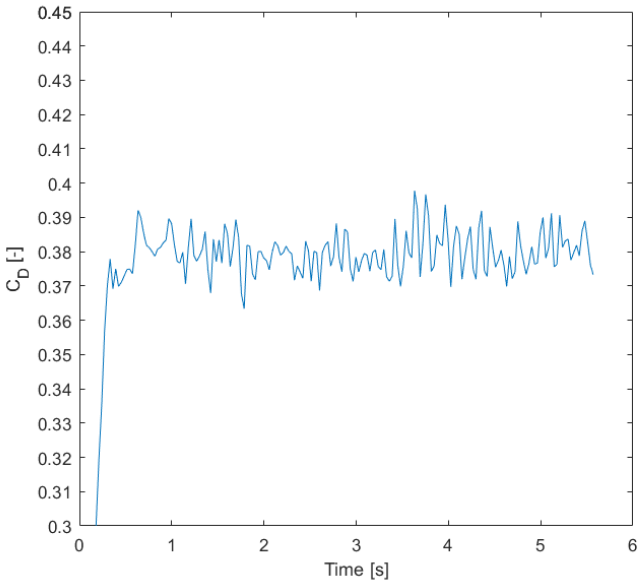

Figure 3.2: Drag coefficient vs. physical time for the fine validation run

An averaged drag coefficient of 0.380 was found. Table 3.1 shows how this compares to the values found by Mulkens and Kruijssen. It can be seen that the drag coefficient found here is closer to the experimental values than the RANS simulations performed in the earlier studies. Unfortunately, the drag coefficient is the only thing that can be compared to the experimental data. However, a more detailed comparison can be made with the simulation data.

Table 3.1: Drag coefficient comparison with previous research

	C_D [-]	
	Numerical	Experimental
Mulkens	0.395	0.373
Kruijssen	0.414	0.363
Current	0.380	

For the numerical data, the distribution of pressure and viscous drag can be evaluated. The viscous drag was determined by integrating the skin friction over all vehicle surfaces. The pressure drag was taken to be the remaining part of the total drag. The results are compared to those found in the other two studies in table 3.2. As expected for a bluff body, the contribution of the pressure drag is way higher than the viscous drag. It was found that the difference between the studies is mainly caused by the pressure drag. The absolute value of the viscous drag is almost the same for all three studies. It has to be noted that the results of the two other studies are based on the last iteration and not on the average of the multiple frames. The results of this study are still based on the average over the last 1.8 *s*.

Table 3.2: Distribution of the pressure and viscous drag compared with previous research

	Pressure drag [%]	Viscous drag [%]
Mulkens	83.2	16.8
Kruijssen	85.3	14.8
Current	82.6	17.4

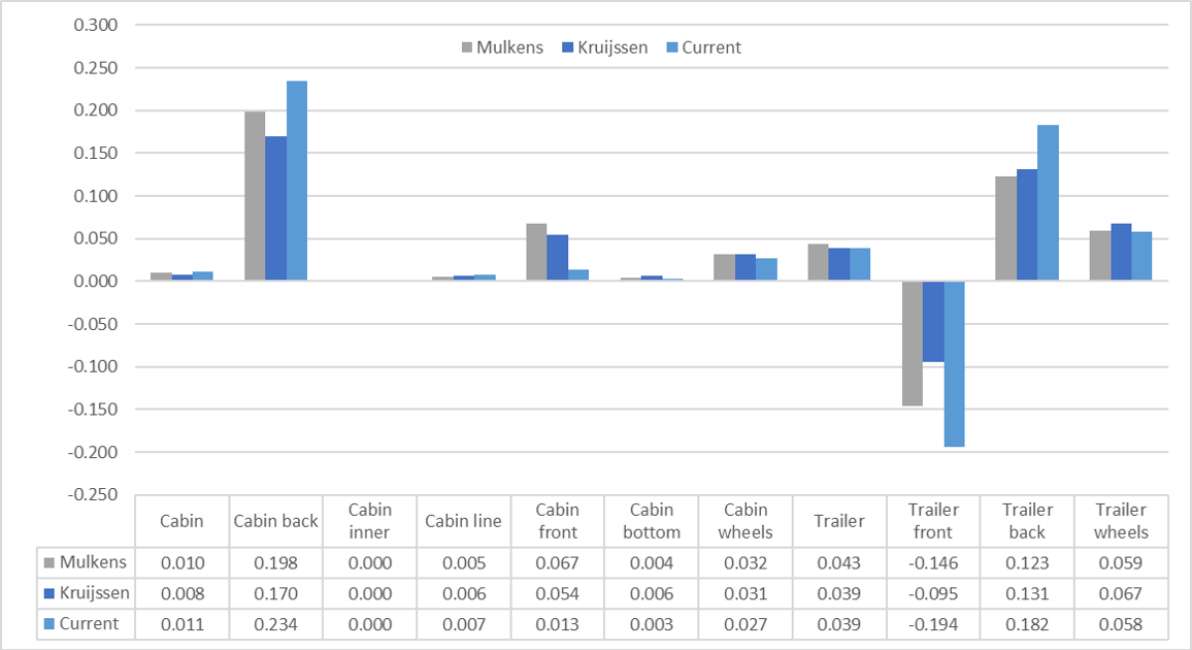

	Cabin	Cabin back	Cabin inner	Cabin line	Cabin front	Cabin bottom	Cabin wheels	Trailer	Trailer front	Trailer back	Trailer wheels
Mulkens	0.010	0.198	0.000	0.005	0.067	0.004	0.032	0.043	-0.146	0.123	0.059
Kruijssen	0.008	0.170	0.000	0.006	0.054	0.006	0.031	0.039	-0.095	0.131	0.067
Current	0.011	0.234	0.000	0.007	0.013	0.003	0.027	0.039	-0.194	0.182	0.058

Figure 3.3: Overview of the drag contributions of different parts of the model found by Mulkens [43], Kruijssen [23] and in the current study

An overview of the drag coefficient for different parts of the model as defined by Kruijssen is shown in figure 3.3. It can be seen that the simulations done here give a way lower drag contribution for the front of the cabin. This is probably caused by higher suction forces over the leading edges. Kruijssen did not record more detailed data on how this drag was distributed, fortunately Mulkens did. Comparing the data of the two simulations shows that the main difference is caused by the bottom edge. Mulkens reports this edge does not experience suction, but has a positive drag contribution of 0.024, while for the simulation performed here a suction force of -0.044 was found.

Large differences can also be seen for the cabin back and trailer front. Where the drag contribution of the cabin is found to be higher in this study, while the suction on the trailer front is stronger as well. This indicates that the pressure in the tractor-trailer gap is lower. This will be further investigated by looking at the flow field in this area. Figure 3.4 shows a top view with pressure and streamlines from Kruijssen and this study. Both figures show two vortices inside the tractor-trailer gap although in the left figure they are much bigger. Besides the difference in streamlines some differences can also be seen in the pressure distribution. The influence of the low pressure areas at the leading edges seem to go further backwards in the RANS results, where the curves of the lower pressure regions reach till behind the tractor-trailer gap. The LBM results on the other hand show curves of lower pressure not further than three quarters of the cabin length and some new low pressure regions round the leading edges of the trailer. On top of that the RANS results show some high pressure regions at the front face of the trailer, one in the middle and at the corners, which are not visible in the LBM results. The ones at the corners indicate flow separation. However, Kruijssen did not observe flow separation in her experiments and concluded that the amount of flow leaving the gap at that point was over-predicted by the CFD method.

A side view of the tractor-trailer gap with streamlines and Z-velocity is shown in figure 3.5. The RANS results of Mulkens show two vortices, one at the top and one at the bottom of the gap. The LBM results only show one big vortex of which the centre is located in the top, but spans across the complete tractor-trailer gap. This results in differences in Z-velocity as well. First, it should be noted that the used scales differ for the two figures. Using the scale used by Mulkens would not show any differences in the LBM results. Therefore it can be concluded that higher vertical velocities are predicted by the RANS method. The distribution is different as well. The LBM results show an upward velocity near the back of the cabin and a downward velocity at the front of the trailer. While the RANS results mainly show a region of upwards velocity in the top of the gap.

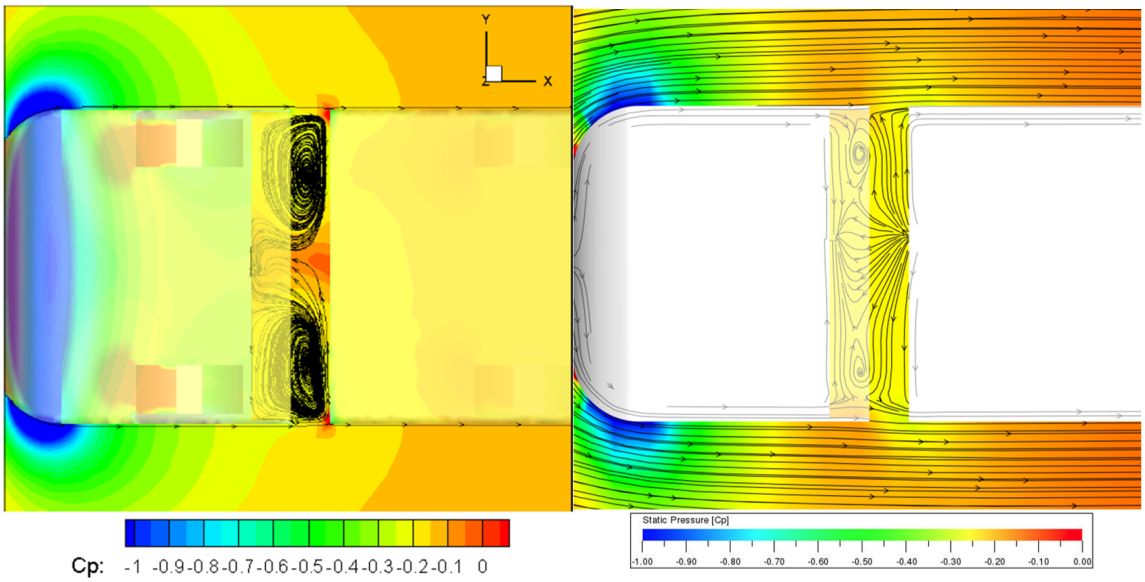

(a) Kruijssen [23] (b) Current

Figure 3.4: Flow field in the tractor-trailer gap in the XY plane

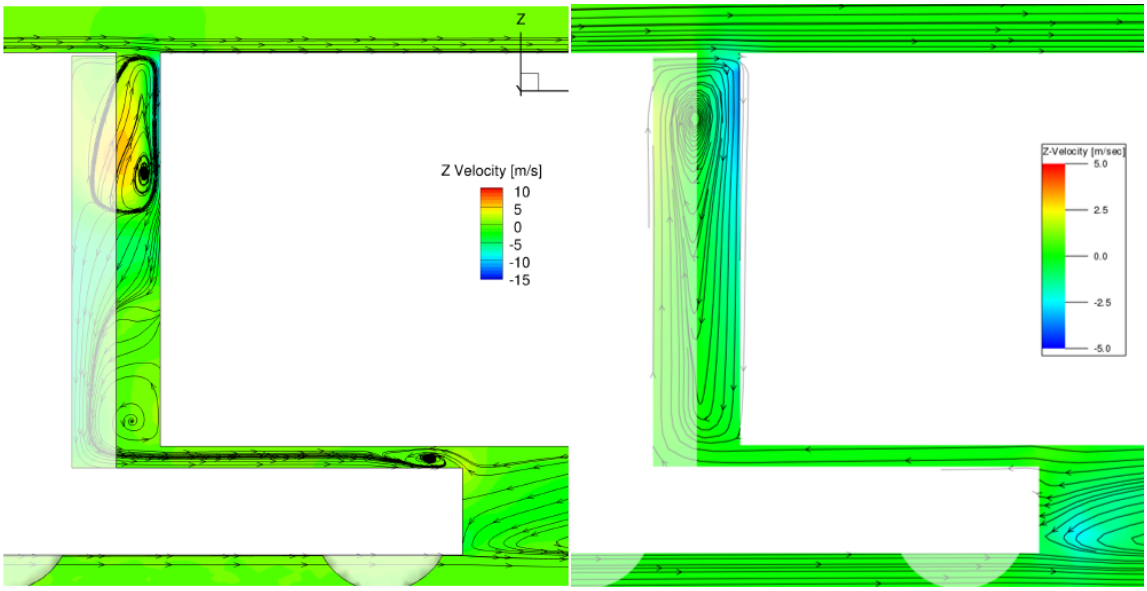

(a) Mulkens [43] (b) Current

Figure 3.5: Flow field in the tractor-trailer gap in the XZ plane in the midplane of the vehicle

Finally, figure 3.3 shows a big difference for the drag generated at the trailer back. Therefore the flow field in the wake was studied more closely as well. Figure 3.7 shows the static pressure distribution and streamlines in the wake in the XZ plane found by Kruijssen and in this study. Some important differences can be seen. First of all the streamlines show a different pattern. Both figures show a vortex originating from the underbody of the trailer. However, the size differs. In the left figure it spans about two thirds of the back of the trailer, while that is completely covered in the right figure. The S-shaped streamlines forming a second vortex on the top can be seen in the right figure as well. Although they do not form a vortex there. Instead they push the streamlines coming from the top of the trailer upwards, while they go slightly downwards in the left figure. It can also be seen that the pressure is lower in the right figure where a large dark blue region is visible. This means that the C_p is around -0.3 there, while the light blue region in the left figure indicates a C_p between -0.2 and -0.25. This explains the higher drag contribution of the trailer back in the simulations of this study.

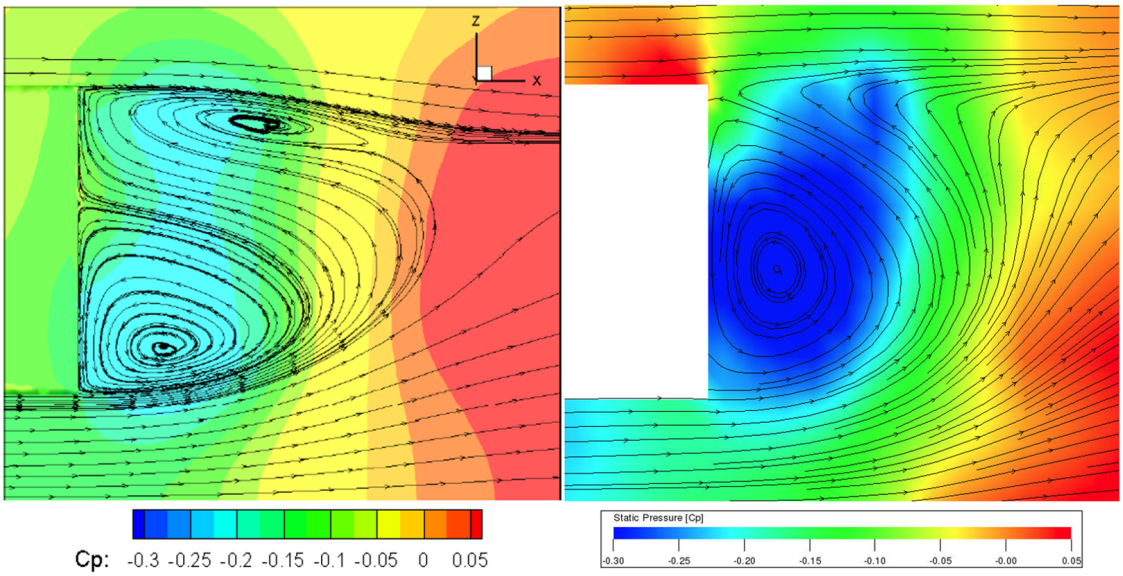

(a) Kruijssen [23] (b) Current

Figure 3.6: Flow field in the wake behind the vehicle in the XZ plane in the midplane of the vehicle

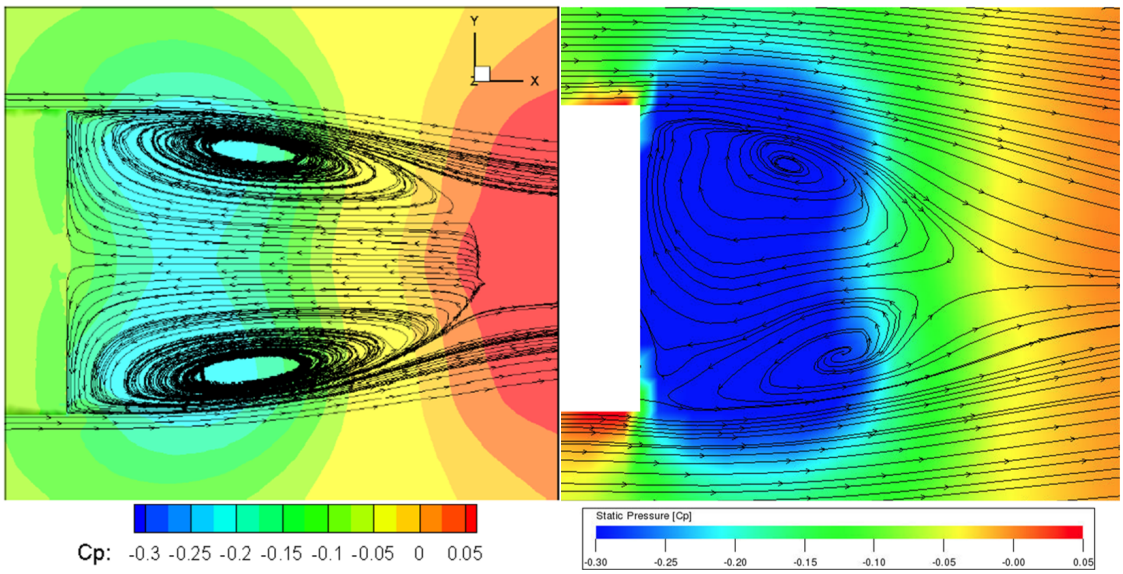

(a) Kruijssen [23] (b) Current

Figure 3.7: Flow field in the wake behind the vehicle in XY plane

The flow field in the XY plane of the trailer wake is shown in figure 3.7. Here again a lower pressure is found in the right figure. The streamlines look more similar than in the previous plane. The vortices are more clear in the left figure. However, this can probably be explained by the difference between steady and transient simulations. When the transient results are averaged over a longer period of time, the results probably look more like the left figure.

The results discussed above show that some differences between the studies can be identified. This is not surprising since completely different methods were used. It is difficult to draw hard conclusions on what is correct and what is wrong here since both are generally accepted simulation methods, but the flow field was not captured during the experiments. The LBM results are closer to the experimental results, but also those results can contain mistakes and uncertainties, as is shown by the difference in results between Mulkens and Kruijssen, while the experimental setup should have been the same.

4

Isolated vehicle

As discussed before, the leading edge radius and underhood flow will be altered to see how they influence the performance in a platoon. Therefore the influence should first be investigated on isolated vehicles. As discussed in section 2.1.3, three different leading edge radii and three versions of the underhood will be tested. This means that nine runs have been performed on the isolated vehicle, to test all combinations. The total drag and underhood mass flow results can be found in tables 4.1 and 4.2 respectively. In this chapter the results of these simulations will be discussed. First the effect of the leading edge radius will be treated in section 4.1, after that the effect of underhood flow in section 4.2.

Table 4.1: Total drag coefficient of all isolated vehicle runs

Underhood model	Total drag coefficient [-]		
	R135	R270	R540
UH0	0.453	0.445	0.446
UH1	0.456	0.460	0.453
UH2	0.467	0.461	0.472

Table 4.2: Underhood mass flow of all isolated vehicle runs

Underhood model	Underhood mass flow [kg/s]		
	R135	R270	R540
UH0	-	-	-
UH1	2.56	2.57	2.61
UH2	4.83	4.86	4.96

4.1. Effect of leading edge radius

To study the results of the leading edge radius separately, the results of the simulations without underhood flow will be discussed first. The results for the different parts of the front for all three leading edge radii are shown in table 4.3. It can be seen that for a larger radius the drag of the frontal surface is reduced, this is explained by the smaller area of this surface due to the bigger edges. However, due to the larger radius the flow speed over the edges is reduced, resulting in less suction. This effect can be seen in figure 4.1. For R270 and R540 these effects exactly cancel each other out. This corresponds to what was found in literature. As discussed in section 1.2.2 when the flow stays attached at a certain radius, increasing the radius further has very little effect on the drag. However, for the R135 case a drag increase was found. Although the suction over the edges is still a bit higher than for the R270 case, it is not enough to compensate for the increase in frontal surface. However, the level of suction indicates that the flow is still not fully separated. Since this would result in a strong decrease in suction. For the bottom edge a strong increase in suction can be seen, this can be explained by the presence of the moving floor, which helps the flow to stay attached.

The influence of the leading edge radius on the drag of an isolated model was studied before by Gheyssens [16] on the GETS model with roughly the same Reynolds number using RANS simulations. Since the front end of the GETS model is similar to the basic GEM model used here it is interesting to compare the results found it both studies. It has to be noted that the GETS model has a higher ride height compared to the GEM tractor and the frontal area is a bit smaller. Therefore the absolute numbers do not coincide, but the trends can still be compared. Gheyssens found that a model with a radius of 270 mm already experienced an increase in drag compared to the 540 mm case. With a radius of 135 mm the flow was fully separated, except for the bottom edge, resulting in an even stronger drag increase. This indicates that in Gheyssens' simulations the flow already started to separate for the 270 mm case, while this was not the case in this study.

Table 4.3: Drag coefficient for the frontal surface and leading edges of the models without underhood flow

Part	Drag coefficient [-]		
	R135	R270	R540
Frontal surface	0.557	0.525	0.367
LE left	-0.176	-0.174	-0.129
LE right	-0.177	-0.176	-0.131
LE bottom	-0.031	-0.012	0.027
LE top	-0.112	-0.110	-0.083
Total front	0.061	0.052	0.052

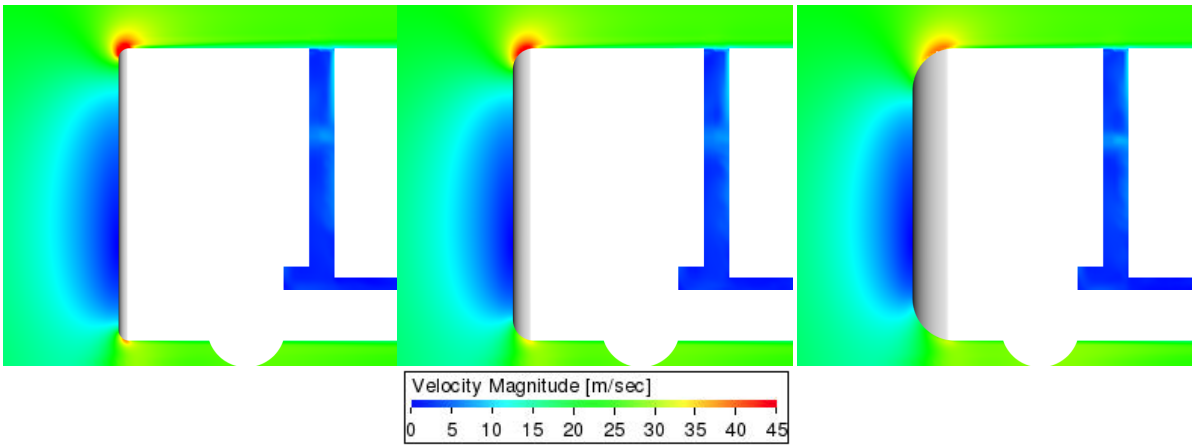

Figure 4.1: Velocity magnitude around the UH0 cases

Gheyssens also noted a decrease in drag for the rear of the model when the radius was decreased. He explained this by the thicker boundary layer that leads to an increased back pressure. To investigate this here, an isosurface of the outer limit of the boundary layer, defined as 99% of the freestream velocity, was created. This surface was exported as a mesh. In this way the exact position can be measured in a CAD program.

First the tractor-trailer gap is analysed. The GETS model does not have one, but the same effect is expected here. Table 4.4 shows a summary of the results found for the tractor-trailer gap for each leading edge radius. Because the boundary layer shows some small variations near the end of the cabin, the boundary layer thickness was measured at approximately 7.5 cm before the end of the top extender near the middle of the vehicle. This is equivalent to 14.3% of the vehicle length measured from the front of the vehicle. It can be seen that a larger leading edge radius gives indeed a thinner boundary layer. As predicted, this results in a lower pressure inside the tractor-trailer gap. The displayed value is the average pressure in the XZ plane in the middle of the vehicle. The lower pressure is beneficial for the front of the trailer, which experiences more suction, but for the rear of the cabin it gives more drag. The area of the back of the cabin is bigger, which means that a lower pressure should lead to an increase in drag for the total tractor-trailer gap, which also includes the inner and rear parts of the cabin extenders. However, since the difference in area and pressure is small this difference is barely noticeable.

Table 4.4: Summary of the results concerning the tractor-trailer gap, where the tractor-trailer gap C_D is the sum of the contributions of the cabin back, trailer front and cabin extenders

	BL thickness [mm]	Tractor-trailer gap C_P [-]	Cabin back C_D [-]	Trailer front C_D [-]	Tractor-trailer gap C_D [-]
R135	93	-0.233	0.181	-0.171	0.010
R270	74	-0.236	0.181	-0.171	0.010
R540	61	-0.254	0.193	-0.183	0.011

When the flow has passed the tractor-trailer gap and forms a new boundary layer on the trailer the case with the smallest leading edge radius still has the thickest boundary layer. This is also translated towards the end of the trailer as can be seen in table 4.5. The shown values for the top were measured at 0.5 meters before

the end of the trailer in the midplane. The side values were measured at the same distance from the rear, three meters above the ground on the left side of the trailer. Although both values for boundary layer thickness are smaller for larger leading edge radii, this does not result in a higher drag contribution for the back of the trailer. Why this is not the case is hard to say. It might be because of the uncertainty of the simulation method. The trailer wake is a highly transient area of flow, therefore simulating with a longer physical runtime might improve the results in this case.

Table 4.5: Summary of the results concerning the back of the trailer

	BL top thickness [mm]	BL side thickness[mm]	Trailer back C_D [-]
R135	290	253	0.163
R270	257	226	0.161
R540	236	208	0.162

Figure 4.2 shows the difference in drag development over the complete vehicle, where the R540 case is used as a baseline. It can be seen that besides the front part and the tractor-trailer gap, the differences are very small. Some differences were observed for rearward facing parts like the back of the trailer and the wheels. However the differences are small and do not show a trend. Since the parts are blunt and facing rearwards the differences can probably be explained by the uncertainty of the simulation method.

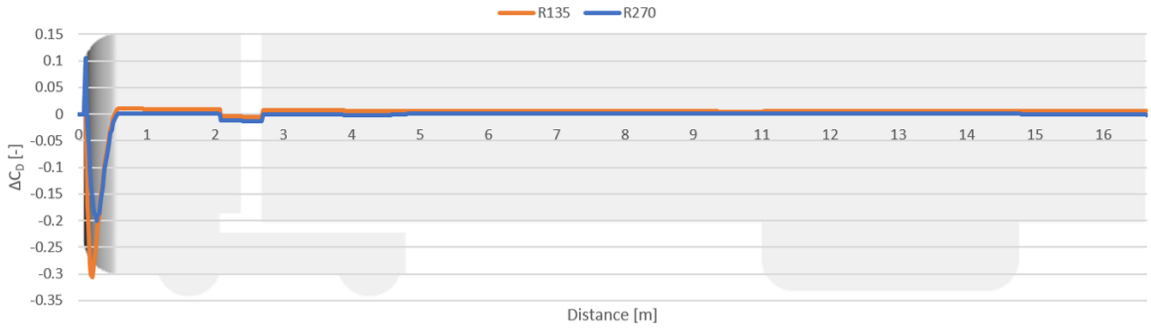

Figure 4.2: Difference in drag development for the basic model with different leading edge radii, R540 is used as baseline

4.2. Effect of underhood flow

Figure 4.3 shows the difference in drag development of the whole vehicle for the R135 models with different underhood versions. UH0, the model without underhood flow is used as the baseline in this figure, UH1 is the version with the half size underhood model and UH2 has the full size model. In this section a closer look will be taken at what causes the differences that are visible in figure 4.3.

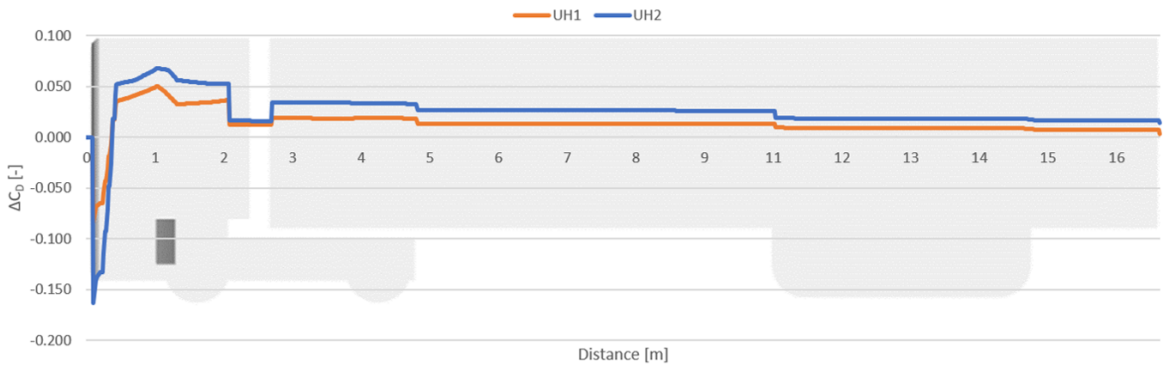

Figure 4.3: Difference in drag development for the R135 model with different underhood models, UH0 is used as baseline

First it will be analysed how the addition of an underhood model changes the observations made for the front of the vehicle in the previous section. Looking at the contributions of the individual parts, shown in table 4.6, the largest difference can be seen for the frontal surface. This makes sense since its area is decreased by the inlet of the underhood model. This explains the strongly decreasing trends in this area in figure 4.3. For the leading edges the suction decreases when the underhood mass flow increases. This can be explained by the fact that because some mass flow is entering the underhood, less mass flow is passing over them. However, the differences are not that big, in the order of a few counts, where a count is defined as a difference in C_D of 0.001. This is not surprising when you look at the total mass flow around the vehicle. The model has a frontal area of 9.7 m^2 with the driving speed and air density used in the simulations this means that roughly 280 kg/s have to be deflected over the leading edges. The flow going through the underhood only represents a small part of that, about 1% in the UH1 case and 2% for UH2. For the top edge which is placed the furthest away from the inlet, the effect is negligible. The effect of having underhood flow is illustrated nicely in figure 4.4 where the difference in static pressure between UH0 and UH1 (left) and UH0 and UH2 (right) is shown for the R135 case. The red areas on the leading edges around the inlet indicate a higher pressure, less suction, for the cases with underhood flow. It can be seen that the increase in pressure is stronger for the model with higher underhood mass flow and that the top parts of left and right edge and the top edge are not influenced.

Table 4.6: Drag coefficient for the frontal surface and leading edges of the models with underhood flow

Part	C_D [-]					
	UH1_R135	UH1_R270	UH1_R540	UH2_R135	UH2_R270	UH2_R540
Frontal surface	0.481	0.453	0.323	0.403	0.373	0.242
LE left	-0.174	-0.172	-0.125	-0.171	-0.169	-0.121
LE right	-0.175	-0.173	-0.127	-0.172	-0.169	-0.123
LE bottom	-0.024	-0.010	0.037	-0.020	-0.005	0.009
LE top	-0.112	-0.110	-0.082	-0.111	-0.110	-0.082
Total front	-0.041	-0.011	-0.008	-0.072	-0.079	-0.075

Table 4.2 already showed that changing the leading edge radius also has an influence on the amount of air entering the underhood. The underhood mass flow slightly increases for larger leading edge radii. It was found for both UH1 and UH2, although it is stronger for UH2. A possible explanation is that due to the lower suction over edges with a larger radius, less flow is sucked towards the sides and flows through the underhood instead. This extra mass flow also gives extra porous medium drag, which is visible as the strongly increasing part immediately behind the leading edges in figure 4.3. The porous medium drag accounts for a significant part of the total drag of the vehicle, around 22% for UH1 cases and around 40% for the UH2 cases. Figure

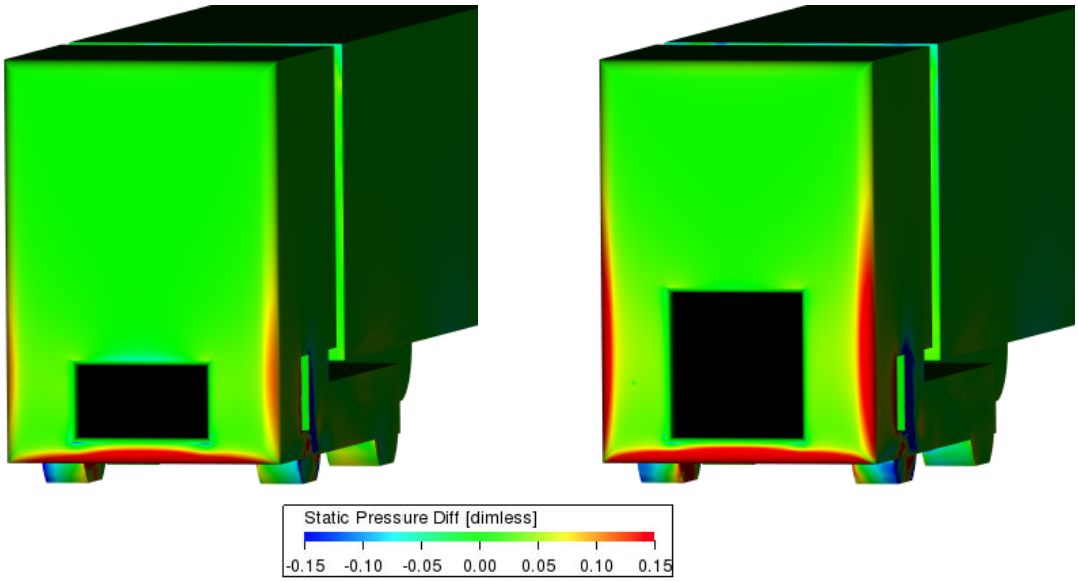

Figure 4.4: Static pressure difference between the models with underhood models compared to the one without for the R135 case

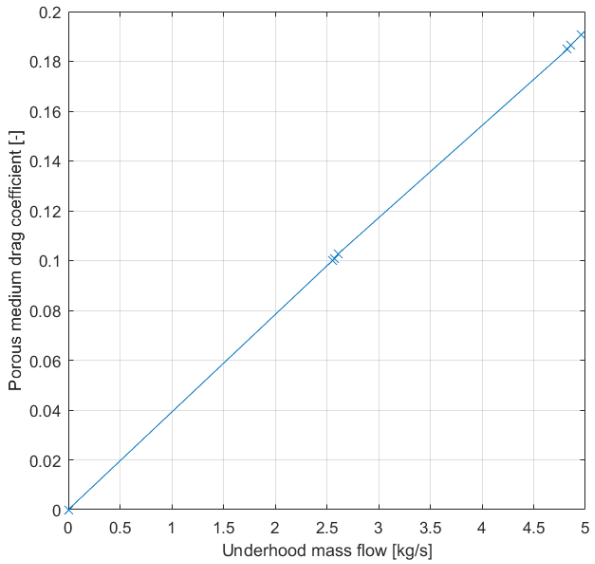

Figure 4.5: Drag coefficient of the porous medium vs. underhood mass flow for all isolated vehicle runs

4.5 shows a plot of the porous medium drag vs. underhood mass flow for all isolated vehicle runs. A linear relationship can be seen in this plot, this is in accordance with the findings of Bäder et al. [28].

Between the strong increase caused by the porous medium and the back of the cabin, figure 4.3 shows some more alterations in drag. These alterations were found to be caused by the underhood model itself. Therefore the underhood components need to be analysed as well. As mentioned before, the walls are defined as frictionless since they do not represent actual geometry found in a real truck. Table 4.7 shows that the influence of each underhood component for all the models that have an underhood. The inlet, being four straight frictionless surfaces placed in flow direction, does not have a drag contribution in all cases. The left and right ducts give a little thrust. This can be explained by the shape of the ducts. Because the inlet is narrower than the outlet, the curvature of the wall towards the rear of the cabin has a higher curvature than the wall towards the front. This gives a higher flow velocity and therefore a lower static pressure on the back wall and thus a bit of thrust. The difference in velocity can also be seen in figure 4.6. The higher thrust generated by in the UH2 cases compared to the UH1 cases can be explained by the increased mass flow through the side ducts. Unfortunately some small differences between left and right can be observed. Since the model is completely symmetric this should not be the case. Therefore this can be seen as a flaw in the simulation method.

Similar behaviour can be seen in the bottom duct, where the curvature of the back wall is also higher than that of the front one. However, a separation region is present on the front wall, counteracting this effect. In the UH1 cases the increased velocity on the back wall is sufficient to generate a little thrust, in the UH2 cases it is not, resulting in some drag. The top duct also shows some difference in results between UH1 and UH2. In the UH2 cases there is only a small separation region immediately after the start of the duct, as can be seen in figure 4.6. In the UH1 case however, the flow does not reattach and large separation regions can be seen. This explains why the upper duct in the UH1 case generates more drag than the one in the UH2 case. The vertical blue stripe in the UH2 picture is caused by the top edge of the outlet. It is not visible in the UH1 picture, because it was taken at a different height, due to the difference in duct shape. The differences between UH1 and UH2 for the bottom and top duct are rather big. Fortunately they cancel each other out for a big part. Therefore the differences in total drag of the underhood are small and do not influence the total drag numbers too much.

In the previous section the influence of the leading edge radius on the pressure inside the tractor-trailer gap was discussed. Adding a underhood model also influences the pressure in this area, as can be seen for the R135 cases in table 4.8. Via the rear outlet, at the bottom of the cabin back, air is directly injected to the tractor-trailer gap, increasing the pressure. More underhood mass flow gives a higher pressure increase, which is of the same order of magnitude as the decrease caused by the boundary layer. Therefore the average C_P in the tractor-trailer gap for the UH0_R135 case is almost the same as for the UH2_R540 case.

Table 4.7: Drag coefficients of the underhood components in isolated vehicle cases

Part	Drag coefficient [-]					
	UH1_R135	UH1_R270	UH1_R540	UH2_R135	UH2_R270	UH2_R540
UH_inlet	0.000	0.000	0.000	0.000	0.000	0.000
UH_left	-0.004	-0.004	-0.004	-0.006	-0.006	-0.006
UH_right	-0.003	-0.003	-0.004	-0.005	-0.005	-0.006
UH_bottom	-0.000	-0.001	-0.003	0.011	0.009	0.005
UH_top	0.009	0.010	0.010	0.002	0.002	0.002
UH_total	0.002	0.002	-0.000	0.002	0.000	-0.004

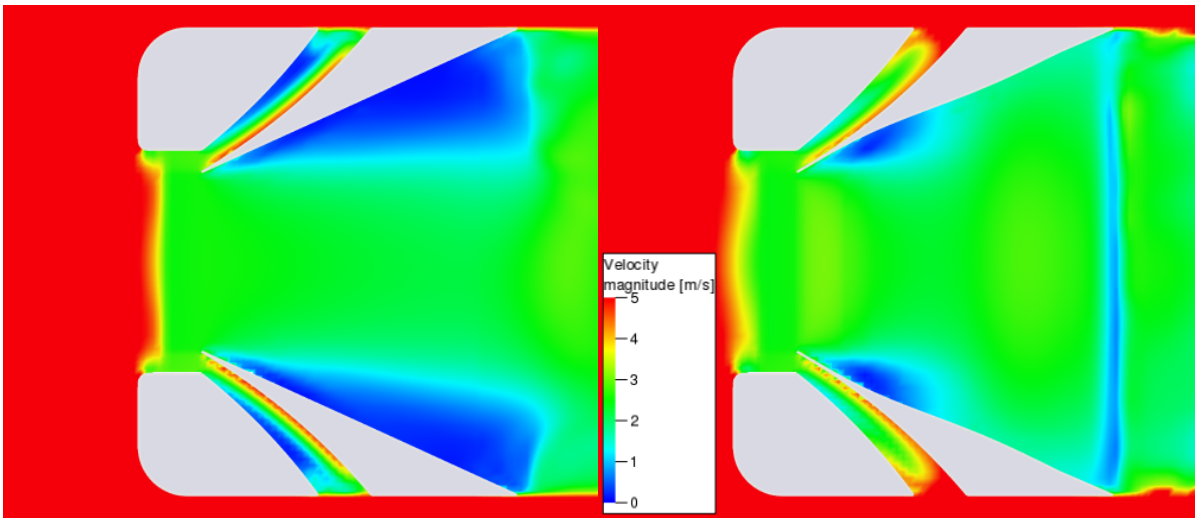

(a) UH1_R270 (b) UH2_R270

Figure 4.6: Velocity magnitude in the XZ plane, shows large separated flow areas for the UH1 case and only small ones for the UH2 case

For the UH0 case it was observed that this pressure difference hardly influences the total drag, because when the drag increases for the back of the cabin, it decreases for the front of the trailer. Since the area of the back of the cabin is slightly bigger, a pressure decrease increases the drag by a very small amount. However, this relation changes when a underhood model is added. The area of the back of the cabin is reduced by the 30x260 cm outlet, reducing the drag generated by this part. This explains the fact that the total drag of the tractor-trailer gap is converted to a small thrust force for the UH1 and UH2 cases. It also means that the area of the rear of the cabin is now smaller than the front of the trailer, so a pressure decrease now results in a small drag decrease. However, the pressure differences found here were not big enough to see a difference in drag counts.

Table 4.8: Pressure and drag data of the tractor-trailer gap for the three R135 cases

	C_P [-]	Cabin back C_D [-]	Trailer front C_D [-]	Tractor-trailer gap C_D [-]
UH0	-0.234	0.048	-0.171	0.017
UH1	-0.224	0.043	-0.164	-0.001
UH2	-0.207	0.042	-0.153	-0.002

A large portion of the air injected into the tractor-trailer gap through the rear outlet, leaves through the horizontal part of the tractor-trailer gap. Figure 4.3 shows that this reduces the drag generated by the rear of the tractor. This can be explained by the reduced size of the wake as visualised in figure 4.7. The flow passing through the horizontal part of the tractor-trailer gap increases the pressure in wake behind the tractor and thus reduces the drag.

Behind the tractor, the lines in figure 4.3 become rather straight. However, round the trailer wheels it can be seen that the vehicles with underhood generate fewer drag than one without. The X-velocity and streamlines in the underbody area of a UH0 and UH2 case are shown in figure 4.8. The figure shows that

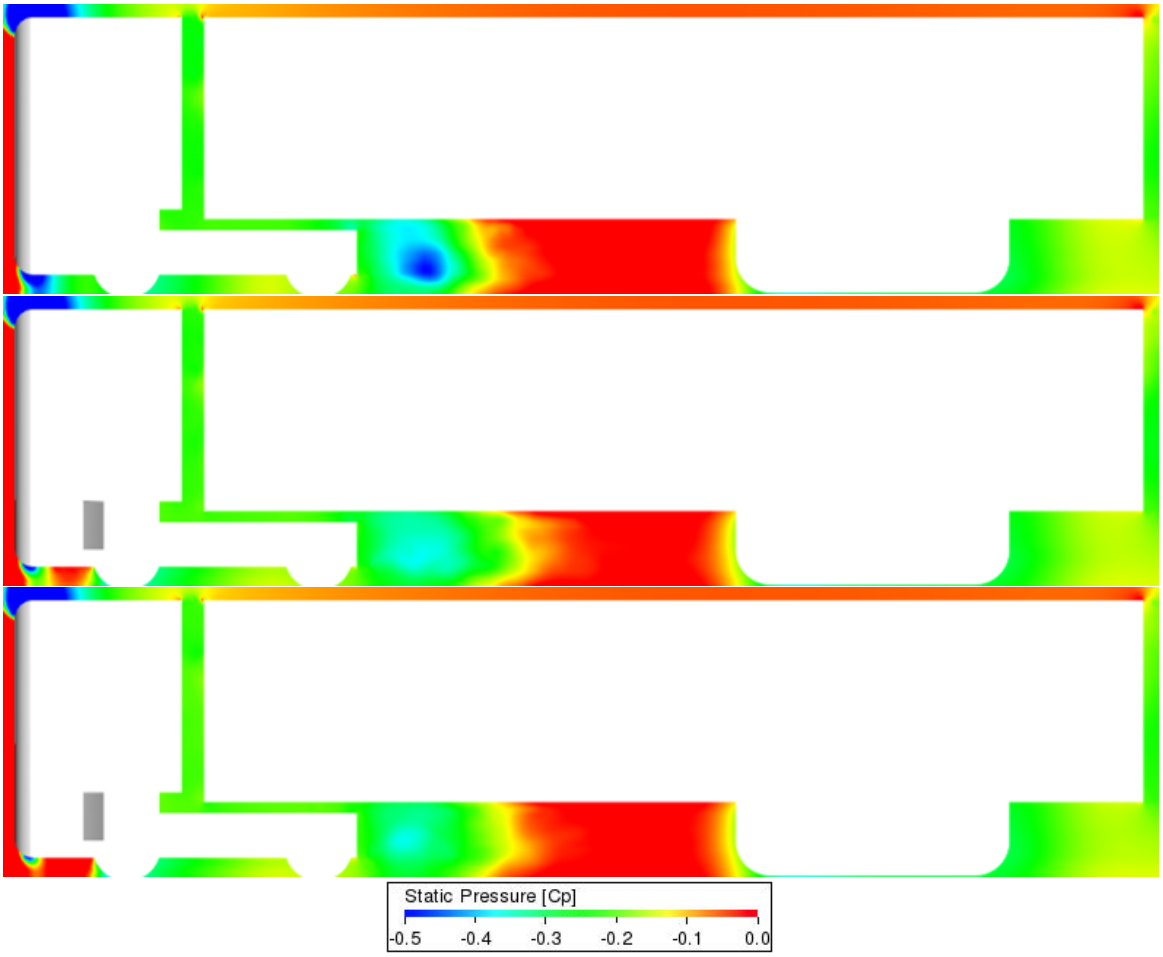

Figure 4.7: Static pressure behind the tractor back for the UH0 (top), UH1 (middle) and UH2 (bottom) cases with a leading edge radius of 270 mm

higher velocities occur in between the two sets of wheels for UH0 than for UH2. It was determined that this difference is also reflected in the mass flow between the wheels. The hypothesis is that this is caused by the differences in the wake behind the lower part of the tractor. For the cases with underhood flow this wake is less intense, but actually bigger in size. Because it is bigger, less high momentum flow from the outside enters the underbody part of the trailer. This means less flow has to pass through the trailer wheels and thus less drag is generated. The fact that low momentum flow from the side ducts of the underhood model are injected here as well might also contribute to this.

For the cases without underhood flow it was already seen that the differences in boundary layer thickness were not translated into differences in drag for the back of the trailer. The difference in underbody mass flow discussed above might also be expected to have an impact. However, table 4.9 shows that no clear trends can be observed. For most models the results are very close, except for UH1_R270 and UH2_R540, which give unexpected high drag values. The difference can also be seen in the pressure distribution over the back of the trailer. However, looking at boundary layer thickness and mass flow in this area did not reveal an explanation for this behaviour. Therefore these variations are probably caused by uncertainty in the simulation method.

Table 4.9: Trailer back and total drag coefficient of all isolated vehicle runs

Underhood	Trailer back C_D [-]			Total C_D [-]		
model	R135	R270	R540	R135	R270	R540
UH0	0.163	0.161	0.162	0.453	0.445	0.446
UH1	0.159	0.169	0.162	0.456	0.460	0.453
UH2	0.161	0.162	0.169	0.467	0.461	0.472

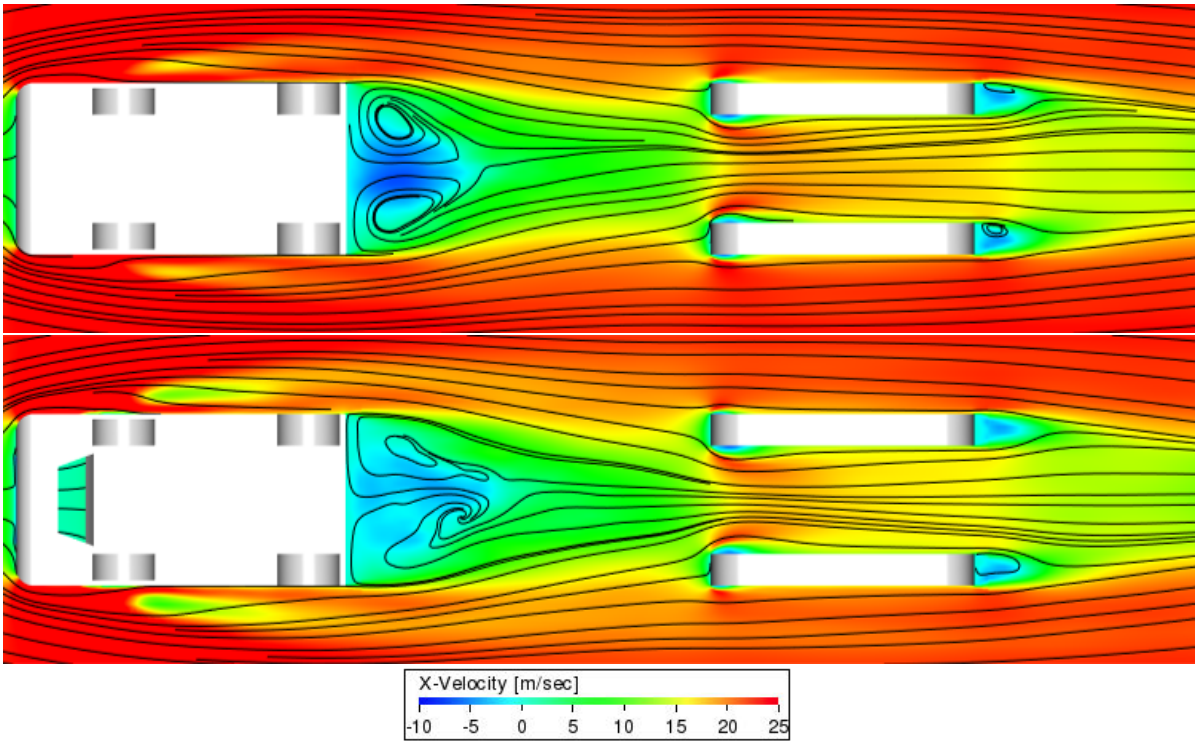

Figure 4.8: X-velocity and streamlines in the XY plane at a height of 0.5 m for the IV_UH0_R270 (top) and IV_UH2_R270 (bottom) case

In general, it can be concluded that more underhood mass flow increases the total drag of the vehicle due to the increased porous medium drag and loss in suction over the leading edges. Despite the beneficial effects for the tractor-trailer gap, back of the tractor and trailer wheels. The models with the smallest leading edge radius have the highest drag values, while they are the same for R270 and R540 models. Looking at the right side of table 4.9 these trends can be identified. However, values for the UH1_R270 and UH2_R540 cases are too high to fit the trend. This can be explained by the high contributions of the rear of the trailer these models have, as discussed above.

5

Platoon

After investigating the effect of changing the leading edge radius and underhood model on an isolated vehicle in the previous chapter, in this chapter the results of the simulations concerning platoons will be shown and discussed. The platoons will be treated in three groups. First the basic platoons will be discussed in section 5.1. For the second group, treated in section 5.2, a boat tail was added to the leading vehicle to see how this influences the aerodynamic behaviour. In the final group of simulations the platoons were placed at a yaw angle. They are discussed in section 5.3. All platoons are composed of two vehicles of which the leading one has no underhood model and a leading edge radius of 540 mm (UH0_R540).

5.1. Basic platoons

In this section 18 different platoons will be treated. Behind the UH0_R540 leading vehicle, another vehicle will be placed at three different distances, with three different underhood models and two different leading edge radii. Since the results of the R270 and R540 models were so similar in the previous chapter it was decided not to use the 270 mm here, to save computational resources. First the effect of inter vehicle distance will be discussed in section 5.1.1, after that the effect of the leading edge radius and underhood flow in sections 5.1.2 and 5.1.3 respectively.

5.1.1. Effect of inter vehicle distance

In this section the results of the most basic platoons, with two UH0_R540 vehicles at three different distances (3.75 m (D23), 7.5 m (D45) and 15 m (D91)), will be discussed. An overview of the total drag coefficient of all vehicles can be found in table 5.1. For the leading vehicle a strong drag reduction was found for the shortest distance, which reduces for longer distances. For the trailing vehicle it is not as straightforward. The largest drag reduction is found for the longest distance and the smallest for the middle distance. This behaviour seems to be similar to that found in literature discussed in section 1.3.1. Due to the large drag reduction of the leading vehicle, the platoon with the shortest inter vehicle distance still gives the lowest total drag.

Table 5.1: Total drag coefficient of the leading vehicle (LV) and trailing vehicle (TV) at different distances compared to the isolated vehicle

	Total C_D [-]			
	IV	D23	D45	D91
LV	0.446	0.310	0.374	0.434
Δ		-0.137	-0.072	-0.013
TV		0.427	0.439	0.384
Δ		-0.019	-0.007	-0.063

To explain the results shown in table 5.1, the drag contribution of different parts of the leading and trailing vehicles and how it changes with inter vehicle distance will be analysed. The drag development of the leading vehicles compared to an isolated vehicle is plotted in figure 5.2. The strong drag reduction of the leading vehicle is explained by the increased pressure in the wake region due to the presence of the other vehicle, as is confirmed by figure 5.1. Therefore it is not surprising that the biggest drag reductions in figure 5.2 are

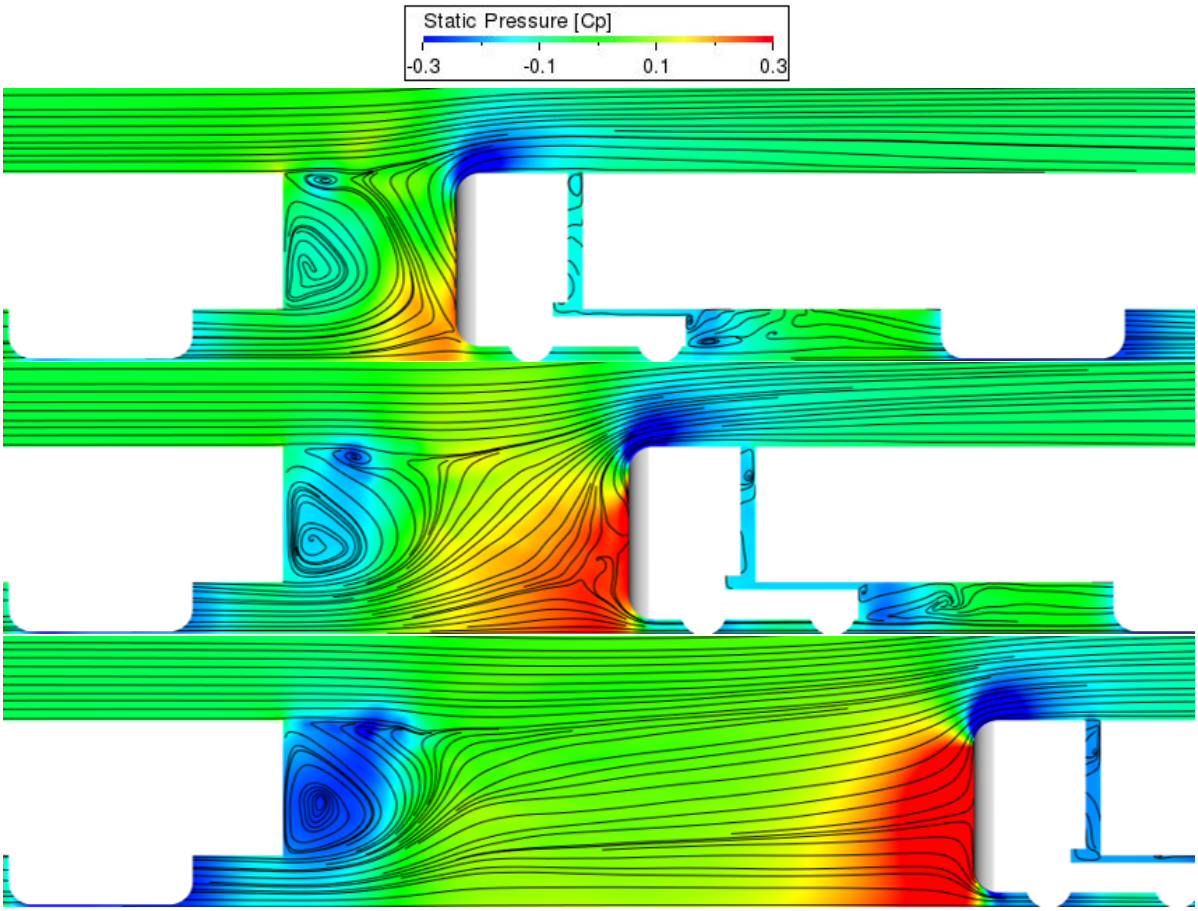

Figure 5.1: Static pressure in the area between the two vehicles for the PL_UH0_R540 cases

found at the back of the trailer and trailer wheels. However, the effect of the increased pressure can still be observed further to the front in the D23 and D45 case. Both cases show a small drag reduction for the back of the tractor. The back of the cabin shows a lower drag as well, while the front of the trailer gives a higher drag, indicating a pressure increase in the tractor-trailer gap. A drag increase can be observed for the front part of the D23 and D45 cases. This behaviour was also found by Gheyssens [16] and Van Tilborg [35] in simulations on platoons of the GETS model.

Figure 5.2 shows some different trends for the largest inter vehicle distance. When the distance is increased it is expected that the effects of the platoon reduce and the drag values converge back to those found for the isolated vehicle. At the rear of the vehicle this is indeed the case. However, at the front a drag reduction compared to the isolated vehicle was found, as well as a pressure decrease in the tractor-trailer gap. This behaviour was not found in literature and a simple explanation is not available either. The same behaviour was found for simulations at the same distance with other underhood models, making it very unlikely that this is caused by the uncertainty of the simulation method.

Initially a mistake was made in the setup for the R135 platooning cases, which caused the length of the simulation volume not to grow compared to the isolated vehicle case. Therefore the simulation volume only stretched 5.1 vehicle lengths behind the trailing vehicle in the D91 case instead of 7. This is different than the setup described in section 2.3, but still lies within the recommendations of the SAE [51]. To investigate the influence of this, a new simulation was done for the PL_UH0_R135_D91 and PL_UH0_R135_D45 cases with the correct simulation volume. Table 5.2 shows an overview of the results.

For the largest distance it can be seen that the strange drag reduction at the front of the leading vehicle described above only appears in case of the large simulation volume. Besides that large differences can also be seen on rear of the leading vehicle and front of the trailing vehicle. For the D45 case differences can be seen as well, although they are not as big for individual parts. To find an explanation for these differences the difference in static pressure between the same cases with different simulation volumes were visualised.

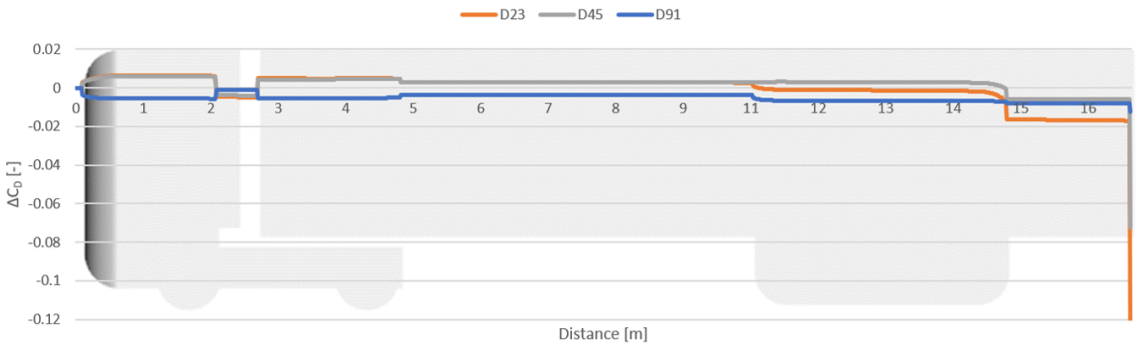

Figure 5.2: Difference in drag development between the leading vehicle at three inter vehicle distances and the isolated vehicle

As can be seen in figure 5.3 this revealed something strange. For the D91 case it can be seen that the static pressure is lower for the simulation with the large volume all around the vehicles. Having a lower static pressure explains the drag reduction at the front and drag increase at the rear of the vehicle. For the D45 case, the same effect is not visible, here the variations are caused by differences in the wakes. The uncertainty in these areas were discussed before. Probably a longer runtime would decrease the difference.

Since all simulation settings besides the size of the simulation volume are identical, the change in static pressure all around the vehicle should not occur. Explaining the observed behaviour is difficult without deep knowledge of the simulation software.

Table 5.2: Summary of the results of the PL_UH0_R135 cases simulated with the wrong (SV1) and correct (SV2) simulation volumes

	C_D [-]					
	D45			D91		
	SV1	SV2	Δ	SV1	SV2	Δ
LV front	0.060	0.058	-0.002	0.059	0.047	-0.012
LV back	0.091	0.085	-0.006	0.147	0.158	+0.011
LV total	0.368	0.360	-0.008	0.434	0.435	+0.001
TV front	0.127	0.125	-0.002	0.065	0.057	-0.008
TV back	0.156	0.153	-0.003	0.154	0.154	0.000
TV total	0.454	0.449	-0.005	0.402	0.394	-0.008

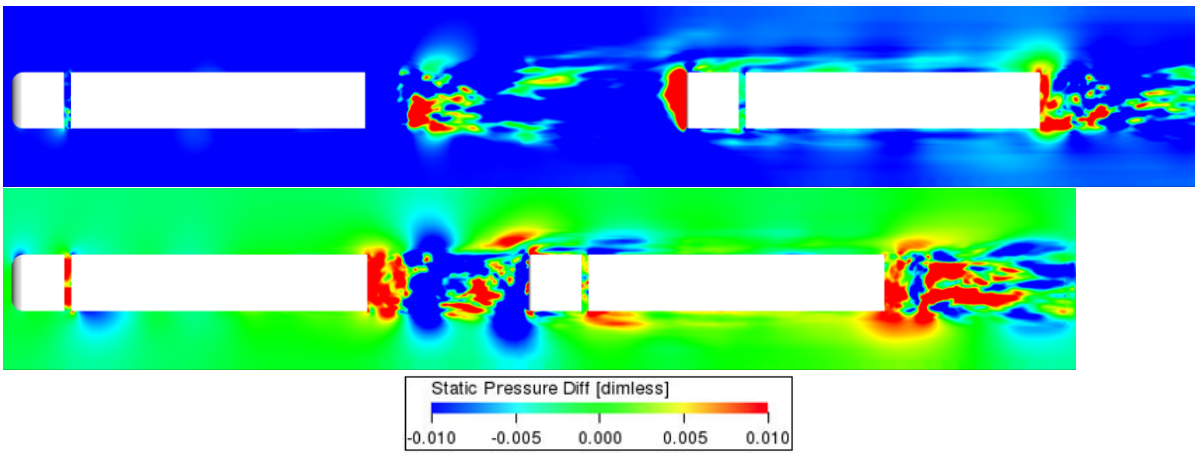

Figure 5.3: Static pressure difference between the same case with small and large simulation volume with an inter vehicle distance of 15 m (top) and 7.5 m (bottom)

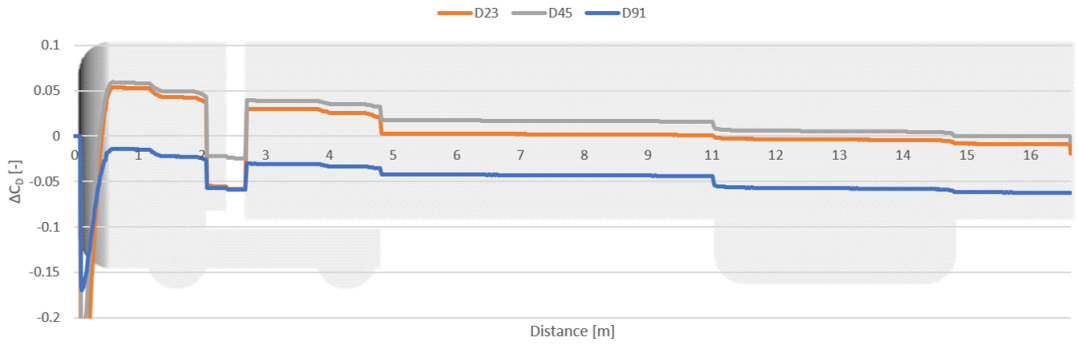

Figure 5.4: Difference in drag development between the trailing vehicle at three inter vehicle distances and the isolated vehicle

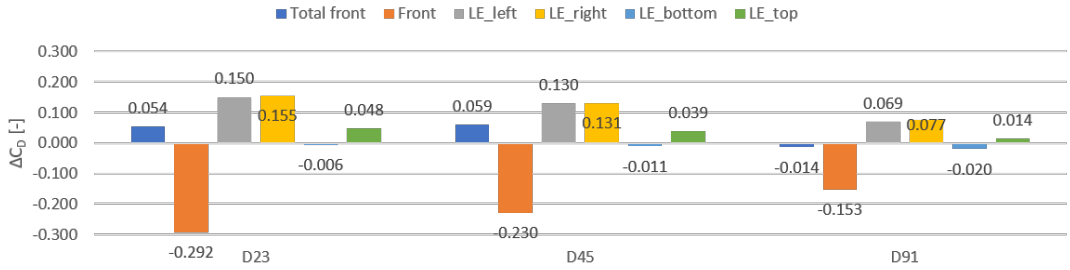

Figure 5.5: Difference in drag contribution of the front parts of the trailing vehicle at different distance compared to the isolated vehicle

The benefit of a platoon for the trailing vehicle is the reduced pressure in the wake of the leading vehicle, reducing its stagnation pressure, as can be seen in figure 5.1. However, a reduced stagnation pressure also reduces the suction over the leading edges. This is the explanation for the non-linear behaviour of the drag of this vehicle. Figure 5.4 shows that the drag contribution of the front stagnation area strongly decreases for all distances. However, only for the largest distance this is sufficient to compensate for the loss in suction. Figure 5.5 shows the change in drag contribution of all the front parts compared to the isolated vehicle.

Behind the leading edges the lines in figure 5.4 are steadily decreasing, because basically every part of the vehicle is benefiting from the lower pressure in the platoon. However, two areas require some extra attention. The first one is the tractor-trailer gap. The figure shows that the back of the cabin experiences a strong drag reduction, while the drag of the front of trailer is increased, indicating an increased pressure inside the gap. Since the overall pressure is decreased, this is a surprising result. Measuring the average pressure in the tractor-trailer confirmed that the pressure indeed increases for shorter inter vehicle distances. For the explanation the boundary layer thickness has to be looked at again. In the previous chapter it was found that a thicker boundary layer gives a higher pressure. In the platoon it is hard to define the boundary layer thickness, since the value of the free stream velocity is altered by the wake of the leading vehicle. However, it is safe to say that the velocity around the tractor trailer gap is reduced in the platoon and that this effect is stronger for shorter inter vehicle distances. This explains the increased pressure in the tractor-trailer gap in a platoon.

The other area with remarkable behaviour is the trailer wheels. Where at every other part the effect of the platoon is the strongest in the D23 case and reduces in strength for larger distances, the trailer wheels show the opposite behaviour. In the D91 case the drag of the trailer wheels is reduced by 17 drag counts compared to the isolated vehicle, while this is 14 and 8 counts for the D45 and D23 case respectively. Since the trailer wheels are placed close to the wake, their drag contribution is prone to some uncertainty. However, looking at the data of all platooning runs, also with different leading edge radii and underhood models, showed that the drag reduction of the trailer wheels is either increasing or staying the same when the inter vehicle distance is increased. It was found that the mass flow between the wheels is decreased by roughly the same amount for all three distances compared to the isolated vehicle. This can be explained by two counteracting phenomena. For a smaller inter vehicle distance, the velocity in the underbody is lower, reducing the mass flow. Increasing the inter vehicle distance increases the velocity but also gives regions of lower velocity next to the underbody, as illustrated in figure 5.6. This means less high momentum flow is entering the underbody area from the sides. The areas of lower velocity are probably the result of a further developed wake of the leading vehicle.

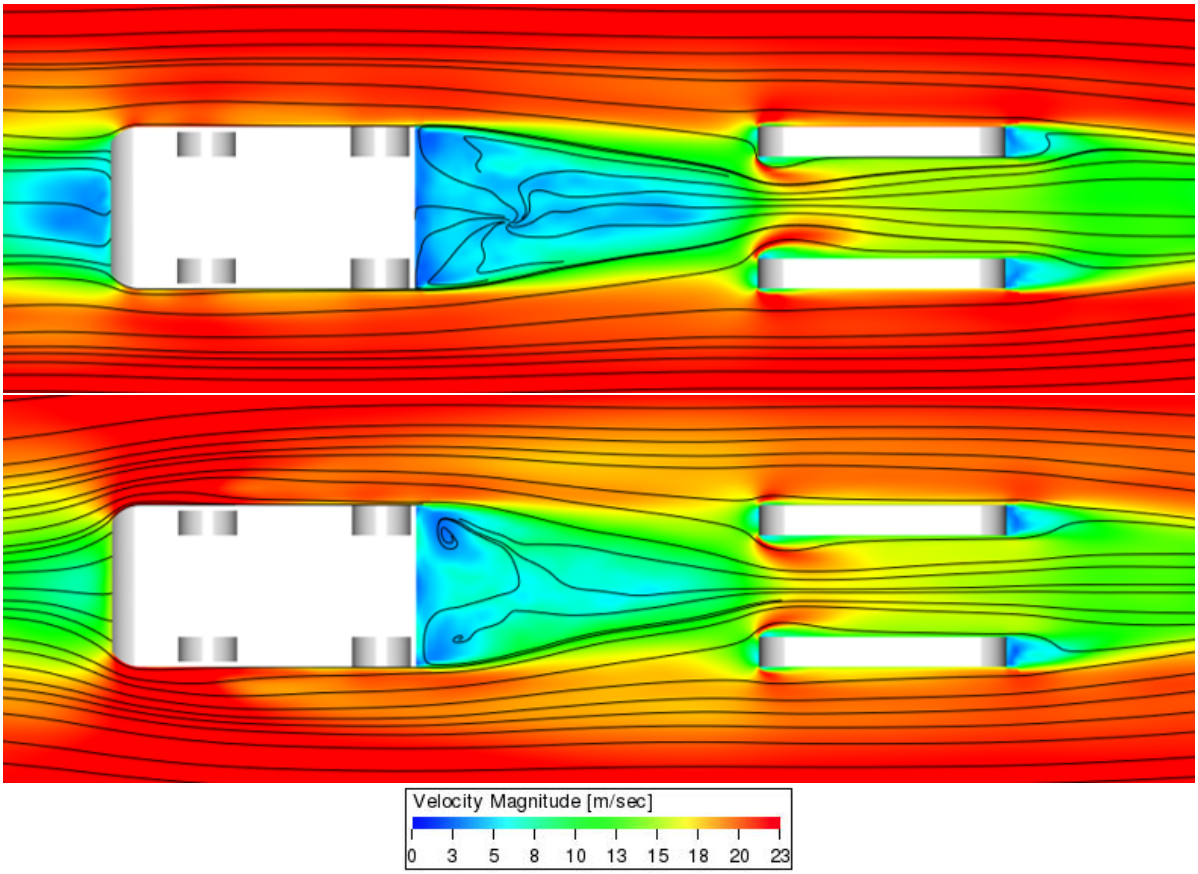

Figure 5.6: Velocity magnitude and streamlines in the XY plane at a height of 0.5 m for the PL_UH0_R540_D23 (top) and PL_UH0_R540_D91 (bottom) case

5.1.2. Effect of leading edge radius

In the previous chapter it was shown that the models with a leading edge radius of 135 mm have a higher drag coefficient. If this is still the case in a platoon will be investigated in this section. As mentioned in the previous section, a mistake was made regarding the length of the simulation volume for the R135 runs. It was decided to use the runs with the large simulation volume here, since it gives a more fair comparison to the R540 cases.

Table 5.3 shows the absolute drag and drag reduction for the leading vehicle of all platoons without underhood flow. It is important to remember that in the R135 cases the leading vehicle is still an UH0_R540. So the observed differences have to be caused by the difference in leading edge radius on the trailing vehicle. It can be seen that for the largest distance the difference is negligible. However, for the other two distances the R135 cases show stronger drag reductions than the R540 ones. Taking a closer look at the drag contributions per part showed that this difference is caused fully by the back of the trailer.

A possible explanation for this behaviour might be that the bigger stagnation area of the R135 models result in a higher pressure in the area between the two vehicles, but that for the D91 case the distance is too large to make a noticeable impact. The static pressure difference in between the two vehicles is shown in figure 5.7 for the D45 case. Due to the transient nature of the wake it is hard to determine if the overall pressure

Table 5.3: Total drag coefficients and drag reductions of the leading vehicles in platoons without underhood flow

	R135		R540	
	C_D [-]	ΔC_D [-]	C_D [-]	ΔC_D [-]
D23	0.303	-0.143	0.310	-0.136
D45	0.360	-0.086	0.374	-0.072
D91	0.435	-0.012	0.434	-0.013

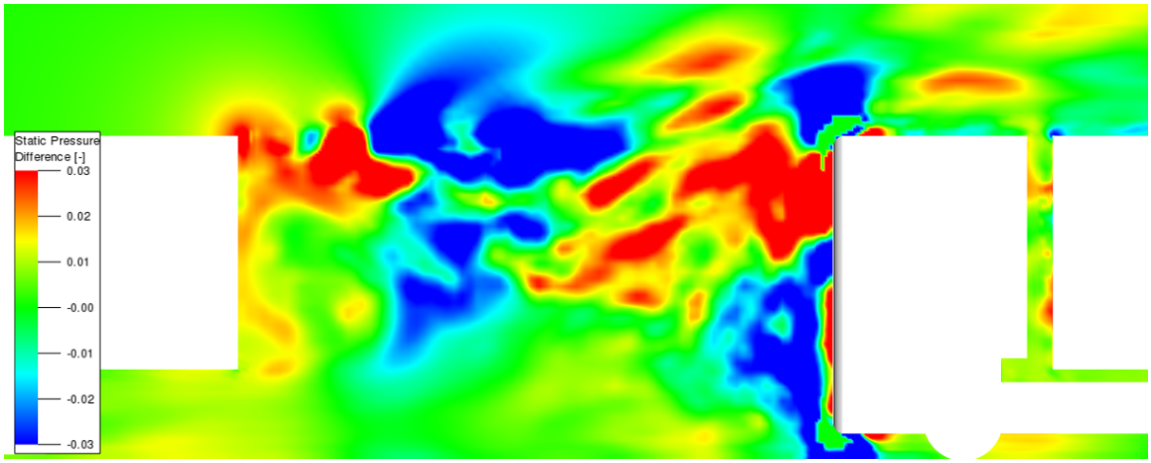

Figure 5.7: Difference in static pressure between the R540 and R135 platoon for an inter vehicle distance of 7.5 m (D45)

has increased, but a clear area of increased pressure can be seen near the back of the trailer. Measuring the average pressure of the area between the two vehicles also showed that the R135 had a slightly higher pressure here.

The total drag and drag reductions of the trailing vehicles can be seen in table 5.4. It can be seen that the vehicles with the highest leading edge radius have both the lowest absolute drag and the highest drag reduction. In the previous section it was already shown that, due to the reduced pressure in the wake, the drag contribution of the frontal stagnation area of the trailing vehicle is strongly decreased. On the other hand the suction over the leading edges is strongly decreased as well. Figure 5.8 shows that the same is true for the R135 cases. For the R540 case it was determined that only for the largest inter vehicle distance the drag of the front of the vehicle was decreased. For the isolated vehicle it was found that a leading edge radius of 135 mm gives more drag on the frontal area, but also more suction over the leading edges. However, the increase in suction is not high enough to compensate the increase in drag, therefore the total drag of the front part is higher than for the R540 case. Comparing figure 5.8 to figure 5.5 shows that the smaller leading edge radius gives a stronger drag reduction for the frontal area, but also a stronger reduction in suction over the leading edges. Another difference can be seen at the bottom edge. In the R540 case, where this edge has a positive drag contribution, the drag is reduced in the platoon. In the R135 case the bottom as has a negative drag contribution, resulting in reduced suction in a platoon.

Table 5.4: Total drag coefficients and drag reductions of the trailing vehicles in platoons without underhood flow

	R135		R540	
	C_D [-]	ΔC_D [-]	C_D [-]	ΔC_D [-]
D23	0.442	-0.011	0.427	-0.019
D45	0.449	-0.005	0.439	-0.014
D91	0.394	-0.059	0.384	-0.063

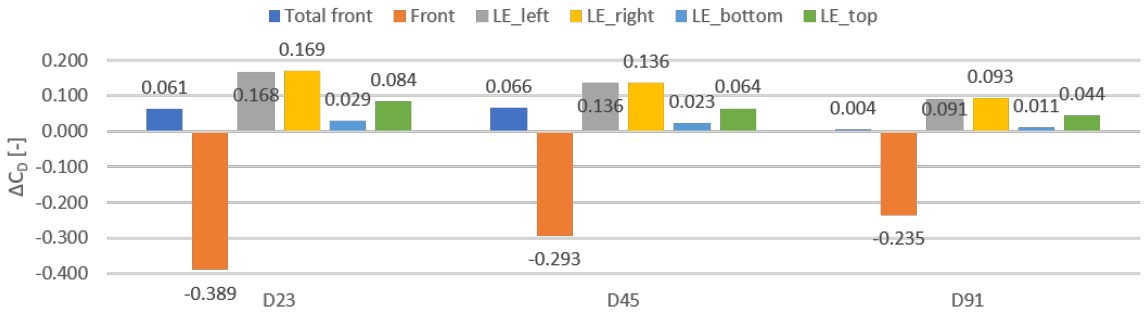

Figure 5.8: Difference in drag contribution of the front parts of the trailing vehicle at different distance compared to the isolated vehicle

Comparing the drag contributions of all parts of the trailing vehicles with different leading edge radii showed, besides the front, only differences in the tractor-trailer gap and at the back of the trailer. It was found that the vehicles with a smaller leading edge radius have higher pressure inside the tractor-trailer gap, which corresponds to the observations made for the isolated vehicle. For the back of the trailer the drag values do not differ too much, in the order of a few counts for the D23 and D45 cases. As discussed before this falls within uncertainty margin of the simulations. However, for the largest distance a difference of 8 counts was found. Where the R540 value is the similar to an isolated vehicle and the R135 value to that of platoons with shorter distances. The results of the platoons with underhood flow show the same trend. Therefore this cannot be explained by uncertainty.

5.1.3. Effect of underhood flow

Having analysed the effect of inter vehicle distance and leading edge radius, It can now be analysed how the observations change when the underhood models are implemented.

For the leading vehicle, which does not have an underhood model in all platoons, only small alterations in total drag coefficient were found in all the runs. The contribution of the front of the vehicle was found to be exactly the same for all platoons with the same inter vehicle distance and leading edge radius of the trailing vehicle. At the rear of the vehicle some small differences were observed, but without a clear trend. Therefore they are probably caused by the uncertainty that has been noticed before for the trailer wake. It can be concluded that adding a underhood model to the trailing vehicle does not effect the leading vehicle.

For the trailing vehicle this is obviously different. Table 5.5 shows the total drag values of the trailing vehicle in all R540 platoons and how they compare to the isolated vehicles. For the isolated vehicle it was found that a higher underhood flow gives a higher drag value. The table shows that in a platoon the models with underhood flow experience a higher drag reduction and that the absolute drag values are closer.

Table 5.5: Total drag coefficient of the trailing vehicle for all R540 platoons

	C_D [-]						
	IV	D23	Δ	D45	Δ	D91	Δ
UH0	0.446	0.427	-0.019	0.439	-0.007	0.384	-0.062
UH1	0.453	0.429	-0.024	0.435	-0.018	0.389	-0.064
UH2	0.472	0.425	-0.047	0.439	-0.033	0.399	-0.073

To see what causes these values to get closer, the drag contributions of different parts will be analysed again. Figure 5.9 shows how the development of the drag reduction compared to the isolated vehicle differs for the three underhood models in a D45 platoon. All three models start with a downward peak because of the reduced stagnation pressure. This peak is the largest for the UH0 model, since this has the largest stagnation area. Behind that the reduction in suction is visible for all three models as well. After that the drag reduction remains constant for the model without underhood flow, but for the ones with underhood flow the lines go down again. This is caused by a reduction in porous medium drag.

The reduced pressure in the platoon reduces the stagnation pressure and therefore the underhood mass flow as well. Figure 5.10 shows how the underhood mass flow is increasing for increasing vehicle distance.

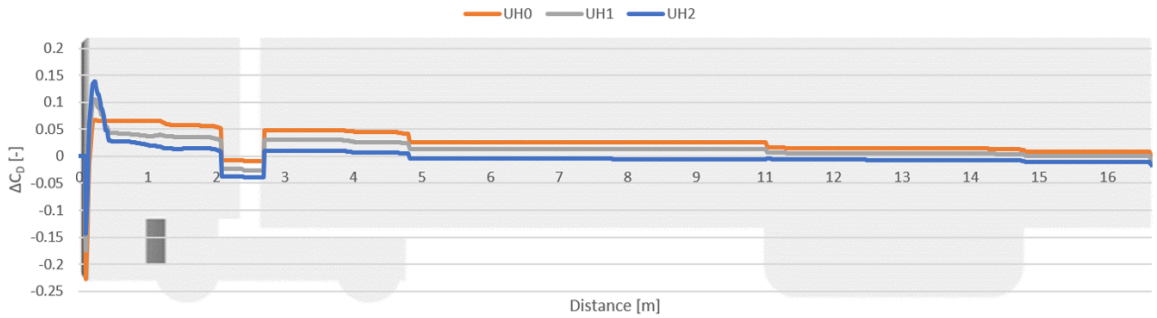

Figure 5.9: Difference in drag development between the R135 trailing vehicles at an inter vehicle distance of 7.5 m with three different underhood models, compared to their respective isolated vehicle

It can be seen that the platoon has a large influence on the mass flow. It was found that for the largest inter vehicle distance around 70% of the mass flow of the isolated vehicle was still available, for the D45 and D23 cases this is around 50% and 35% respectively. The difference caused by the leading edge radius is negligible compared to this effect. The mass flow is reduced by the same percentage for the UH1 and UH2 model, this means that the UH2 model sees the largest absolute reduction. As shown before the porous medium drag is increasing linearly with mass flow. This means that the UH2 model has the strongest porous medium drag reduction because of the platoon. This can also be seen in figure 5.9.

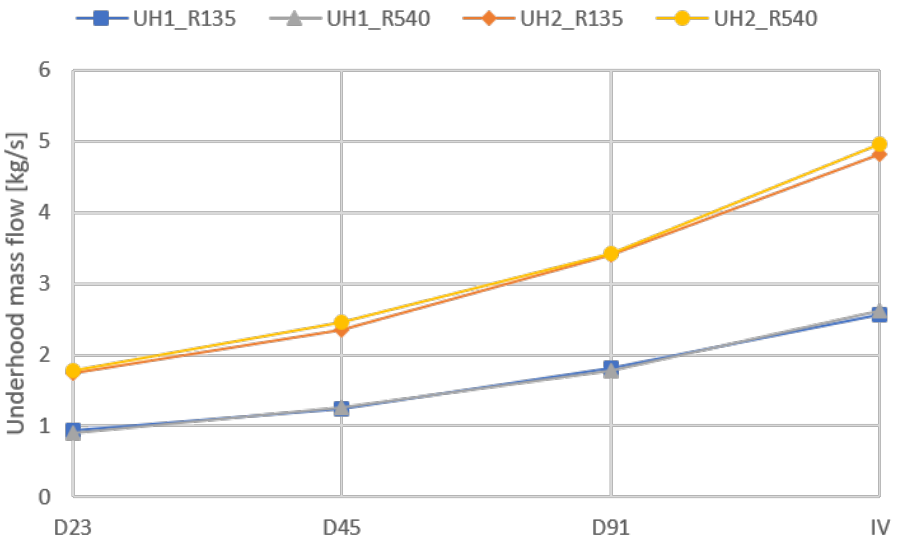

Figure 5.10: Variation in underhood mass flow for all models

Ellis et al. [38] found that around 60% of the mass flow is left for the middle and trailing vehicle in a three vehicle platoon of American style tractor-trailers at an inter vehicle distance of 9 m. For an inter vehicle distance of 5 m this reduced to 40%, as was already shown in figure 1.13. The value found for the shortest distance seem to fit the trend found in this study. However, the mass flow found at a distance of 9 m is higher than to be expected.

Martini [24] found that for a Volvo FH 56% of underhood mass flow of an isolated vehicle was still sufficient to cool the engine in highway conditions. This would mean that already at an inter vehicle distance of 7.5 m fan assistance might be required. However, the required mass flow also depends on the conditions, like air density and temperature and the weight of the vehicle.

Salari and Ortega [37] measured the static pressure in the grille of American style trucks in a platoon as a measure for the underhood mass flow. Figure 5.11 shows a comparison between the values found by Salari and Ortega and in this study. When the inter vehicle distance is increased the data of Salari and Ortega first shows a strong increase in C_P after which it starts increasing more gradually for larger distances. For this study less data points are available, but between the three data points the relation seems to be more linear. It has to be noted that the data of Salari and Ortega is wind averaged, while zero yaw data is used from this study. Comparing the increase in C_P with the increase in mass flow in this study showed that the relationship between the two is not fixed. It was found that when the inter vehicle distance is increased the increase in pressure is stronger than the increase in mass flow.

For the isolated vehicle it was found that an increased underhood mass flow leads to a small reduction of suction over the leading edges. In a platoon the suction is already strongly reduced, as is the underhood mass flow. At an inter vehicle distances of 15 and 7.5 m still some effect is visible, although some random fluctuations caused by the wake seem to be present as well. For the smallest inter vehicle distance, the effect cannot be seen at all.

In the isolated vehicle some differences in drag contribution were found between the two underhood models. Therefore this should be checked in the platoon as well. The contributions of the individual parts of the underhood model and the total in the platoon and isolated vehicle are plotted in figure 5.12. The left and right ducts were found to generate thrust due to the difference in velocity over forward and rearward facing walls. In a platoon this is still the case, but the amount of thrust is reduced because of the reduced mass flow.

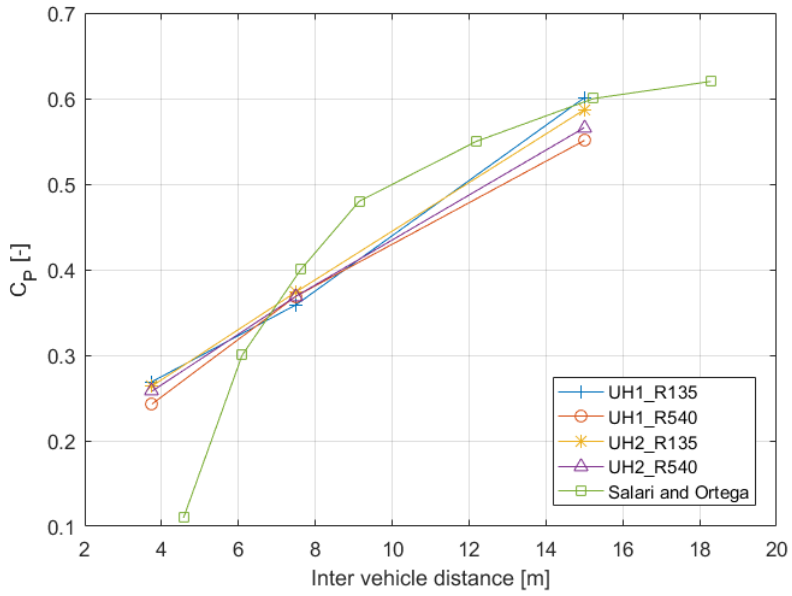

Figure 5.11: Variation of the C_P in the underhood inlet of the trailing vehicle found in this study compared to the data found by Salari and Ortega [37]

For UH1 large regions of separated flow were visible in the top duct of the isolated vehicle, generating drag. In the platoon, this is still the case, but the reduced mass flow reduces the drag as well. The bottom duct shows similar behaviour as the side ducts, as can be seen in the figure. The decrease in thrust of the bottom and side ducts is stronger than the drag reduction of the top duct. Therefore the total drag of the UH1 model is increasing for decreasing inter vehicle distance.

For the UH2 cases, the top duct generates some drag in an isolated vehicle due to two separation bubbles on side walls. In the platoon these regions are still present. The reduced mass flow reduces the drag only slightly. The bottom duct shows some interesting behaviour in the UH2 case. In the isolated vehicle this duct generated quite some drag due to a separation area on the front wall. Figure 5.12 shows that it generates some drag in the platoon as well, but it is reducing for increasing inter vehicle distance. In the D91 case it even gives zero drag. This behaviour can be explained by the average static pressure inside the duct. In the isolated vehicle the C_P is positive, so this gives drag for a forward facing surface and thrust for a rearward facing surface. Since the back wall is much bigger than the front wall of this duct, this results in a drag force. In the platoon a negative C_P is found, giving the opposite effect. The influence of this on the total drag is rather big. Giving an increasing amount of thrust for the total underhood for increasing inter vehicle distance.

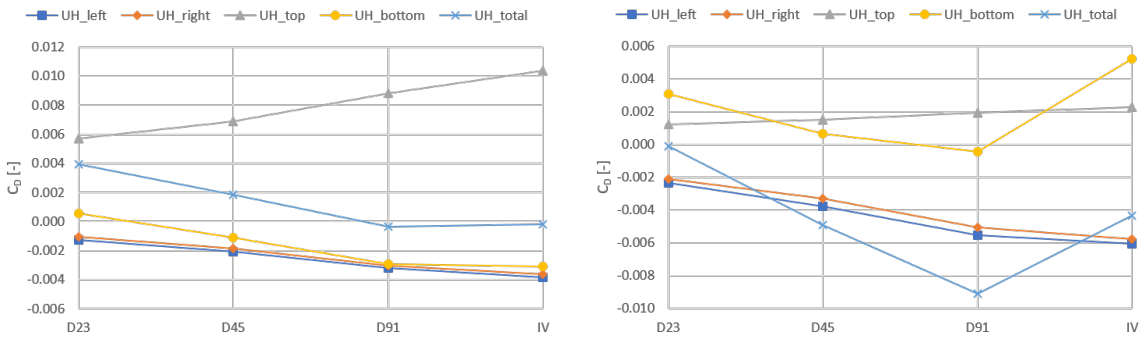

Figure 5.12: Underhood drag contribution of UH1 (left) and UH2 (right) model with a leading edge radius of 540 mm

For the tractor-trailer gap three effects influencing the pressure have already been discussed: a smaller leading edge radius, more underhood flow and a smaller inter vehicle distance all give a higher pressure. All three effects can be found when looking at the average pressure inside the tractor-trailer gap of all the pla-

toons and isolated vehicles. The effect of the inter vehicle distance is the strongest. Therefore the highest pressure is found in the PL_UH2_R135_D23 case. For the cases without underhood flow, a pressure increase gives a drag reduction, while it is the other way round for the cases with underhood flow. For the isolated vehicle the differences were hardly noticeable, in the platoon they are. Although it is still not too big, maximum five counts difference between the isolated vehicle and the platoon with the shortest inter vehicle distance.

The air passing through the top duct mostly passes through the horizontal part of the tractor-trailer gap as well. It was found that this has a beneficial effect on the drag of the tractor back and trailer wheels. The platoon also reduces the drag of these two parts. It was found that in the platoon the models with underhood flow still give the lowest absolute values, but the ones without have the strongest drag reduction. This indicates that the effect is still present in the platoon, but it is reduced in strength.

The analysis of the effect of underhood flow on the trailing vehicle started with the observation that models with underhood flow have the highest drag reduction and the absolute drag values are getting closer together. After looking at the individual parts it can be concluded that this is mainly due to the reduced porous medium drag, caused by the reduced mass flow. The effects of underhood flow on a isolated vehicle, discussed in section 4.2, are still present when the vehicle is placed in a platoon, although their strength is decreased.

5.2. Tail platoons

In this section the results of six additional platoons are discussed. In these platoons a boat tail is attached to the rear of the leading vehicle. The trailing vehicle is placed at the same three distances as used in the previous section. However, only one leading edge radius, R135, and two underhood models, UH0 and UH2, are used. The effect of inter vehicle distance and how this is different than for the basic platoons is discussed in section 5.2.1. The same is done for the effect of underhood flow in section 5.2.2.

5.2.1. Effect of inter vehicle distance

The effect of boat tails has been investigated in earlier studies. It increases the back pressure of the trailer it is mounted on and therefore reduces the drag. Since the trailing vehicle benefits from the lower pressure of the wake of the leading vehicle, this is not necessarily beneficial in a platoon. In earlier studies the effect of adding a boat tail to the leading vehicle was compared to the effect of increasing the inter vehicle distance. Figure 5.13 shows the flow field between the two vehicles when a platoon is applied. Compared to the platoons without tail it can be clearly seen that the pressure close to the back of the trailer is increased. The high pressure areas in front of the trailing vehicle also seem to be bigger. It can also be observed that the large vortex is extended more towards the front end of the trailing vehicle for the D23 case. For cases with a higher inter vehicle distance the stagnation point seems to have moved upwards.

Table 5.6 shows how these changes effect the total drag coefficients of the leading and trailing vehicle, compared to those in the same platoon without a tail. It can be seen that the tail gives a strong drag reduction on the leading vehicle, while its effect on the trailing vehicle is much smaller. For the smallest inter vehicle distance, the drag of the trailing vehicle is increased. However, for the other two distances the tail has a beneficial effect on both vehicles. To investigate the effect of the boat tail in more detail, the drag contribution of individual parts of the vehicle will be analysed again.

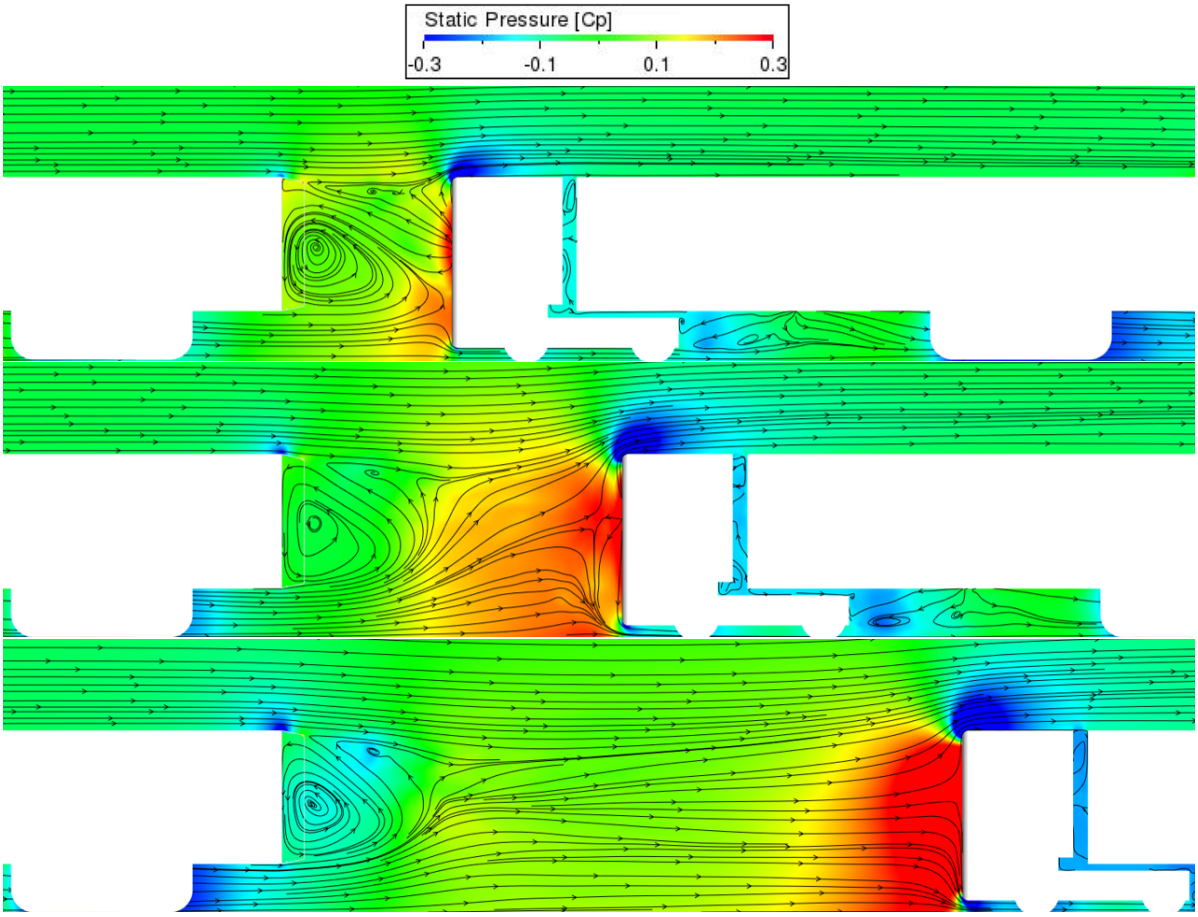

Figure 5.13: Static pressure and streamlines between the vehicles in a platoon with tail, without underhood flow, only the outline of the tail is visualised

Table 5.6: Overview of total drag coefficient of leading and trailing vehicles in platoons with and without tail

	D23		D45		D91	
	LV C_D [-]	TV C_D [-]	LV C_D [-]	TV C_D [-]	LV C_D [-]	LV C_D [-]
No tail	0.303	0.442	0.360	0.449	0.435	0.394
Tail	0.193	0.456	0.287	0.433	0.352	0.384
Δ	-0.110	+0.014	-0.073	-0.016	-0.083	-0.010

For the leading vehicle the differences for the front of the vehicle are negligibly small. This means that all drag reduction can be found at the rear of the vehicle. The drag contribution of the back of the trailer for the platoons with tail is compared to the ones without in table 5.7. It can be seen that for the shortest distance the drag reduction is strongest, the back of the trailer even gives thrust here. In the D45 case, there is approximately zero drag, but the reduction is the smallest. For the largest distance the back of the trailer has a clear positive drag contribution again.

Table 5.7: Drag contribution of the back of the trailer of the leading vehicle with and without tail

	Trailer back C_D [-]		
	D23	D45	D91
No tail	0.043	0.085	0.158
Tail	-0.075	0.001	0.063
Δ	-0.118	-0.084	-0.095

Besides the back of the trailer, the trailer wheels experience a small drag reduction as well, four counts for the smallest inter vehicle distance reducing to one count for the largest. However, most of the difference of drag reduction seen in table 5.6 compared to table 5.7 is caused by the drag contribution of the tail itself. This contribution is rather linearly increasing from nine counts at the shortest inter vehicle distance to fourteen counts at the largest. However, how the drag is distributed over the inner, outer and back side of the tail is changing completely. Figure 5.14 shows the trends of the different parts. It can be seen that the outer part has zero drag at D23 and sees increasing drag for larger distances. The inner part generates quite some drag at D23, which decreases to almost zero drag for D45. At D91 quite some thrust is even generated. The back of the tail shows exactly the opposite behaviour, although it is with smaller numbers.

The behaviour of the outer part can be explained by the pressure distribution over the tail shown in figure 5.15. At the leading edge of the tail, where it is connected to the trailer, a low pressure region can be seen. Towards the trailing edge the pressure is increasing. Since the tail is angled inwards, the outer part is a back facing surface. Therefore a low pressure gives drag and a high pressure thrust. For the shortest distance the

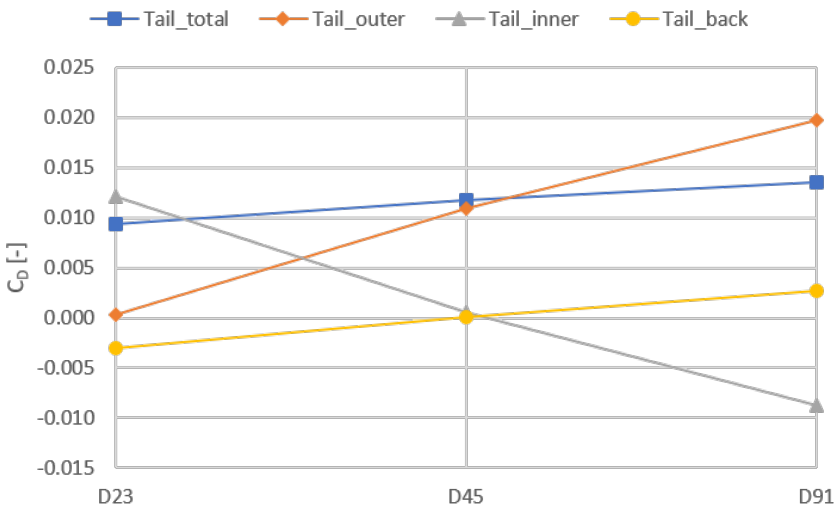

Figure 5.14: Drag contribution of the different parts of the tail at different inter vehicle distances

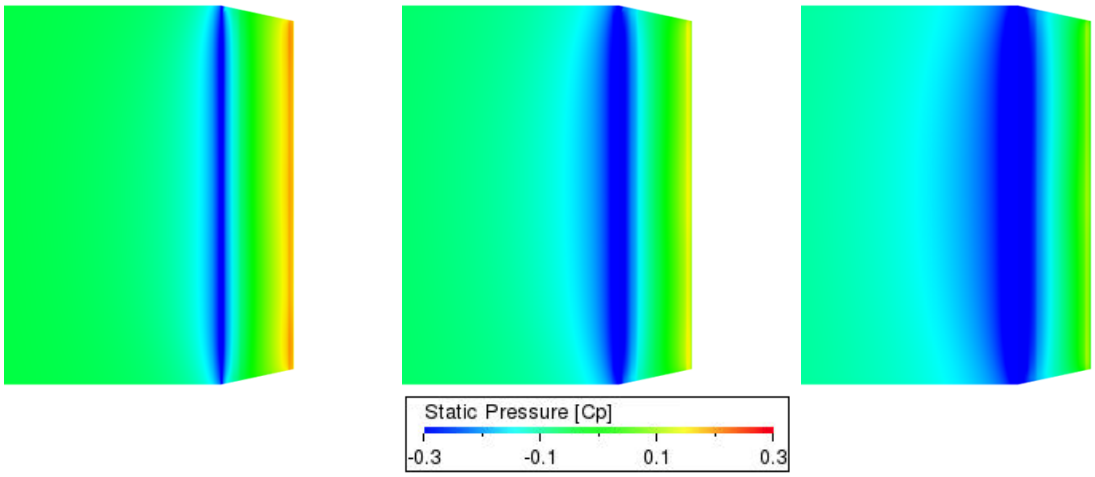

Figure 5.15: Pressure distribution over the top panel of the tail for the D23 (left), D45 (middle) and D91 (right) case

lower pressure region at the leading edge is rather small, while the pressure increases to positive pressures near the trailing edge. These two regions cancel each other out, resulting in practically zero drag. The size of the low pressure region increases for larger inter vehicle distances, while the pressure at the trailing edge reduces as well. Therefore the drag of the outer part of the tail increases.

On the other hand, the inner part of the tail is a forward facing surface. This means that it generates thrust for positive C_P and drag for negative ones. It was found that for the shortest inter vehicle distance a positive C_P is present at the back of the trailer, while this is roughly zero for the D45 case and negative for the D91 case. This explains the behaviour for the inner part seen in figure 5.14. The back of the tail is influenced by the same effect, but is backward facing and has a smaller surface area.

As expected, the trailing vehicle experiences an increase in stagnation pressure on the front surface. Therefore the drag contribution of this part increases, but so does the suction over the leading edges, as can be seen in figure 5.16. This is sufficient to compensate for the drag increase of the front surface when the inter vehicle distance is 7.5 or 15 m. However, it is not for the smallest distance. This is caused by the top edge, which gives a strong drag increase of twelve counts, while the other edges give a suction increase of around four counts. It was already pointed out that for the D23 case, the main vortex of the trailer wake extended all the way up to the trailing vehicle. This might prevent the flow from moving up over the top edge. Figure 5.17 shows the pressure difference between the platoon with and without tail for the D23 and D45 case. It can be seen that the area of increased pressure around the top edge is way bigger for the D23 case. It only shows a tiny area of equal or lower pressure. For the D45 case the pressure is only higher on the frontal surface, around the edge it is equal or lower than for the case without tail.

Figure 5.17 also shows the regions of increased pressure round the tail, except for some green areas directly at the tails leading edges. These are caused by a difference in mesh refinement in those areas. For the cases with tail a layer of smaller cells is applied around the tail surfaces, while these are not present in the cases without tail. Unfortunately the post-processing tool cannot give pressure differences in this case.

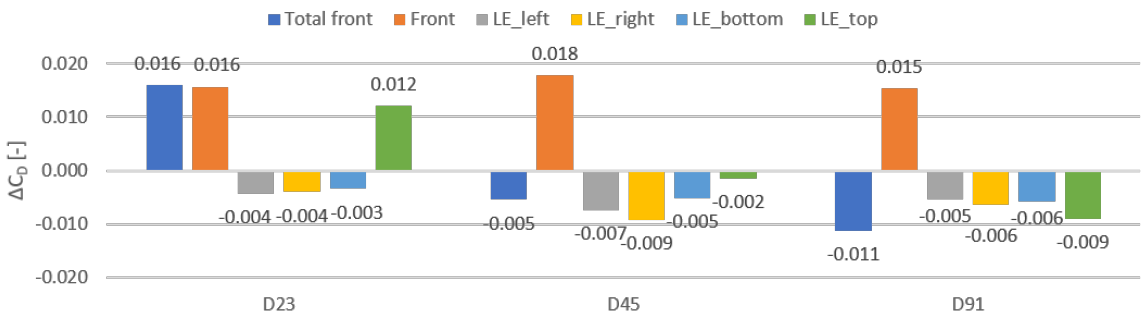

Figure 5.16: Difference in drag contribution for the front parts of the trailing vehicle between the platoons with and without tail

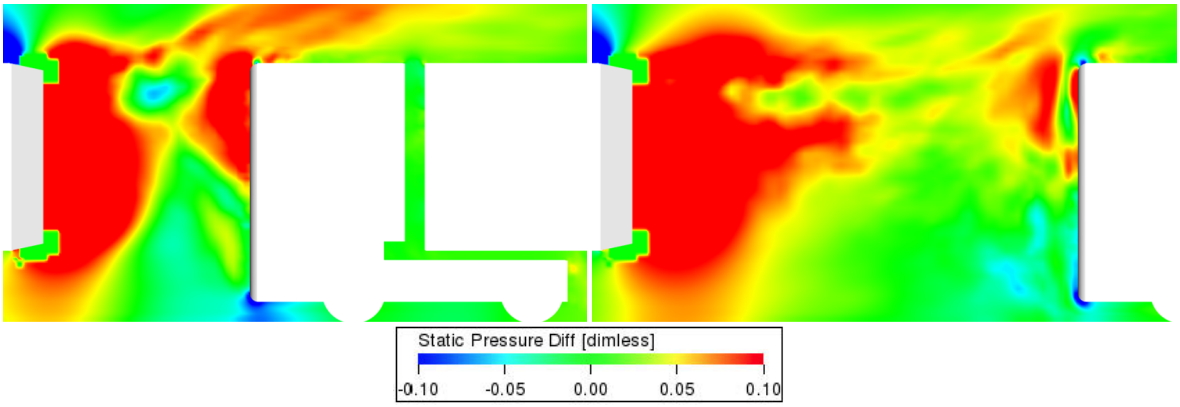

Figure 5.17: Pressure difference between the platoon with and without tail for the D23 (left) and D45 (right) case

Table 5.8 shows that in the platoons with tail, both the wheels of the tractor and those of the trailer have less drag compared to the platoons without tail. This indicates a reduction in mass flow through the underbody region of the tailing vehicle, caused by the tail. This was confirmed by measuring the mass flow between the front wheels of the tractor and the trailer wheels. It was found that between the tractor wheels the mass flow was about 0.5 kg/s lower for the platoons with tail. This might be caused by the higher stagnation point that was found in figure 5.13. However, between the trailer wheels the difference in mass flow is bigger, around 1.5 kg/s. Therefore something more should be going on. An explanation might be found in figure 5.18. It shows that the flow is accelerated over the top part of the trailing vehicle and reduced around the lower part, compared to the case without tail. This means that the air besides the underbody area has less energy and therefore the side inflow to the underbody is reduced.

Since not all boat tails already applied to real trucks use a bottom panel and this might influence the phenomena found above, it was decided to also test two platoons with a tail without bottom panel. Besides removing the panel, the design of the tail remains the same. This means that the side panel still has a twelve degree angle at their bottom edge. This three panel tail was applied to the D23 and D45 case without underhood flow. The flow field between the two vehicles for both cases can be seen in figure 5.19. In the D23 case the flow field is quite different when the bottom plate is removed. For the normal tail the flow field was pretty

Table 5.8: Drag contributions of the tractor and trailer wheels of the trailing vehicle with and without tail applied to the platoon

	D23		D45		D91	
	Tractor wheels	Trailer wheels	Tractor wheels	Trailer wheels	Tractor wheels	Trailer wheels
	C_D [-]	C_D [-]	C_D [-]	C_D [-]	C_D [-]	C_D [-]
No tail	0.016	0.073	0.019	0.070	0.025	0.067
Tail	0.014	0.064	0.017	0.060	0.023	0.064
Δ	-0.002	-0.009	-0.002	-0.010	-0.002	-0.003

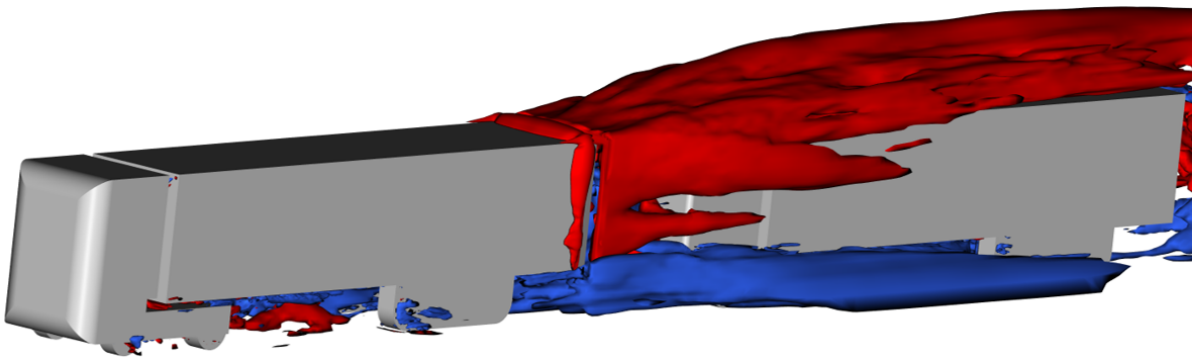

Figure 5.18: Isosurfaces showing the difference in X-velocity around the D23 platoon with tail compared to the platoon without tail, the red surface indicates that the X-velocity is at least 2 m/s higher, the blue one that it is at least 2 m/s lower

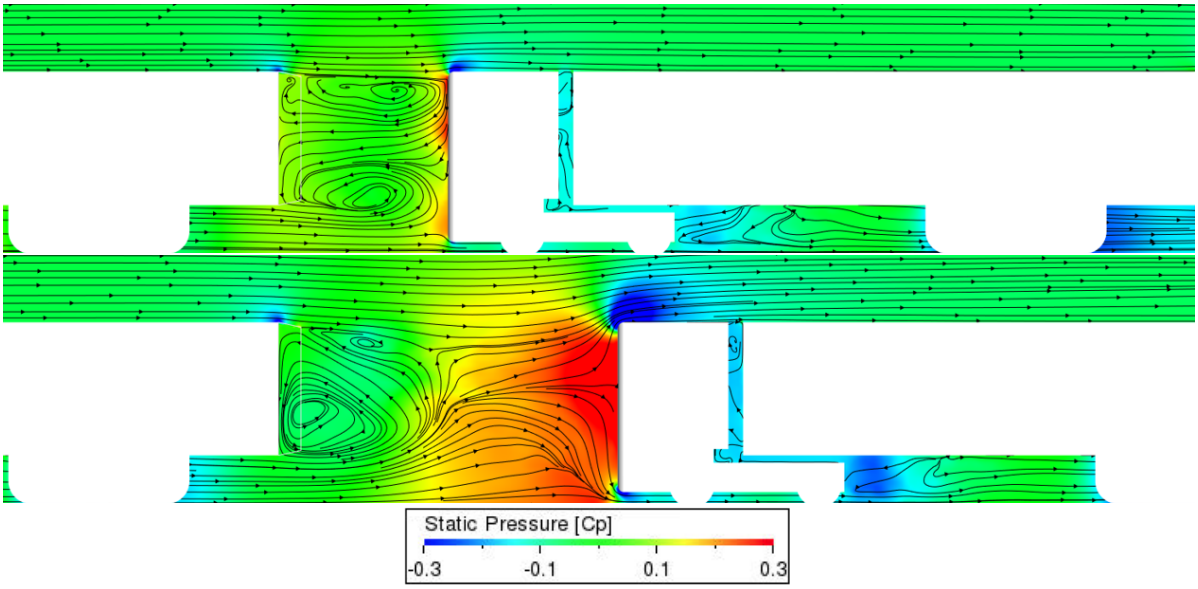

Figure 5.19: Static pressure and streamlines between the vehicles in a platoon with a three panel tail, without underhood flow, only the outline of the tail is visualised

similar to all other wakes, with one large vortex with its centre close to the back of the trailer in the lower part and a small vortex in the upper part. Here two big vortices are found with their centre closer to the trailing vehicle. For the D45 case no dramatic changes in flow field can be seen.

Table 5.9 shows that removing the bottom panel makes the tail less effective, the pressure behind the back of the trailer is lower compared to the four panel tail. However this is compensated by the drag of the trailer wheels which is reduced. The drag reduction of the trailer wheels is caused by an increase in pressure in the area behind them. The kink in the leading edge of the tail gives a pressure reduction, as was shown in figure 5.15. At the top and sides this low pressure does not influence any parts, besides the tail itself. On top of that the drag of the tail itself is reduced slightly because of the lower area. The total drag of the leading vehicle was found to be equal at an inter vehicle distance of 3.75 m. At 7.5 m the drag of the leading vehicle is two counts higher for the three panel tail. However, this is within the margin of uncertainty. Therefore it can be concluded that the bottom panel does not effect the drag of the leading vehicle.

Table 5.9: Drag contributions of the rear parts of the leading vehicle with a three panel tail, compared to other platoons

	Trailer wheels C_D [-]		Tractor back C_D [-]		Tail C_D [-]	
	D23	D45	D23	D45	D23	D45
No tail	0.065	0.074	0.043	0.085	-	-
4 panel tail	0.061	0.072	-0.075	0.001	0.009	0.012
3 panel tail	0.055	0.067	-0.068	0.011	0.009	0.010

The changes in flow field found for the D23 case reduce the pressure on the front surface of the trailing vehicle, as can be seen in figure 5.20. As was found before this reduces the drag contribution of the front surface and reduces the suction over the leading edge. Especially the decrease in suction over the top edge is notable. This can also be seen in figure 5.20 where the low pressure area on top of the vehicle is very small compared those found in all other platoons. For the D45 case the pressure is increased compared to the platoon with a four panel tail. The drag contribution of the front surface is increased, but the higher suction over the leading edges is more than enough to compensate for this. Therefore the total drag of the front part is reduced.

The reason for testing the three panel tail was to look at its influence on the underbody flow. The drag of the tractor wheels does not show a notable difference between the cases with the two different tails. This means that the drag reduction found for the four panel tail is preserved when the bottom panel is removed. For the trailer wheels an even stronger drag reduction was found than for the four panel tail, nine counts more in the D23 case and four more in the D45 case. For the four panel tail is was already noted that the

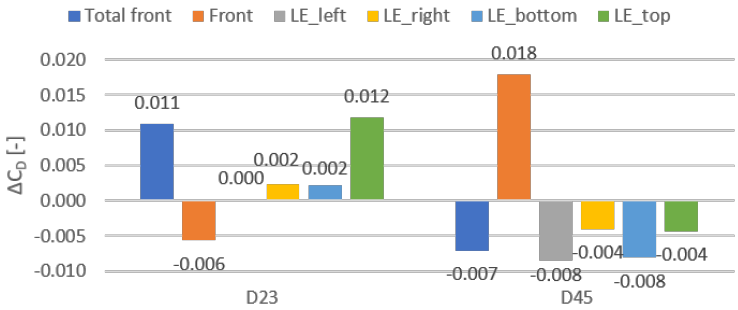

Figure 5.20: Difference in drag contribution for the front parts of the trailing vehicle between the platoons with three and four panel tail

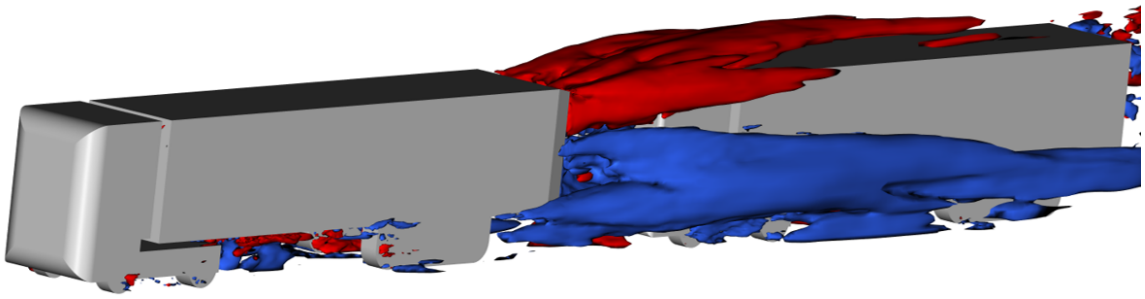

Figure 5.21: Isosurfaces showing the difference in X-velocity around the D23 platoon with a three panel tail compared to the platoon with a four panel tail, the red surface indicates that the X-velocity is at least 2 m/s higher, the blue one that it is at least 2 m/s lower

velocity around the top of the vehicle was increased compared to the cases without tail, while the velocities around the bottom are reduced. Figure 5.21 shows that for the three panel tail this effect is even stronger. So again the energy in the flow entering the underhood has lower momentum and thus the mass flow and drag is reduced.

As was found before, the back of the trailer of the trailing vehicle is subject to variations caused by the uncertainty of the simulation method. However, table 5.10 seems to show that the platoons with tail consistently give a higher drag contribution for the trailer back. By how much is variable, but for all platoons an increase is visible.

Table 5.10: Drag contribution for the back of the trailer of the trailing vehicle

	Trailer back C_D [-]		
	D23	D45	D91
No tail	0.154	0.153	0.154
4 panel tail	0.165	0.155	0.161
3 panel tail	0.159	0.157	-

5.2.2. Effect of underhood flow

After analysing the tail platoons without underhood flow, the ones with will be treated now. The platoons discussed in this section use the UH2 model and only the four panel tail is applied.

For the platoons without tail there seemed to be no influence of the underhood of the trailing vehicle on the leading vehicle. When a tail is applied this does not change. Only some small differences could be observed for the backward facing surface, as has been the case throughout this study. Therefore the uncertainty of the simulation method can be blamed for this.

The total drag coefficient of the trailing vehicles are shown in table 5.11 and compared to those of other platoons. It can be seen that the boat tail gives a larger drag increase for the UH2 model at the shortest inter vehicle distance and a smaller drag decrease for the larger distances. To explain this the drag contributions of the individual parts will be analysed again.

Table 5.11: Total drag coefficient of the trailing vehicle in a platoon with underhood flow and tail compared to other platoons

	C_D [-]		
	D23	D45	D91
UH0	0.442	0.449	0.394
UH0_Tail	0.456	0.433	0.384
Δ	+0.013	-0.015	-0.011
UH2	0.443	0.450	0.402
UH2_Tail	0.465	0.446	0.396
Δ	+0.022	-0.004	-0.006

In the previous section it was shown that a tail accelerates the flow around the top part of the vehicle and slows it down round the lower part. This influences the model with underhood flow in multiple ways. Figure 5.22 shows that the air entering the underhood is coming more from above when a tail is applied to the leading vehicle. This effect is not found at the shortest inter vehicle distance, but can be clearly seen for D45 and D91 case. Table 5.12 shows that this effect also influences the amount of underhood mass flow. For the D23 case the change is negligibly small. But for the other two cases it can be concluded that the tail slightly reduces the mass flow. Ellis et al. [38] also found a reduced mass flow for American style trucks in a platoon when the preceding vehicle had a boat tail. From data presented in their paper it cannot be clearly seen that this effect is reducing for smaller inter vehicle distances. Salari and Ortega [37] also found a lower static pressure in the grille area when a tail is applied. In figure 1.12 the difference seems to be the biggest for small inter vehicle distances. However, it was found before that static pressure and mass flow do not have a fixed relation.

Table 5.12: Underhood mass flow of the platoons with tail, compared to the same platoons without tail

	Underhood mass flow [kg/s]		
	D23	D45	D91
No tail	1.743	2.356	3.398
Tail	1.737	2.211	3.150
Δ	-0.006	-0.145	-0.248

The main effect of a boat tail is the increased pressure between the two vehicles. This increases the drag of the frontal area of the trailing vehicle. Implementing an underhood model decreases the size of this area, due to the cutout for the inlet. Therefore you would expect the drag contribution of the frontal surface to increase less for the UH2 model. However, the data in table 5.13 shows the opposite, for the D23 and D45 cases, while the drag increase is approximately equal for the D91 case. This behaviour can be explained by the difference in static pressure over the front of the vehicle, as shown for the D45 case in figure 5.23. Due to the accelerated air around the top part of the vehicle the pressure is increased on this part. The lower half of the front area

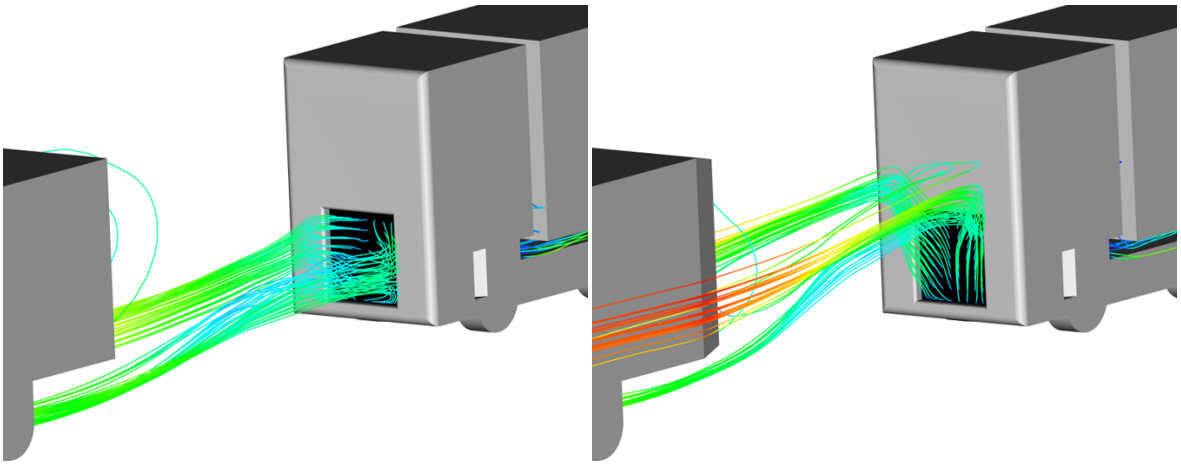

Figure 5.22: Streamlines passing through the underhood area for the D45 platoon without tail (left) and with tail (right)

Table 5.13: Comparison of the drag increase of the frontal area of the trailing vehicle when a tail is applied for the UH0 and UH2 cases

	Frontal area C_D [-]		
	D23	D45	D91
UH0	0.168	0.255	0.319
UH0_Tail	0.184	0.272	0.335
Δ	+0.016	+0.018	+0.015
UH2	0.126	0.185	0.243
UH2_Tail	0.166	0.222	0.256
Δ	+0.039	+0.037	+0.014

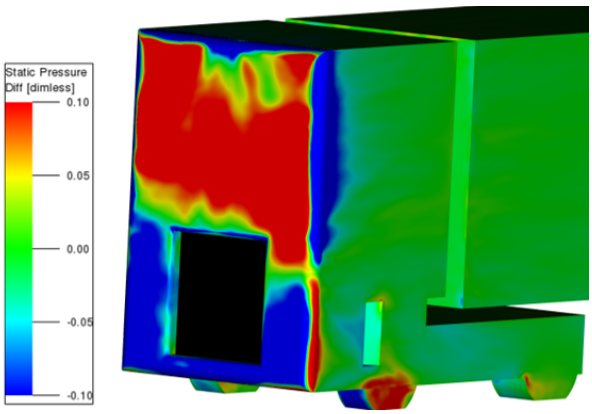

Figure 5.23: Pressure difference between the UH2_R135 model at a inter vehicle distance of 7.5 m in a platoon with and without tail

experiences a lower pressure. However, for the UH2 model a large part of the lower half is occupied by the inlet. Therefore it gives a higher drag increase.

It was found before that the amount of underhood flow has an influence on the suction produced by the leading edges. Because the air that goes through the underhood is not flowing over the edges, the suction is slightly reduced. However, this effect was already small for an isolated vehicle. In a platoon it became hard to notice this effect. This is still the case when a tail is applied.

The lower pressure around the bottom part of the front also results in a lower pressure in the bottom duct of the underhood model. Since the back wall of this duct is way larger than the front one, this results in a decrease in drag. At all distances this decrease was found to be around three counts.

In the previous section it was found that the drag of tractor and trailer wheels is reduced because of the lower velocities around the bottom part of the vehicle. When a underhood model is applied this effect is preserved.

5.3. Yawed platoons

The last group of platoons to be discussed is placed at a yaw angle of six degrees. This has been done for six platoons in which the trailing vehicle is placed at three different distances with two underhood models and always has the same leading edge radius of 135 mm. The effect of changing the inter vehicle distance and how it differs from the zero yaw angle cases is discussed in section 5.3.1. The same is done for the effect of underhood flow in section 5.3.2.

5.3.1. Effect of inter vehicle distance

First, the platoons without underhood flow will be treated. The total drag coefficients of the leading and trailing vehicle, compared to those without yaw, are shown in table 5.14. It can be seen that the drag of all vehicles is increased when a yaw angle is introduced. This increase is much stronger for the trailing vehicle than for the leading vehicle and in both cases it varies for different inter vehicle distances.

Table 5.14: Total drag coefficient of the leading and trailing vehicle in the platoons with yaw angle, compared to the same platoons without yaw angle

	LV C_D [-]			TV C_D [-]		
	D23	D45	D91	D23	D45	D91
0 deg yaw	0.303	0.360	0.435	0.442	0.449	0.394
6 deg yaw	0.318	0.374	0.440	0.495	0.488	0.441
Δ	+0.014	+0.014	+0.005	+0.053	+0.039	+0.047

Figure 5.24 shows the drag development of the leading vehicles in a yawed platoon compared to the same vehicles in a platoon without yaw. The very left of the plot shows that the front of the vehicle actually experiences a drag reduction. In figure 5.25 it can be seen how this is distributed over the different components of the front part. The front surface experiences a small drag decrease, indicating a lower stagnation pressure. This can be explained by the angle this surface now has with the flow, because of this angle the flow does not fully stagnate here anymore. The only part which is completely perpendicular to the flow is now in the left leading edge. The drag contribution is therefore steeply increased. This is also caused by the reduced flow speed around this edge. However, this is compensated by the right edge, which is on the leeward side of the vehicle. Due to the yaw angle the flow speed around this edge is increased and therefore the suction is increased. This is also indicated by the size of the low pressure region around the edges, visible in figure 5.27. It can be seen that this increase is even bigger than the decrease found at the left edge. Finally it can be seen that the influence of the yaw angle on drag of the top and bottom edge is negligible.

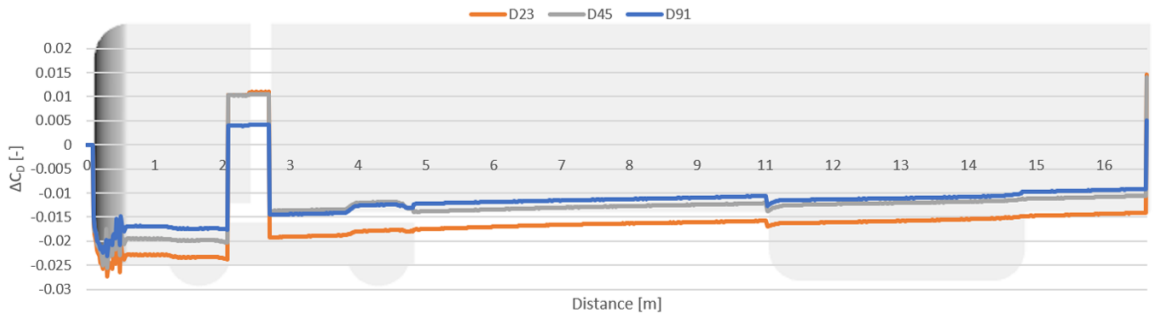

Figure 5.24: Difference in drag development of the leading vehicle of the yawed platoons compared to the same platoons without yaw

Moving further to the right in figure 5.24 the next area of changes is found at the tractor-trailer gap. The drag increase for the back of the cabin and drag decrease of the front of the trailer indicate a reduced pressure in this area. As was found before, for models without underhood flow this results in an increase of the total drag coefficient.

Behind the tractor-trailer gap the lines start to rise slowly but steadily. This is explained by the flow around the trailer surfaces. Figure 5.26 shows how the pressure distribution over the trailer changes when a yaw angle is applied. The most distinctive feature is the low pressure stripe on the top of the trailer, which indicates a

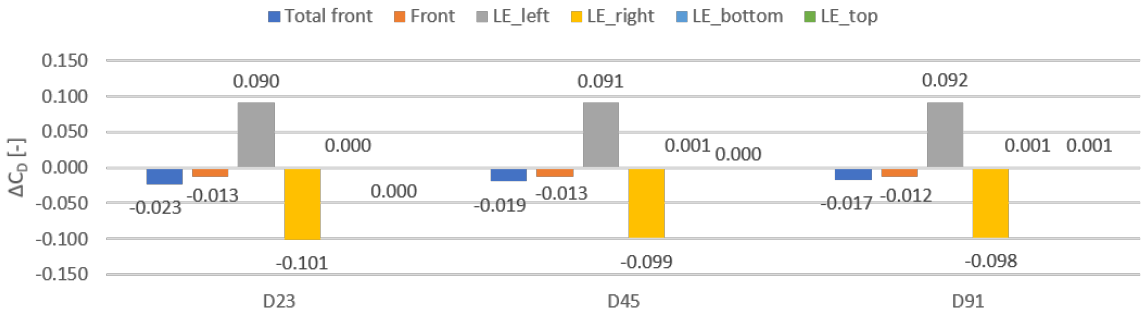

Figure 5.25: Difference in drag contribution of the front parts of the leading vehicle of the yawed platoons compared to the same platoons without yaw

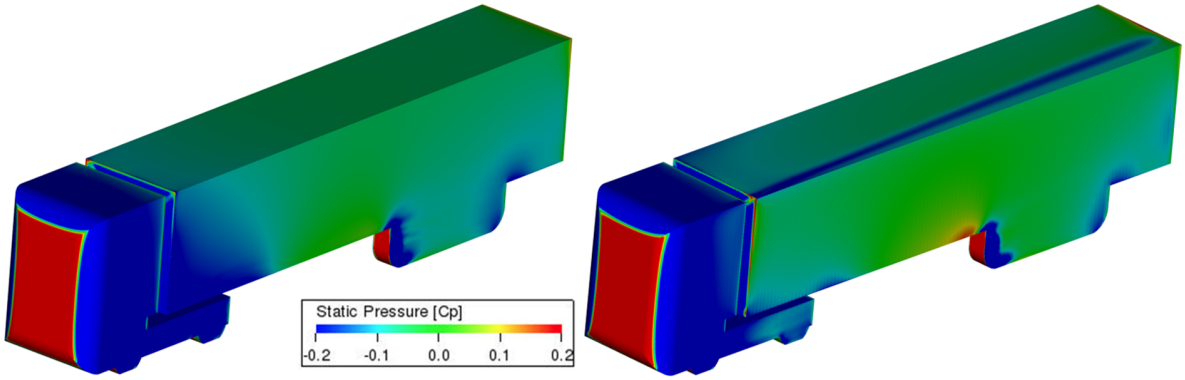

Figure 5.26: Pressure distribution over the leading vehicle in a D91 platoon without yaw (left) and with yaw angle (right)

vortex generated by the left top edge of the trailer. In total the drag differs one or two counts per surface. Given the size of the trailer surfaces it can be concluded that the effect is not that strong.

The very right of figure 5.24 shows that the back of the trailer experiences a strong drag increase. This is confirmed by the numerical values in table 5.15. The table also shows that the effect is strongest for small inter vehicle distances. Figure 5.27 shows that the drag increase can be explained by a lower pressure behind the vehicle.

Table 5.15: Drag contribution of the trailer back of the leading vehicle with and without yaw

	Trailer back C_D [-]		
	D23	D45	D91
0 deg yaw	0.036	0.085	0.158
6 deg yaw	0.065	0.109	0.172
Δ	+0.029	+0.024	+0.014

Besides the reduced pressure near the leading vehicle, figure 5.27 also shows an increased size of the high pressure area in front of the trailing vehicle. This translates to an increased drag contribution for the front part of this vehicle, as can be seen in figure 5.28. How this increase is divided over the different components of the front is shown in figure 5.29. As mentioned before, the stagnation pressure is increased. Therefore the drag of the front surface is increased. This should mean that the suction over the leading edges increases as well. However, as was observed for the leading vehicle, the yaw angle influences this as well. This explains the small reduction in suction seen for the left, windward, edge. The right, leeward, edge does see an increase in suction, which is getting stronger for larger inter vehicle distances. For the leading vehicle the top and bottom edge were both not influenced by the yaw angle. Here they show a notable difference in behaviour. Although the pressure is increased, the bottom edge only experiences a significant increase in suction for the largest inter vehicle distance. On the other hand, the top edge always gives an increase in suction, which is getting less strong for the larger distances.

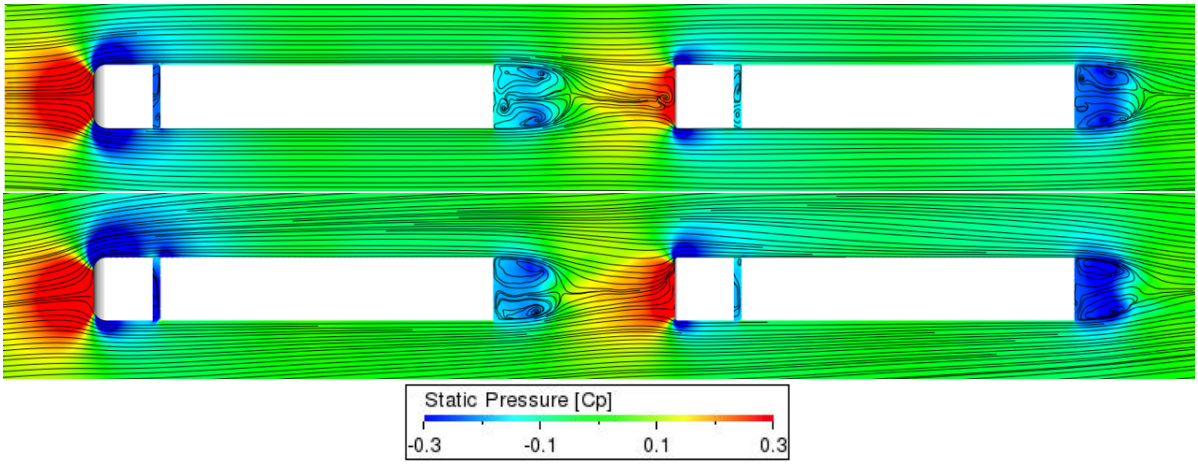

Figure 5.27: Static pressure and streamlines around the UH0_R135 platoon with zero yaw (top) and with six degrees of yaw (bottom)

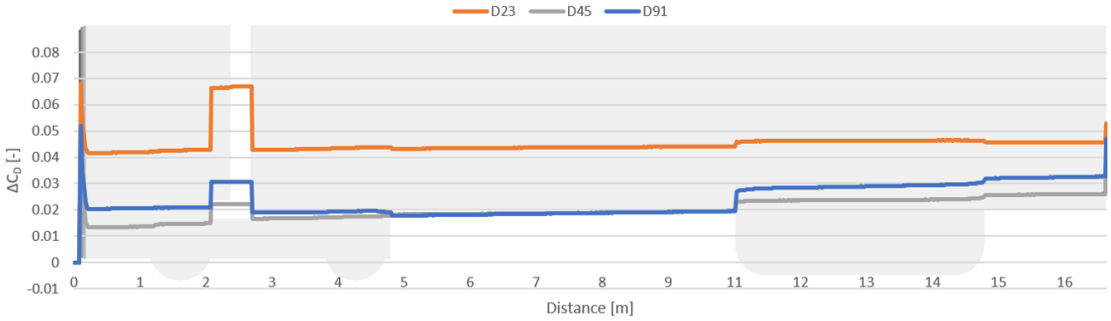

Figure 5.28: Difference in drag development of the trailing vehicle of the yawed platoons compared to the same platoons without yaw

Behind the front part, figure 5.28 shows similar behaviour as for the leading vehicle. The pressure inside the tractor-trailer gap is decreased, mostly for short inter vehicle distances, and the drag is slightly increasing over the length of the trailer. However, the effect is less strong than for the leading vehicle. Finally the back of the trailer experiences an increase in drag. This is again caused by a lower back pressure, which is also visible in figure 5.27. In contrast to what was found for the leading vehicle, this effect is stronger for larger inter vehicle distances. A drag increase can also be seen for the trailer wheels, for the D23 case it is very small, but it increases in strength for the larger distances. In previous studies it was already found that the leading vehicle has a straightening effect on the trailing vehicle. Therefore the effects of yaw angle are reduced. When the inter vehicle distance is increased this influence becomes less strong, so the trailing vehicle experiences more side flow, especially towards its back end. This explains the behaviour seen on the wheels and back of the trailer.

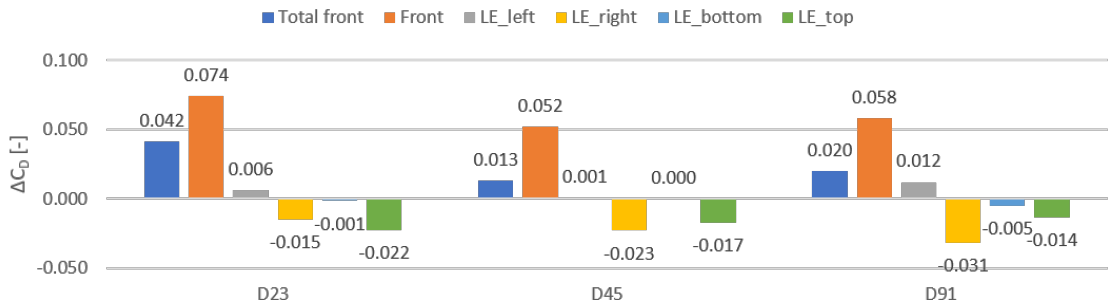

Figure 5.29: Difference in drag contribution of the front parts of the trailing vehicle of the yawed platoons compared to the same platoons without yaw

Due to the yaw angle, the side force acting on the vehicle becomes important as well. The total side force coefficients of both the leading and trailing vehicle can be found in table 5.16. The side force of the leading vehicle is highest for the D45 case. Figure 5.30 shows how the side force develops over the length of the vehicle. It shows that the slope of the development lines is equivalent to the area in y-direction at that point. This can be seen by the almost flat part at the tractor-trailer gap and the strong increase at the start of the trailer wheels. The increase in side force found for the D45 case compared to the other two cases is found at the rear of the vehicle. Further to the front the three cases show almost identical behaviour.

Table 5.16: Total side force coefficient for the leading and trailing vehicle in a platoon with six degree yaw, without underhood flow

	C_S [-]		
	D23	D45	D91
LV	0.867	0.896	0.861
TV	0.299	0.327	0.361

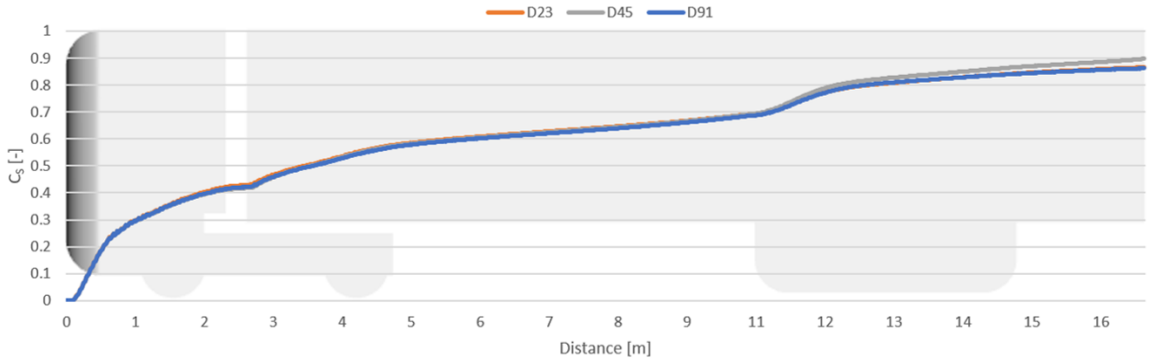

Figure 5.30: Side force development of the leading vehicle of the yawed platoons

The side force of the trailing vehicle is way lower than for the leading vehicle. This can be explained by the straightening effect the leading vehicle has on the flow. It can also be seen that the side force increases for increasing inter vehicle distance, indicating that the straightening is becoming weaker. The development of the side force over the vehicle length is shown in figure 5.31. The D23 and D45 cases show a similar trend for the parts before the trailer wheels. From that point onwards the side force of the D45 starts to increase more rapidly. The D91 case sees a strong increase in side force at very front of the vehicle, after that it follows basically the same trend as the other two cases.

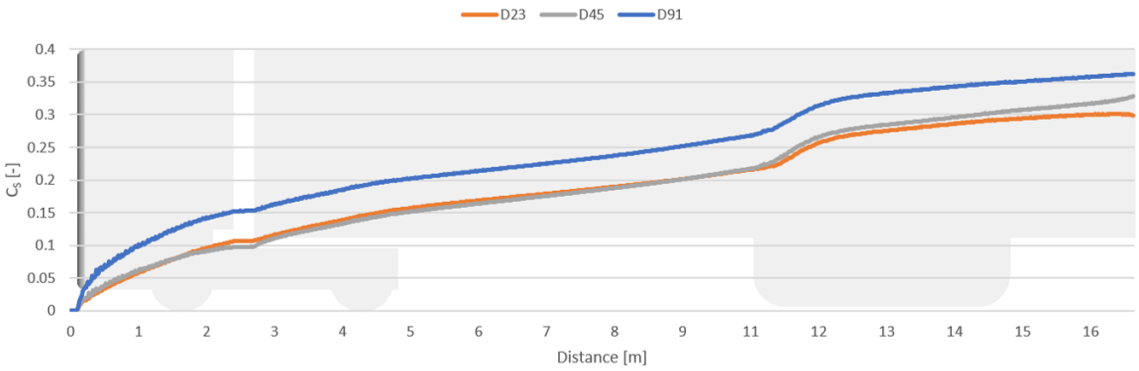

Figure 5.31: Side force development of the trailing vehicle of the yawed platoons, without underhood flow

5.3.2. Effect of underhood flow

After investigating the influence of yaw in the previous section, now it can be analysed how adding underhood flow changes the observations made earlier. The total drag coefficients of the leading and trailing vehicle in the yawed platoons with underhood flow are compared to those for the platoons without underhood flow in table 5.17. The found differences are small, except for the leading vehicle in the D45 case and the trailing vehicle in the D91 case.

Table 5.17: Total drag coefficient of the leading and trailing vehicle in a yawed platoon with underhood flow, compared to the yawed platoons without

	LV C_D [-]			TV C_D [-]		
	D23	D45	D91	D23	D45	D91
UH0	0.318	0.374	0.440	0.495	0.488	0.441
UH2	0.319	0.387	0.437	0.493	0.486	0.454
Δ	+0.001	+0.013	-0.003	-0.002	-0.002	+0.013

For the leading vehicle no influence of the underhood flow is expected, since none has been found so far. However, comparing the drag contributions of the individual components of yawed platoons with and without underhood flow still shows some differences. For all three cases a higher pressure was found in the tractor-trailer gap. For the D23 and D45 cases a small drag increase was found for the trailer wheels. This can be explained by uncertainty. The trailer back saw a drag increase of ten counts for the D45 case.

For the trailing vehicle, effects are expected. The effects found for the trailing vehicle in the basic platoon are also found here. Since the platoons are identical, except for the six degree yaw angle, this is not surprising. To look a bit deeper it will be checked how the strength of these effects is influenced by the yaw angle.

First, the underhood mass flow is treated. The total mass flow for the platoons with and without yaw are compared in table 5.18. The table shows that the yaw angle increases the mass flow, but the effect is reducing for increasing inter vehicle distance. An increased mass flow also results in more porous medium drag, an increase of 12, 8 and 7 counts was found for the D23, D45 and D91 cases respectively.

Table 5.18: Underhood mass flow for the trailing vehicle in yaw configuration

	Underhood mass flow [kg/s]		
	D23	D45	D91
0 deg yaw	1.743	2.356	3.398
6 deg yaw	1.985	2.501	3.517
Δ	+0.242	+0.145	+0.119

It was also found before that the underhood mass flow reduces the suction over the leading edges. This could be seen clearly for the isolated vehicle, but is not that clear in a platoon because of other variations in the same area. This is also the case for the yawed platoons. In general the suction is a bit lower compared to the yawed platoons without underhood flow, but this is not the case for every edge. Compared to the platoons with underhood flow but without yaw it is even harder to see this effect, since the difference in mass flow is relatively small.

Also the drag contributions of the underhood components are influenced by the difference in mass flow. It was also found that due to the yaw angle the mass flow distribution over the different ducts was altered. The mass flow through the left duct stays approximately the same when a yaw angle is applied, while the right duct sees the biggest increase. This can be explained by the angle of the inlet compared to the side inflow. The flow is entering the area between the vehicles from the left. Therefore it has to take a sharp turn around the left corner of the inlet, while it more naturally flows towards the right end of the inlet. Since the side ducts are placed directly at the left and right edges of the porous medium they are very sensitive to this. It was found before that the left and right duct generate small amounts of thrust due to their shape. In the yawed platoon the thrust of the left duct is decreased, while the thrust of the right duct is increased. However, both vary by approximately one drag count, making it a very small influence.

The pressure inside the tractor-trailer gap was found to decrease when a yaw angle is applied, underhood flow on the other hand increases the pressure. It was found that the pressure in the tractor-trailer gap with underhood flow still decreases compared to the same platoon without yaw, but the effect is smaller than for the platoons without underhood flow. After leaving the tractor-trailer gap, the underhood flow still has

a beneficial effect on the back of the tractor. This effect is still present when yaw is applied and shows no significant changes in strength.

In the previous section it was shown that the drag of the trailer wheels is not increased for the shortest distance when yaw is applied. However, it does increase when the inter vehicle distance becomes longer. It was found before that the underhood flow has a beneficial effect on the trailer wheels. This is also found here. At the shortest distance the drag contribution is approximately equal for all configurations. For the D45 case the contribution increases for the platoon without underhood flow, while it stays roughly the same for the model with underhood flow. For the largest distance the drag increases for both cases, but stronger for the one without underhood flow.

Finally, the drag of the back of the trailer is increased for all cases with yaw. Where a larger inter vehicle distance gives a higher drag contribution. The drag increase was found to be slightly higher for the models with underhood flow. However, given the uncertainty encountered for this part of the vehicle, it is too small to draw hard conclusions from this.

Table 5.19 shows the difference in side force between the yawed platoon with and without underhood flow. It can be seen that the results are quite different for different inter vehicle differences. For the D23 case the difference is negligibly small, for the D45 case the side force reduced for both vehicles and for the D91 case the side force is increased for both vehicles.

Table 5.19: Side force coefficient for the leading and trailing vehicle in yawed platoons with and without underhood flow

	D23 C_S [-]		D45 C_S [-]		D91 C_S [-]	
	LV	TV	LV	TV	LV	TV
UH0	0.867	0.299	0.896	0.327	0.861	0.361
UH2	0.868	0.300	0.883	0.316	0.868	0.373
Δ	+0.001	+0.001	-0.013	-0.011	+0.007	+0.012

Figure 5.32 and 5.33 show the difference in side force over length of the vehicle between the platoon with underhood flow and without underhood flow for the leading and trailing vehicle respectively. Both figures do not indicate clear trends.

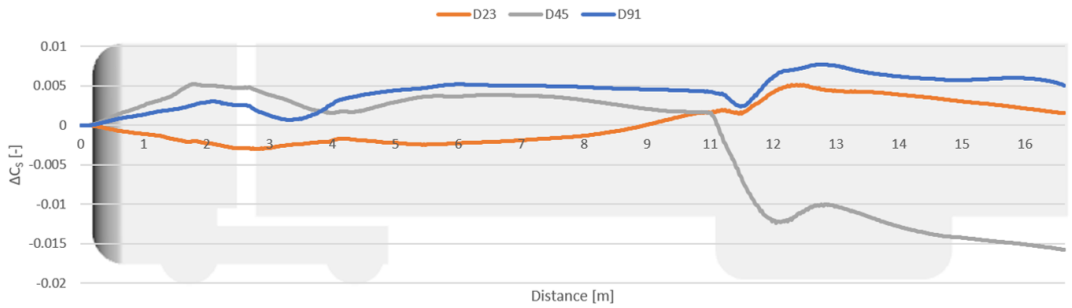

Figure 5.32: Difference in side force development of the leading vehicle of the yawed platoons with underhood flow compared to the ones without

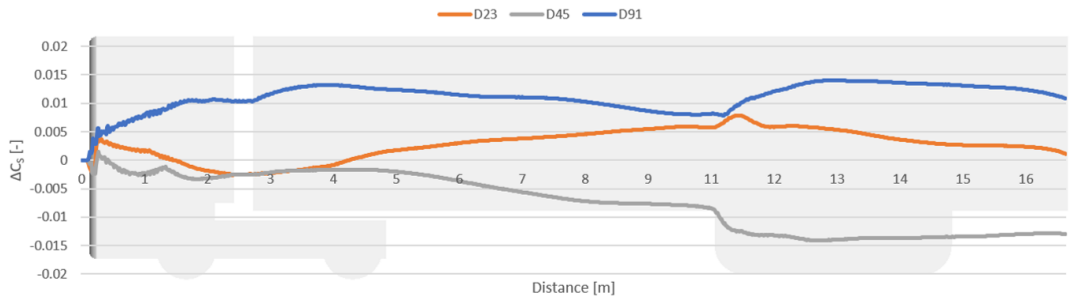

Figure 5.33: Difference in side force development of the trailing vehicle of the yawed platoons with underhood flow compared to the ones without

6

Discussion of results

In the previous chapter the results of all tested platoons were shown. It was mainly zoomed in on the influence on individual components. In this chapter the analysis will be zoomed out a bit more to give an overview of the total drag of the different vehicles and platoons and their drag reduction compared to the isolated vehicles. First the results for the leading vehicle in all platoons will be discussed in section 6.1. After that the same will be done for the trailing vehicle in section 6.2. Finally the two are combined to give the drag of the complete platoons in section 6.3. An overview of the total drag of all vehicles can be found in Appendix D.

6.1. Leading vehicle

All tested platoons used the same vehicle model as leading vehicle, the basic model without underhood flow and a leading edge radius of 540 mm. This makes it easy to compare the performance of the leading vehicle in all platoons.

The total drag coefficient of the leading vehicle in all basic platoons is shown in figure 6.1. It can be seen that for all platoons the drag follows approximately the same trend when the inter vehicle distance is altered. At the shortest distance the highest drag of 0.310 was found for the UH0 and UH1 cases with a leading edge radius of 540 mm. The lowest drag was found for the UH1 case with a 135 mm leading edge radius. An average C_D is 0.305, which means that there is a variation of around 2% in both directions. Compared to the isolated vehicle, which was found to have a drag coefficient of 0.446, the drag reduction is between 30 and 33%.

At an inter vehicle distance of 7.5 m the drag coefficient of the leading vehicle was found to vary between 0.360 and 0.375, with an average of 0.368. This again gives a variation of around 2% in both directions. The drag reduction has been decreased to 16 to 19% compared to the isolated vehicle. The lowest drag reduction is found for the leading vehicle at a distance of 15 m. The total drag coefficient varies between 0.428 and

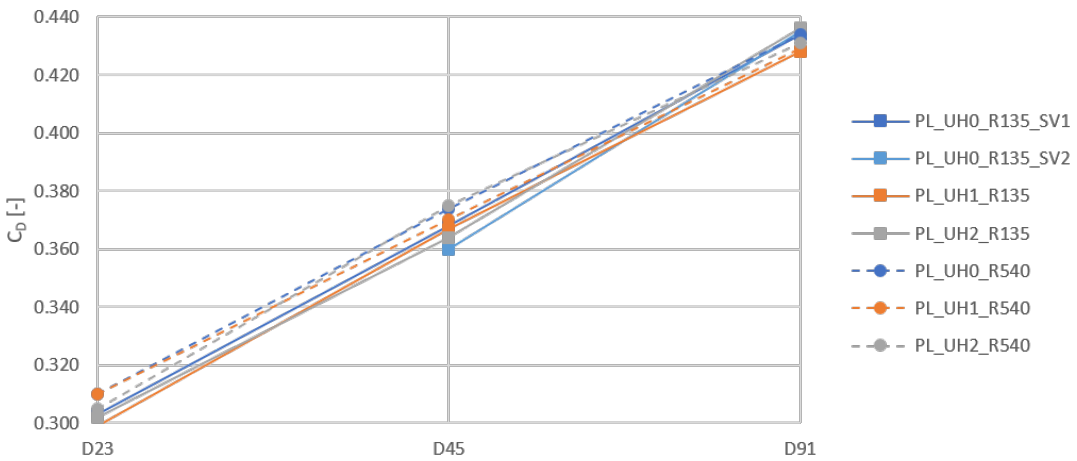

Figure 6.1: Total drag coefficient of the leading vehicle in all basic platoons

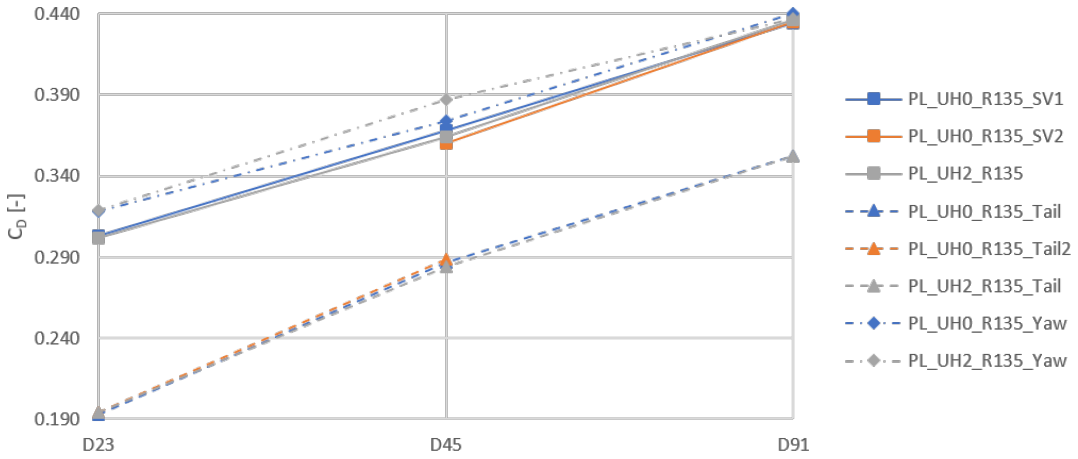

Figure 6.2: Total drag coefficient of the leading vehicle in basic platoons compared to platoons with boat tail or yaw angle

0.436 at this distance, with an average of 0.432. This means that the variation is only 1% in both directions. The drag reduction compared to the isolated vehicle is reduced to only 2 to 4%.

Figure 6.2 shows that the differences in drag are bigger when a boat tail or yaw is applied. When a boat tail is applied the drag of the leading vehicle is significantly reduced. Compared to the isolated vehicle without tail the drag reduction is 57% for the shortest inter vehicle distance, 36% for the middle distance and 21% for the longest one. The three panel tail, called Tail2 in the figure, was only tested at 3.75 and 7.5 m inter vehicle distance. At these distances it shows values very close to those of the platoons with the four panel tail.

The dotted lines in figure 6.2 show that with a yaw angle of six degrees the drag of the leading vehicle slightly increases. This does not have a dramatic effect on the drag reduction compared to the isolated vehicle. The isolated vehicle was only tested with zero yaw.

Van Tilborg [35] and Gheyssens [16] found the same trend for the leading vehicle, although they found larger drag reductions. This is explained by the difference in model. They used The GETS model which has basically the same front end as the GEM model used here, but behind that it is a simple block. Therefore the drag contribution of the back surface is bigger compared to the total drag. The area of the rear is also bigger, therefore a larger absolute drag reduction is found as well.

6.2. Trailing vehicle

Figure 6.3 shows that the drag of the trailing vehicle follows a different trend. For the basic platoons the highest drag is found for the middle inter vehicle distance, except for the UH1_R135 case, while the lowest values are found at the largest distance. The figure also shows that the leading edge radius has a stronger effect on the total drag than the underhood flow.

For the isolated vehicle the difference in drag coefficient was found to be 14 counts between the UH0 and the UH2 model with a leading edge radius of 135 mm. In a platoon the differences are reduced and the UH0 model does not even have the lowest value in all cases. This indicates that the drag reduction is stronger for the vehicles with underhood flow.

To illustrate this, the drag reduction compared to isolated vehicles of the same type is plotted for the basic platoons in figure 6.4. It can be seen that the vehicles with more underhood mass flow experience a stronger drag reduction. The figure also shows that the drag reduction is stronger for the larger leading edge radius.

Figure 6.5 shows that the trend found for the trailing vehicle is slightly changed when a boat tail or yaw is applied. The figure shows that in both cases the highest drag is found for the shortest inter vehicle distance and not for the middle distance. For the platoons with a boat tail the drag of trailing vehicle at the shortest distance is higher than for the basic platoons. However, at the larger distances the drag is lower. It can also be seen that for the platoons with tail the drag of the UH2 model is notably higher than for the UH0 model, while this is not the case for the basic platoons. Figure 6.6 shows that the relative drag reduction is almost identical for the UH0 and UH2 models, while for the basic platoons the reduction for the UH2 model is clearly higher. The drag of the trailing vehicle in the yawed platoon is clearly higher than for zero yaw. As was found for the basic platoons, the drag of the UH2 model is almost the same as for the UH0 model. This means that the UH2

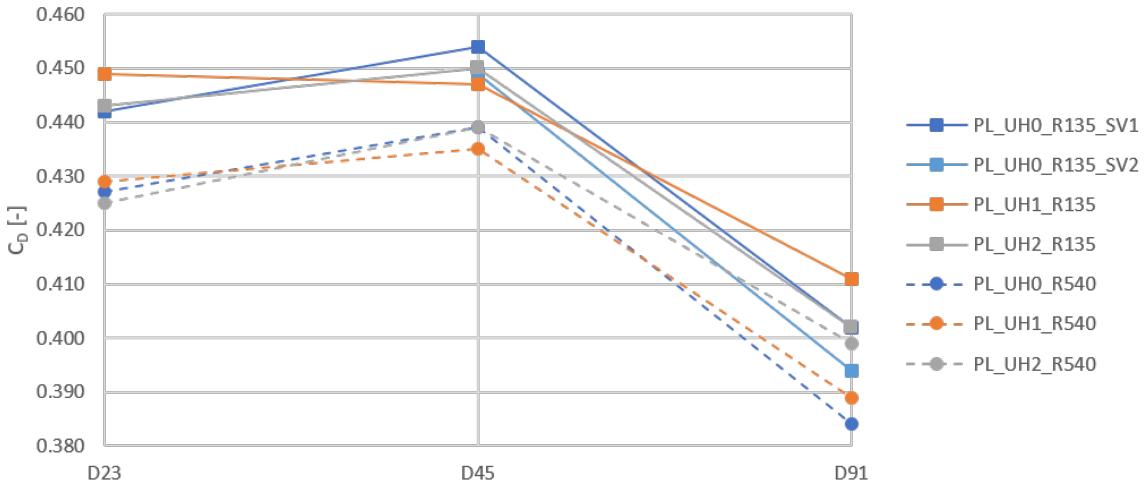

Figure 6.3: Total drag coefficient of the trailing vehicle in all basic platoons

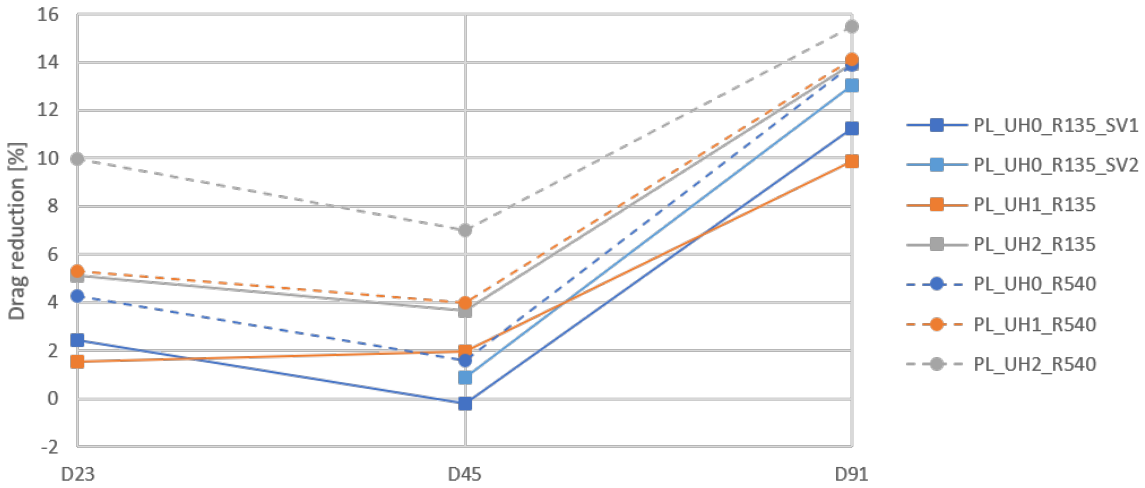

Figure 6.4: Drag reduction of the trailing vehicles in percentage compared to an isolated vehicle of the same type

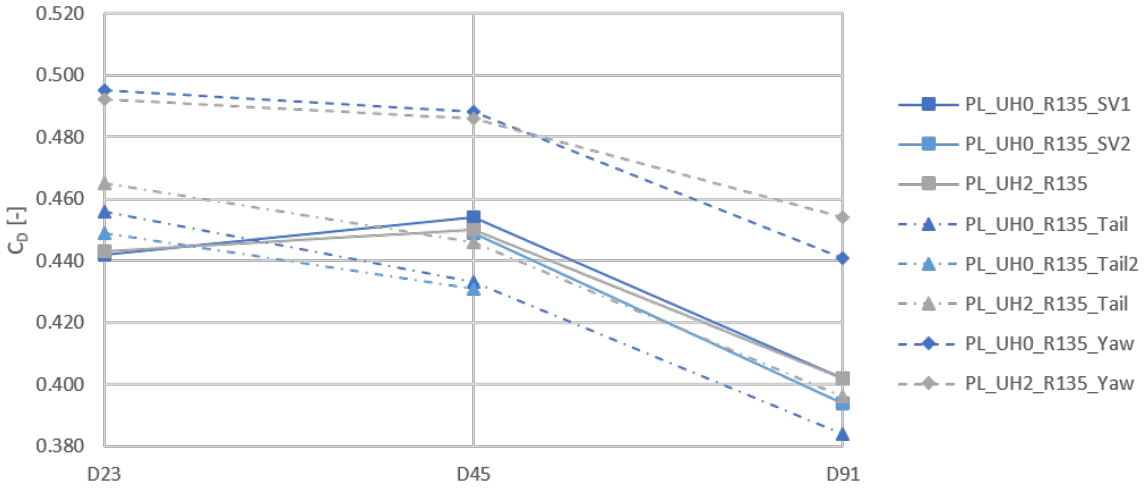

Figure 6.5: Total drag coefficient of the trailing vehicle in platoons with tail or yaw angle, compared to the basic platoons

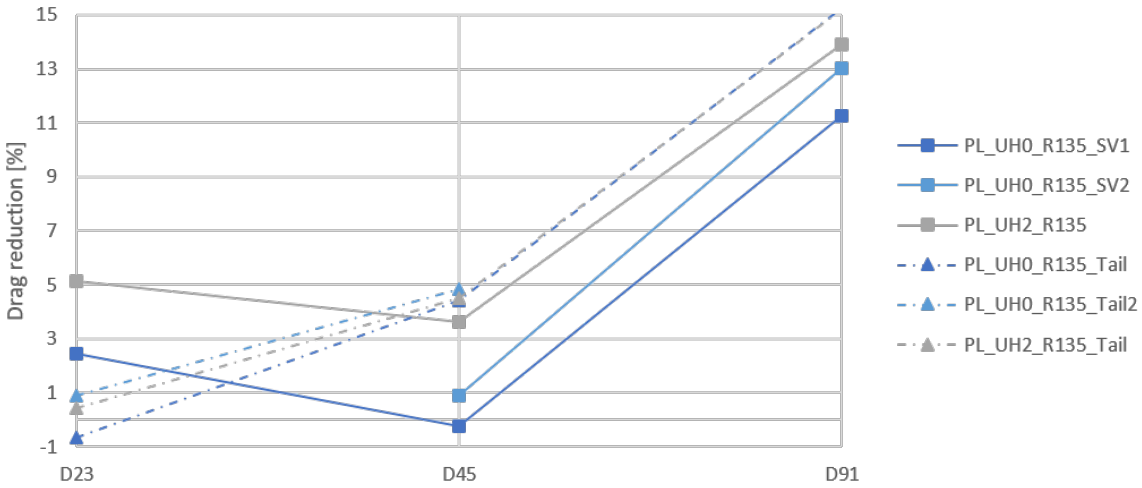

Figure 6.6: Drag reduction of the trailing vehicle in percentage compared to an isolated vehicle of the same type

experiences a higher drag reduction in the platoon. However, since the isolated vehicles were not tested in yaw conditions it is impossible to give a drag reduction for these platoons in figure 6.6

Comparing the results for the trailing vehicle to those of Van Tilborg [35] and Gheyssens [16] shows that they also found the highest drag values at an inter vehicle distance of 0.45 vehicle lengths. In some cases these values were even higher than the drag for an isolated vehicle. That this was not found here can again be explained by the level of detail of the models. The lower the amount of details the bigger the influence of the platoon.

6.3. Total platoon

In the previous sections it was found that the drag of the leading vehicle is reducing for smaller inter vehicle distances. However, for the trailing vehicles the largest inter vehicle distance gives lower drag values. Therefore it is interesting to look at the drag of the complete platoon to see which distance gives the lowest total drag. The total drag of the basic platoons is plotted in figure 6.7. It can be seen that the shortest inter vehicle distance clearly gives the lowest drag. The highest drag is found for the largest inter vehicle distance, although the difference with the D45 cases is small. This can be explained by the fact that for the trailing vehicle the D45 cases give the highest drag.

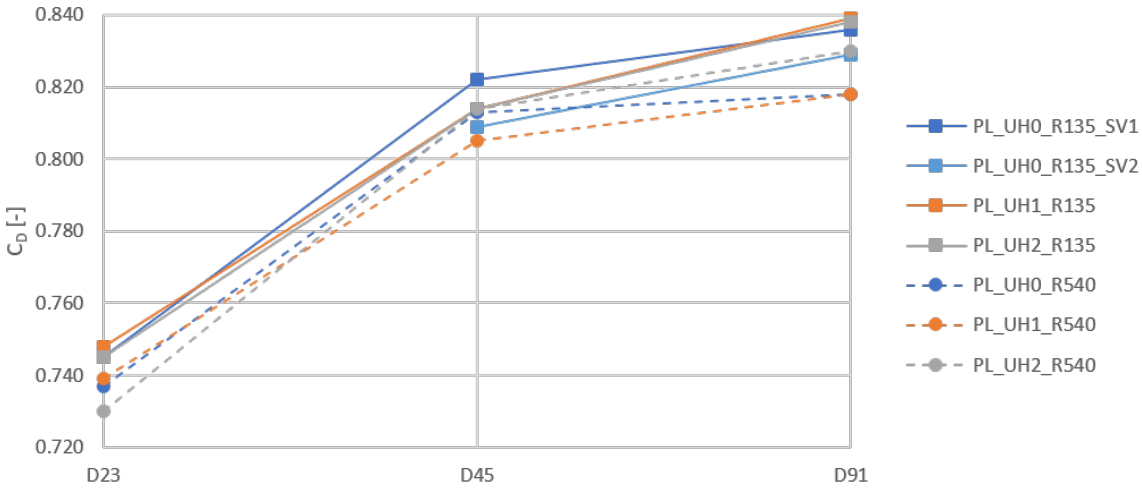

Figure 6.7: Total drag coefficient of all basic platoons

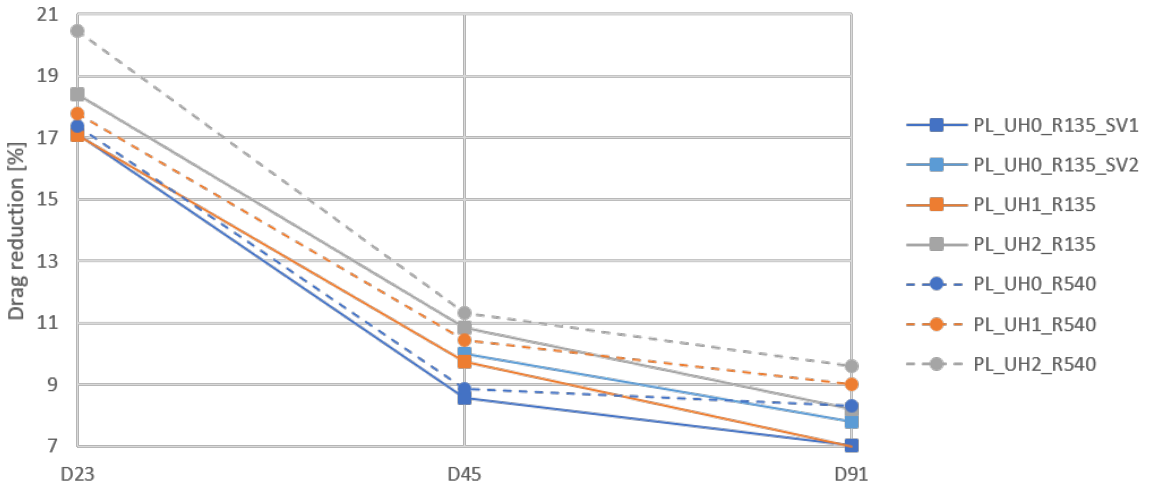

Figure 6.8: Drag reduction in percentage of the total platoon compared to the same two vehicles in isolation

Figure 6.8 shows that at the largest distance the drag is still reduced by 7 to 10% compared to two vehicles in isolation. However, at an inter vehicle distance of 3.75 m the reduction is significantly higher, between 17 and 21%. Same as for the trailing vehicle the highest drag reduction is found for the UH2_R540 model and the lowest for the UH0_R135. This is logical because this was the case for the trailing vehicle and the results for the leading vehicle are almost the same in all platoons.

To illustrate the significance of these drag reductions the fuel that is saved by it will be calculated. To do this the absolute drag reduction in Newtons is used. The engine power that would have been required to overcome this drag can be determined using the following equation [52]:

$$P = \frac{Fv}{\eta} \tag{6.1}$$

Where P is the engine power, F the drag reduction, v the vehicle speed and η the engine efficiency. An engine efficiency of 44% is used based on [53]. The outcome of this equation can be transformed to the amount of energy saved per 100 km. Dividing this by the calorific value of diesel (38.6 MJ/l [54]) gives the fuel saving. The highest drag reduction was found for the UH2_R540 platoon at an inter vehicle distance of 3.75 m. A fuel saving of 2.8 $l/100km$ was found for the leading vehicle, while this is 0.9 $l/100km$ for the trailing one. Assuming that both trucks drive 150.000 km per year of which 85% takes place in highway conditions[1] of which 50% in a platoon this would save almost 2350 l of diesel per year. This is obviously good for reducing emissions, but also for the companies operating the vehicles. With an average diesel price of €1 per liter without VAT in the European Union [55], they save €2350 in fuel costs for both trucks or €1175 per truck, if they split the benefits evenly. Unfortunately, the underhood flow will not be sufficient in most cases at this inter vehicle distance. However, the same platoon at an inter vehicle distance of 15 m still gives a fuel saving of 1.7 $l/100km$ or 1100 $l/year$ for both vehicles combined.

For the trailing vehicle the highest drag values were found for the D23 case when a boat tail or yaw angle is applied. However, figure 6.9 shows that this does not alter the trend found for the total platoon. It can be seen that a boat tail on the leading vehicle is a large benefit for the complete platoon at all distances, while a yaw angle gives a clearly higher total drag.

[1] Typical values for trucks in long haul transport, supplied by Gandert van Raemdonck of WABCO OptiFlow in personal correspondence

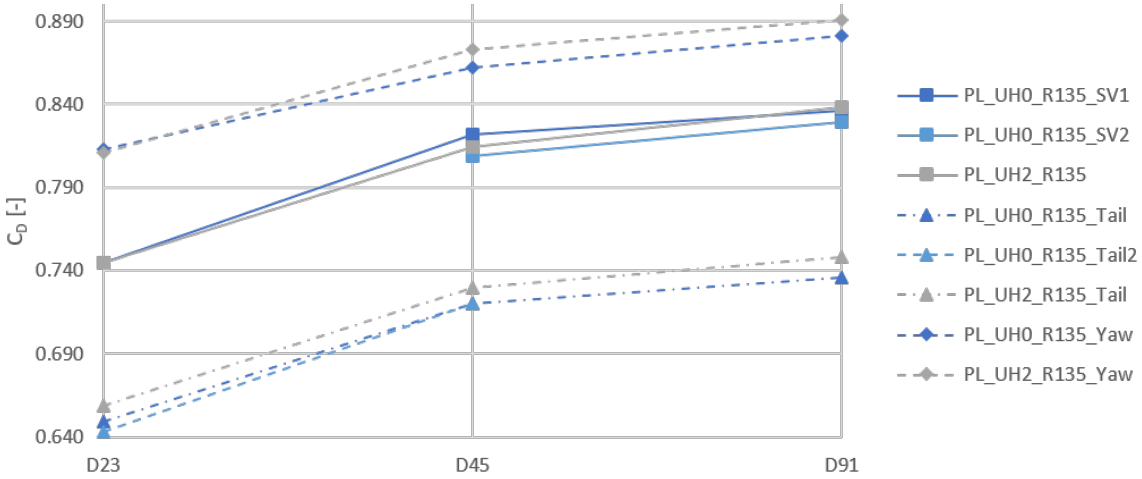

Figure 6.9: Total drag coefficient of the platoons with a boat tail or yaw angle compared to the basic platoons

7

Conclusion and recommendations

In this chapter the conclusions of this study will be drawn. Section 7.1 will reflect on the effects of the different changes made to the isolated vehicle and platoons. Finally in section 7.2 the recommendations for future work will be stated.

7.1. Conclusion

Isolated vehicle

The study was started by investigating the effect of the leading edge radius and underhood flow on an isolated vehicle, in order to later compare it to the behaviour in platoons. Three leading edge radii were used: 135, 270 and 540 mm. It was found that the drag contribution of the front parts of the models with 270 and 540 mm were equal. This indicates that the flow is fully attached in both cases. For the model with the 135 mm radius the drag was higher, although the suction over the leading edges was still slightly higher than for the 270 mm radius model. This indicates that the flow is not fully attached anymore, but also not completely separated yet, as this would give a larger drag increase. A larger leading edge radius also gives a thinner boundary layer. This results in a lower pressure inside the tractor-trailer gap, but this has a very small influence on the total drag. At the rear of the vehicle a difference in boundary layer thickness could still be observed, but this did not translate in a higher drag contribution for the rear of the trailer.

When an underhood model is added, the drag of the vehicle is increased due to the high drag of the porous medium. Models with a larger leading edge radius had a higher mass flow, probably because a small leading edge radius gives a lower pressure, which sucks more air away from the inlet. For all leading edge radii the suction over the leading edges is reduced when an underhood model is applied. This is caused by the flow entering the underhood decreasing the mass flow over the leading edges. Although this is a small effect. Besides this, the underhood flow actually has beneficial effects on other parts of the vehicle. The pressure inside the tractor-trailer gap is increased, reducing the total drag of the components surrounding it. Most air leaves the tractor-trailer gap through its horizontal part, which reduces the drag for the rear part of the tractor. The same effect, in combination with the low momentum flow leaving the cabin from the sides reduces the side inflow to the underbody area of the trailer. This reduces the drag of the trailer wheels.

Effect of inter vehicle distance

The tested platoons all consisted of two vehicles of which the leading one had a leading edge radius of 540 mm and no underhood flow. The trailing vehicle was placed at either 3.75, 7.5 or 15 m behind that. Altering the distance between the vehicles has by far the strongest effect on the drag of the platoon. The leading vehicle gives the lowest drag for the shortest inter vehicle distance. This is explained by the presence of the trailing vehicle increasing the pressure in the area behind the trailing vehicle, reducing the drag contribution of the back of the trailer and trailer wheels. The closer it is, the stronger this effect. For the trailing vehicle it is not as straightforward. The presence of the leading vehicle reduces the stagnation pressure as well as the static pressure around the vehicle. The reduced stagnation pressure reduces the drag contribution of the front area of the vehicle, but also reduces suction over the leading edges. It was found that the trailing vehicle has the strongest drag reduction for an inter vehicle distance of 15 m and the weakest at 7.5 m. Since the drag

reduction of the leading vehicle is stronger for small inter vehicle distances, the lowest drag of the complete platoon is found at 3.75 m.

Effect of leading edge radius

Since the results of the isolated vehicles with a leading edge radius of 270 and 540 mm were very similar, only the 135 and 540 mm radii were tested on the trailing vehicle of the platoon. It was found that the smaller radius gives a larger drag reduction for the leading vehicle at small inter vehicle distances. This is probably caused by the larger stagnation area of this model giving a bigger high pressure region between the two vehicles. At an inter vehicle distance of 15 m this effect is no longer noticeable. For the trailing vehicle a leading edge radius of 540 mm gave both the lowest absolute drag and the strongest drag reduction.

Effect of underhood flow

When an underhood model is added to the trailing vehicle, this does not effect the leading vehicle. This is not surprising since the underhood mass flow is very small compared to the overall mass flow around the vehicle. For the trailing vehicle it was found that the total drag of the models with and without underhood flow are closer together than they are for the isolated vehicle. This means that the drag reduction is stronger for the vehicles with underhood flow. The cause of this is the reduction in mass flow compared to the isolated vehicle. It was found that at an inter vehicle distance of 15 m only 70% of the mass flow was still available, while this was further reduced to 50 and 35% for the 7.5 and 3.75 m distances respectively. Since the porous medium drag is decreasing linearly for reducing mass flow, this has a strong effect on the total drag. For the isolated vehicle some beneficial effects of the underhood flow on the drag of different components were found. These effects are still present in the platoon, but have reduced in strength. Compared to the isolated vehicle the vehicles without underhood flow saw the biggest drag reduction for these parts inside the platoon. However, the models with underhood flow still had the lowest absolute values.

Effect of boat tail

A boat tail was placed on the back of the leading vehicle. A boat tail increases the back pressure and with that reduces the drag of the leading vehicle. However, for the trailing vehicle this might not be beneficial, since it counteracts the effect of the platoon. As expected an increased stagnation pressure was found for the trailing vehicle compared to platoons without tail. However, as mentioned before, this also increases the suction over the leading edges. For the shortest inter vehicle distance the total drag of the trailing vehicle was increased, but for the other two distances this actually resulted in a drag reduction. Besides this, it was found that the boat tail gives higher velocities over the top of the trailing vehicle and lower velocities round the bottom. This results in reduced drag contributions for both the tractor and trailer wheels.

The same effect gives an increased pressure on the top part of the stagnation surface of the trailing vehicle and a reduced pressure on the bottom part. When an underhood model is applied, the inlet reduces the area of the bottom part. Therefore the drag contribution of the frontal area sees a higher increase in this case. It also slightly reduces the underhood mass flow compared to platoons without tail.

Effect of yaw angle

When a platoon is put at a yaw angle the drag of both vehicles increases. The leading vehicle gives a reduced drag contribution of the front and a big drag increase for the back of the trailer. Most other parts give a slight drag increase, because they are no longer perfectly aligned with the flow. The drag increase is stronger for the trailing vehicle, because for this vehicle the drag contribution of the front part is increased as well. This is caused by an increased stagnation pressure. This also causes the platoon with the shortest inter vehicle distance to give the highest drag for the trailing vehicle. The effect of yaw on the other components is reduced compared to the leading vehicle, because the flow is more aligned with the trailing vehicle in a platoon.

The underhood mass flow increases when a yaw angle is applied, this can be explained by the side inflow in the area between the two vehicles. The effect is strongest for the smallest inter vehicle distance. The division of the mass flow over the different ducts also becomes asymmetrical because of this. The underhood flow still gives the same advantages for other parts of the vehicle as were found before.

Finally, it can be concluded that underhood flow does not have a strong effect on the aerodynamic performance of a platoon. The leading vehicle is not effected by the underhood of the trailing vehicle at all. Models with underhood flow do give a stronger drag reduction when placed in a platoon as a trailing vehicle. This is

caused by the reduced underhood mass flow. The effects underhood flow has on an isolated vehicle are still present in a platoon, but reduce in strength. The highest drag reduction for the total platoon is found at the shortest inter vehicle distance, where the underhood mass flow is the lowest. In practice the shortest inter vehicle distance where the trailing vehicle still has sufficient cooling should be found.

7.2. Recommendations

After concluding this study, in this section some recommendations are given that could improve the simulations performed in this study and verify and validate them better. Also some interesting possible topics extending this research will be discussed.

Simulation setup

Throughout this study varying results were found for backwards facing surfaces due to uncertainty in the wake regions. It is suspected that the results can be improved by using longer physical run times and average over a longer period. At the leading edges little separation was found compared to other studies on similar models. This might be changed when a finer mesh is applied round the leading edges.

Verification and validation

For this study the verification and validation possibilities have been limited. Chapter 3 showed that only the total drag coefficient of an isolated vehicle could be compared to wind tunnel tests. The RANS simulations performed on this case showed a different wake structure than the LBM simulations in this study. Performing PIV measurements during a wind tunnel test with the same model are needed to find out what the correct structure is.

Vehicle models

The vehicle models used is this study are highly simplified. Even though this makes sense because manufacturer or model specific features in mainly the underhood area are not influencing the results, some features of real trucks are probably good to add. Rotating wheels, especially in the front, will make it possible to better simulate the flow leaving the underhood through the wheel arches. Most of the benefits of underhood flow were found in the trailer underbody area. In the GEM model this area is completely empty, while this is not the case for most trailers found on the road. Therefore it might be interesting to see how more underbody components and aerodynamic features, like trailer side skirts, influence the effects caused by underhood flow.

Further research

The total drag of a platoon was found to be lowest for the smallest inter vehicle distance, mainly due to the drag reduction for the leading vehicle. However, in practice it will be difficult to use this inter vehicle distance because the underhood mass flow will be decreased too far to maintain sufficient cooling capacity. It might be possible to solve this using a fan behind the cooling package, to suck more air through. However, operating this fan will require energy, reducing the fuel savings of the platoon. Therefore it should be investigated if this can be an economically viable option. When such a critical case is considered it might be necessary to also include temperature into the simulation. The air entering the underhood of the leading vehicle might already be heated up by the leading vehicle, reducing effectiveness of the heat exchangers of the trailing vehicle.

Bibliography

[1] R. Muncrief and B. Sharpe, *Overview of the heavy-duty vehicle market and CO2 emissions in the European Union*, Tech. Rep. (ICCT, 2015).

[2] J. D. Miller and C. Façanha, *The state of clean transport policy - A 2014 synthesis of vehicle and fuel policy developments*, Tech. Rep. (ICCT, 2014).

[3] Harwell and Didcot, *Good practice guide: Truck aerodynamic styling*, Department for Transport, Tech. Rep. (2001).

[4] ACEA, *Platooning roadmap*, `http://www.acea.be/uploads/publications/Platooning_roadmap.pdf` (2017), accessed: 15-01-2018.

[5] D. Rondini, *Trucking Efficiency Confidence Report: Two-Truck Platooning*, Tech. Rep. (North American Council for Freight Efficiency, 2016).

[6] M. P. Lammert, A. Duran, J. Diez, K. Burton, and A. Nicholson, *Effect of platooning on fuel consumption of class 8 vehicles over a range of speeds, following distances, and mass*, SAE International Journal of Commercial Vehicles **7**, 626 (2014).

[7] A. Dávila and M. Nombela, *Sartre - safe road trains for the environment reducing fuel consumption through lower aerodynamic drag coefficient*, in *SAE Technical Paper Series* (SAE International, 2011).

[8] F. Browand, J. McArthur, and C. Radovich, *Fuel Saving Achieved in the Field Test of Two Tandem Trucks*, Tech. Rep. (University of Southern California, 2004).

[9] B. Gaudet, *Review of cooperative truck platooning systems*, Tech. Rep. (National Research Council Canada, 2014).

[10] B. R. McAuliffe, M. Croken, M. Ahmadi-Baloutaki, and A. Raeesi, *Fuel-economy testing of a three-vehicle truck platooning system*, Tech. Rep. (National Research Council Canada, 2017).

[11] W. Hucho and G. Sovran, *Aerodynamics of road vehicles*, Annu. Rev. Fluid Mech. 1993.25 : 485-537 (1993).

[12] R. Wood, *A Discussion of a Heavy Truck Advanced Aerodynamic Trailer System*, Tech. Rep. (SOLUS-Solutions and Technologies LLC, 2006).

[13] E. G. Duell and A. R. George, *Experimental study of a ground vehicle body unsteady near wake*, in *SAE Technical Paper Series* (SAE International, 1999).

[14] W.-H. Hucho, ed., *Aerodynamics of Road Vehicles* (Butterworth-Heinemann, 1987).

[15] R. Wood, *A review of reynolds number effects on the aerodynamics of commercial ground vehicles*, SAE International Journal of Commercial Vehicles **5**, 628 (2012).

[16] T. Gheyssens, *Aerodynamic analysis of a platoon of bluff bodies subjected to cross wind*, Master's thesis, TU Delft (2016).

[17] K. R. Cooper, *Commercial vehicle aerodynamic drag reduction: Historical perspective as a guide*, in *The Aerodynamics of Heavy Vehicles: Trucks, Buses, and Trains* (Springer Berlin Heidelberg, 2004) pp. 9–28.

[18] K. R. Cooper, *The effect of front-edge rounding and rear-edge shaping on the aerodynamic drag of bluff vehicles in ground proximity*, in *SAE Technical Paper Series* (SAE International, 1985).

[19] M. Hammache and F. Browand, *On the aerodynamics of tractor-trailers*, in *The Aerodynamics of Heavy Vehicles: Trucks, Buses, and Trains* (Springer, 2004).

[20] G. van Raemdonck, *Design of low drag bluff road vehicles*, Ph.D. thesis, TU Delft (2012).

[21] B. Storms, D. Satran, J. Heineck, and S. Walker, *A Summary of the Experimental Results for a Generic Tractor-Trailer in the Ames Research Center 7- by 10-Foot and 12-Foot Wind Tunnels*, Tech. Rep. (NASA Ames Research Center, 2006).

[22] EU, *Directive 2015/719 of the european parliament and of the council of 29 april 2015,* (2015).

[23] F. Kruijssen, *The effect of asymmetric base flaps on the drag of a tractor-trailer for four crosswind angles*, Master's thesis, TU Delft (2017).

[24] H. Martini, *Perspectives of Aerodynamic Drag and Cooling, Airflow for Heavy-Duty Trucks - Reconsidering European Total-Length Legislation*, Ph.D. thesis, Chalmers University of Technology (2016).

[25] R. Barnard, *Road Vehicle Aerodynamic Design - An Introduction* (Longman, 1996).

[26] T. Hallqvist, *The cooling airflow of heavy trucks - a parametric study,* SAE International Journal of Commercial Vehicles **1**, 119 (2008).

[27] R. Barnard, *Theoretical and experimental investigation of the aerodynamic drag due to automotive cooling systems,* in *Proceedings of the Institution of Mechanical Engineers, Part D: Journal of Automobile Engineering* (2000).

[28] D. Bäder, T. Indinger, N. A. Adams, P. Unterlechner, and G. Wickern, *Interference effects of cooling airflows on a generic car body,* Journal of Wind Engineering and Industrial Aerodynamics **119**, 146 (2013).

[29] D. Baeder, T. Indinger, N. Adams, and P. Unterlechner, *Aerodynamic investigation of vehicle cooling-drag,* in *SAE Technical Paper Series* (SAE International, 2012).

[30] C. Pfeifer, *Evolution of active grille shutters,* in *SAE Technical Paper Series* (SAE International, 2014).

[31] M. Hammache, M. Michaelian, and F. Browand, *Aerodynamic forces on truck models, including two trucks in tandem,* in *SAE 2002 World Congress Detroit, Michigan* (2002).

[32] A. Davila, *SARTRE - Report on Fuel Consumption*, Tech. Rep. (Applus+ IDIADA, 2013).

[33] M. Zabat, N. Stabile, S. Farascaroli, and F. Browand, *The Aerodynamic Performance of Platoons: A Final Report*, Tech. Rep. (California Partners for Advanced Transportation Technology UC Berkeley, 1995).

[34] J. Smith, R. Mihelic, B. Gifford, and M. Ellis, *Aerodynamic impact of tractor-trailer in drafting configuration,* SAE International Journal of Commercial Vehicles **7**, 619 (2014).

[35] F. van Tilborg, *Flow analysis between two bluff bodies in a close distance platooning configuration*, Master's thesis, TU Delft (2018).

[36] B. Marcu and F. Browand, *Aerodynamic forces experienced by a 3-vehicle platoon in a crosswind,* in *SAE International Congress and Exposition Detroit, Michigan* (1999).

[37] K. Salari and J. Ortega, *Experimental investigation of the aerodynamic benefits of truck platooning,* in *SAE Technical Paper Series* (SAE International, 2018).

[38] M. Ellis, J. I. Gargoloff, and R. Sengupta, *Aerodynamic drag and engine cooling effects on class 8 trucks in platooning configurations,* SAE International Journal of Commercial Vehicles **8**, 732 (2015).

[39] L. Larsson and H. Martini, *Aerodynamic Drag Reduction of a Heavy Truck with Variable Cooling Air Intake Area*, Master's thesis, Chalmers University of Technology (2009).

[40] C. Bonnet and H. Fritz, *Fuel consumption reduction in a platoon: Experimental results with two electronically coupled trucks at close spacing,* in *SAE Technical Paper Series* (SAE International, 2000).

[41] A. Alam, *Fuel-Efficient Distributed Control for Heavy Duty Vehicle Platooning*, Ph.D. thesis, KTH (2011).

[42] *PowerFLOW Best Practices Guide, ExaBP2.0, Revision 3*, Exa Corporation.

[43] W. Mulkens, *Aerodynamic Analysis of Drag Reduction Devices for the Tractor-Trailer Gap*, Master's thesis, TU Delft (2016).

[44] T. Scheeve, *Truck wheelhouse aerodynamics*, Master's thesis, TU Delft (2013).

[45] *Semi | tesla nederland,* https://www.tesla.com/nl_NL/semi (2018), accessed: 13-07-2018.

[46] *PowerCASE User's Guide, Release 5.5*, Exa Corporation (2018).

[47] *The technology behind powerflow: Exa's lattice boltzmann-based physics,* http://exa.com/en/company/exa-lattice-boltzmann-technology (2018), accessed: 7-3-2018.

[48] Y. Li, R. Shock, R. Zhang, and H. Chen, *Numerical study of flow past an impulsively started cylinder by the lattice-boltzmann method,* Journal of Fluid Mechanics **519**, 273 (2004).

[49] K. Horrigan, B. Duncan, A. Keating, A. Gupta, and J. Gargoloff, *Aerodynamic simulations of a generic tractor-trailer: Validation and analysis of unsteady aerodynamics,* in *SAE Technical Paper Series* (SAE International, 2008).

[50] *PowerFLOW User's Guide, Release 5.5*, Exa Corporation (2018).

[51] *Sae international - surface vehicle recommended practice: Guidelines for aerodynamic assessment of medium and heavy commercial ground vehicles using computational fluid dynamics,* (2013).

[52] *Engineering toolbox, car -required power and torque,* https://www.engineeringtoolbox.com/cars-power-torque-d_1784.html (2011), accessed: 28-11-2018.

[53] N. Lutsey, *The ever-improving efficiency of the diesel engine | international council on clean transportation,* https://www.theicct.org/blogs/staff/ever-improving-efficiency-diesel-engine (2015), accessed: 28-11-2018.

[54] *Engineering toolbox, fuels - higher and lower calorific values,* https://www.engineeringtoolbox.com/fuels-higher-calorific-values-d_169.html (2003), accessed: 28-11-2018.

[55] *Fuel price breakdown - fuels europe,* https://www.fuelseurope.eu/knowledge/refining-in-europe/economics-of-refining/fuel-price-breakdown/ (2018), accessed: 28-11-2018.

A

Results of model with angled roof

While testing the underhood models some differences were found in the behaviour of the flow in the tractor-trailer gap of tested model compared to the reference cases. In the reference cases, the flow leaving the underhood at the back of the cabin was mostly flowing out via the top of the tractor-trailer gap, while it flows through the horizontal part of the gap in models used in this study. In section 2.1.2 it was already shown that this can be explained by the angle of the roof. Here the differences between the two models are discussed in some more detail.

The model with angled roof is based on the UH2_R540 model. Therefore it will be compared to that. The simulation of the model with angled roof was also used to determine the desired coefficients of the porous medium. Therefore they are slightly different then the ones used in the regular UH2_R540 case. I and V were 97 $1/m$ and 390 $1/s$ respectively in the angled roof case, while the final values were set at 101 and 404. This resulted in slightly more underhood mass flow for the model with angled roof, 0.2 kg/s more, resulting in 4 counts extra porous medium drag.

Figure A.1 shows the difference in drag development between the model with angled roof compared to that of the regular UH2_R540 model. At the very front of the vehicle some variations can be seen. Due to the angled roof, the area of the front surface is smaller, reducing the drag. However, this also reduces the area of the left and right leading edges, resulting in less suction. Part of the suction is transferred to the angled roof, but it is not enough to compensate. Therefore the model with angled roof has a higher drag contribution of the front part. The peak in the tractor-trailer gap shows that the pressure is decreased here, when the roof is angled. However, in total this only gives a 2 count difference. For the regular model, adding underhood flow had a beneficial effect on the trailer underbody area. This could be explained by the mass flow leaving through the horizontal part of the tractor-trailer gap. In the model with angled roof the flow is taking a different route. Therefore it is not surprising to see higher drag contributions for the back of the tractor and trailer wheels in figure A.1. The drag contribution of the back of the trailer was found to be unexpectedly high for the regular UH2_R540 isolated vehicle. Therefore it is also higher than for the model with angled roof, which shows a contribution at the expected level.

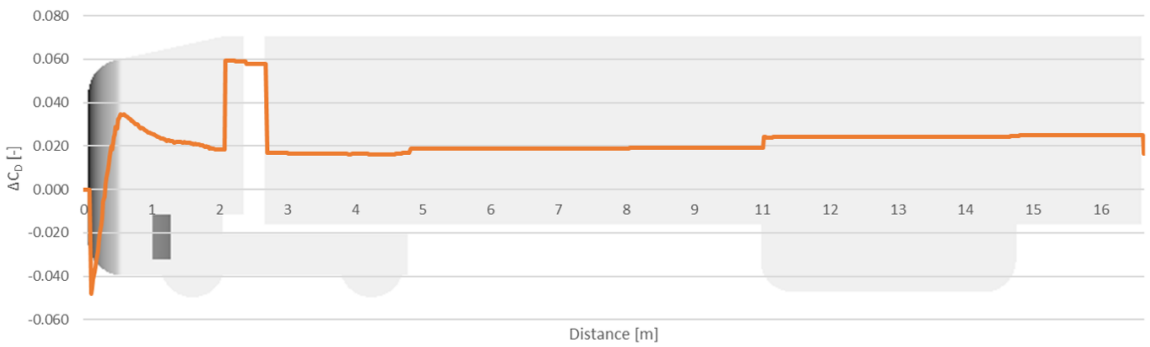

Figure A.1: Difference in drag development between the model with angled roof and the regular UH0_R540 isolated vehicle

In total the drag of the model with angled roof is 16 counts higher than that of the regular model. This is caused mainly by the difference in the front, the extra mass flow due to different coefficients and the lack of beneficial effects in the trailer underbody area. This is also shown in table A.1.

Table A.1: Overview of drag contributions of key components of UH2_R540 model with and without angled roof

	C_D [-]		
	Regular model	Angled roof	Δ
Front	0.242	0.194	-0.047
LE_left	-0.121	-0.100	+0.021
LE_right	-0.123	-0.102	+0.021
LE_bottom	0.009	0.010	+0.001
LE_top	-0.082	-0.043	+0.039
Total_front	-0.075	-0.041	+0.034
Porous_medium	0.191	0.194	+0.004
Cabin_top	0.002	-0.020	-0.022
Cabin_back	0.165	0.206	+0.041
Tractor_back	0.042	0.044	+0.002
Trailer_front	-0.174	-0.215	-0.041
Trailer_wheels	0.074	0.080	+0.006
Trailer_back	0.169	0.160	-0.009
Total	0.472	0.488	+0.016

B

Model division

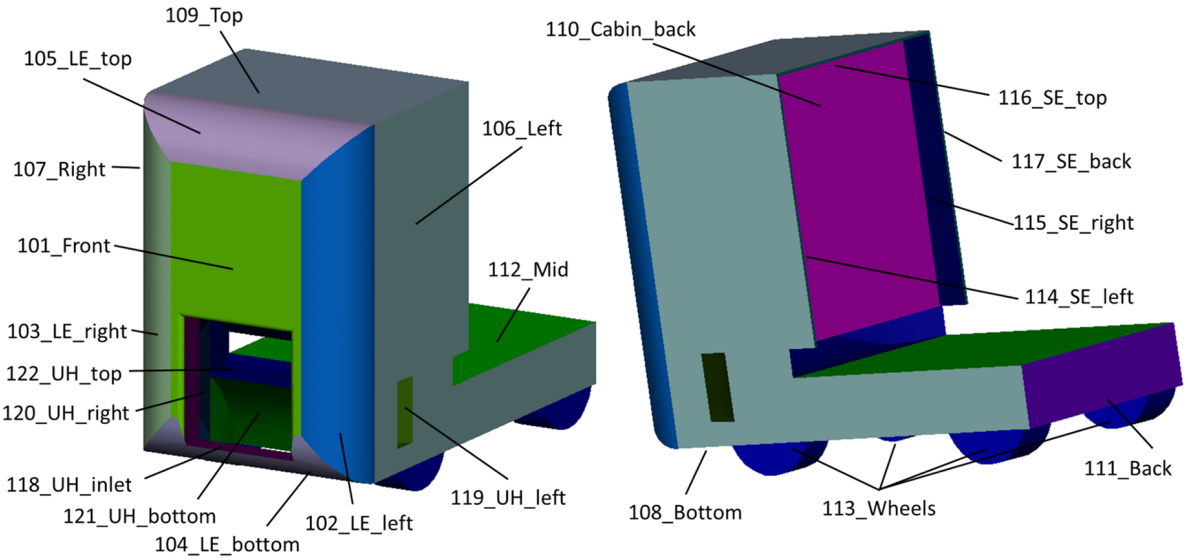

Figure B.1: Model division of the tractor used in simulations, numbering is for automatic ordering purposes

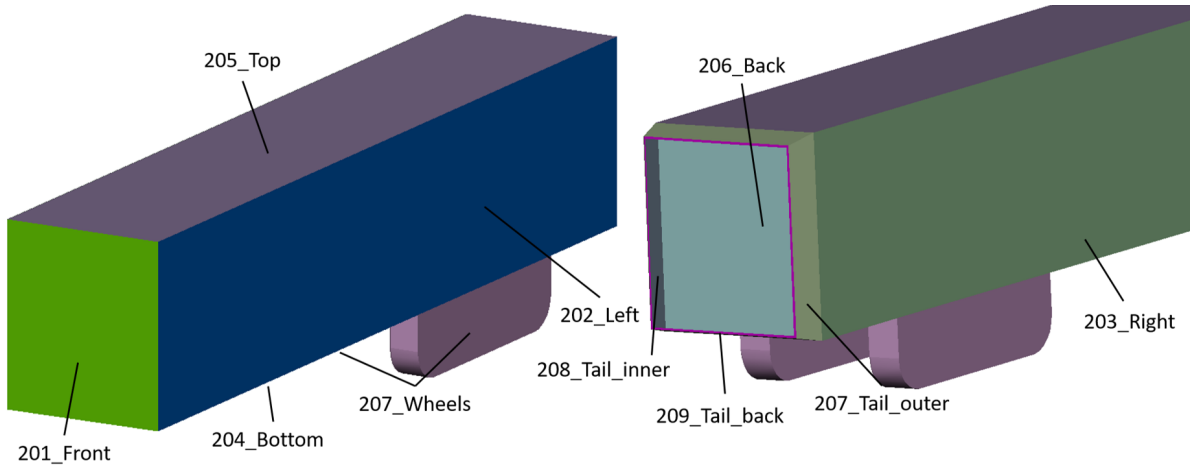

Figure B.2: Model division of the trailer, including boat tail, used in simulations, numbering is for automatic ordering purposes

C

Wind tunnel setup

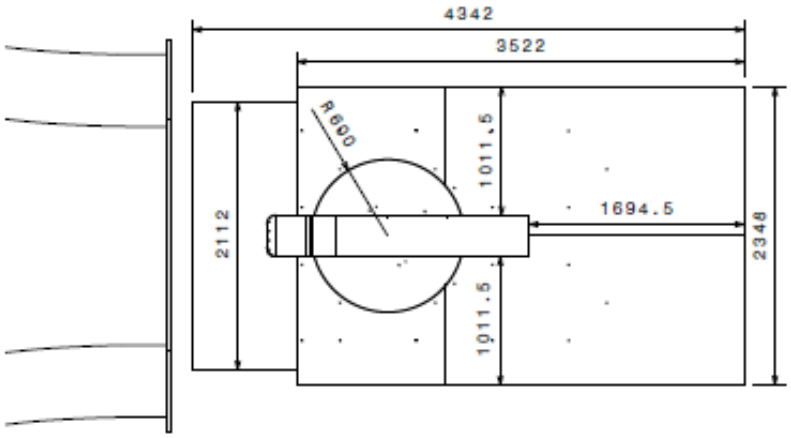

Figure C.1: Top view of the wind tunnel setup used by Mulkens en Kruijssen, dimensions are in mm [43]

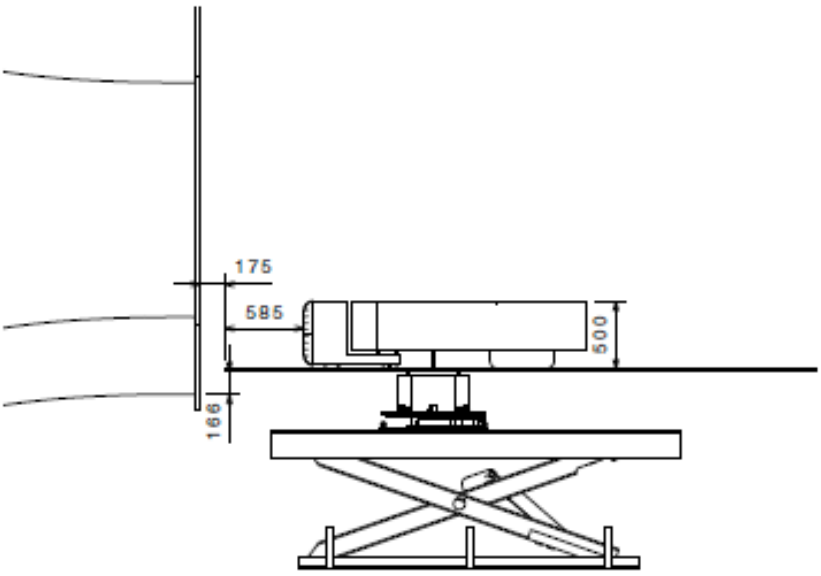

Figure C.2: Side view of the wind tunnel setup used by Mulkens en Kruijssen, dimensions are in mm [43]

D

Overview of results

D.1. Isolated vehicle

Table D.1: Total drag coefficient of all isolated vehicle runs

Underhood model	Total C_D [-]		
	R135	R270	R540
UH0	0.453	0.445	0.446
UH1	0.456	0.460	0.453
UH2	0.467	0.461	0.472

D.2. Platoons

Table D.2 shows the total drag coefficient of the leading vehicle in all tested platoons, this is an UH0_R540 model in all cases. The second part of the table shows the absolute difference in drag compared to an isolated vehicle. In the third part of the table the drag difference is shown as a percentage of the total C_D. The isolated vehicles were not tested with a tail or yaw angle. Therefore the drag reduction is still compared to an isolated vehicle without those features.

The same is done in table D.3 and table D.4 for the trailing vehicle and total platoon respectively. The trailing vehicles are compared to the isolated vehicles of the same type. The drag of the total platoon is compared to the sum of the drag of the two vehicles it consists of, when operated in isolation.

Table D.2: Total drag and drag reductions of the leading vehicle in all tested platoons

	Total C_D [-]			ΔC_D [-]			ΔC_D [%]		
	D23	D45	D91	D23	D45	D91	D23	D45	D91
PL_UH0_R135_SV1	0.303	0.368	0.434	-0.143	-0.078	-0.012	-32	-17	-3
PL_UH0_R135_SV2		0.360	0.435		-0.086	-0.011		-19	-2
PL_UH1_R135	0.299	0.367	0.428	-0.147	-0.079	-0.018	-33	-18	-4
PL_UH2_R135	0.302	0.364	0.436	-0.144	-0.082	-0.010	-32	-18	-2
PL_UH0_R540	0.310	0.374	0.434	-0.136	-0.072	-0.012	-30	-16	-3
PL_UH1_R540	0.310	0.370	0.429	-0.136	-0.076	-0.017	-30	-17	-4
PL_UH2_R540	0.305	0.375	0.431	-0.141	-0.071	-0.015	-32	-16	-3
PL_UH0_R135_Tail	0.193	0.287	0.352	-0.253	-0.159	-0.094	-57	-36	-21
PL_UH0_R135_Tail_3panel	0.194	0.289		-0.252	-0.157		-57	-35	
PL_UH2_R135_Tail	0.194	0.284	0.352	-0.252	-0.162	-0.094	-57	-36	-21
PL_UH0_R135_Yaw	0.318	0.374	0.440	-0.128	-0.072	-0.006	-29	-16	-1
PL_UH2_R135_Yaw	0.319	0.387	0.437	-0.127	-0.059	-0.009	-28	-13	-2

Table D.3: Total drag and drag reductions of the trailing vehicle in all tested platoons

	Total C_D [-]			ΔC_D [-]			ΔC_D [%]		
	D23	D45	D91	D23	D45	D91	D23	D45	D91
PL_UH0_R135_SV1	0.442	0.454	0.402	-0.011	0.001	-0.051	-2	0	-11
PL_UH0_R135_SV2		0.449	0.394		-0.004	-0.059		-1	-13
PL_UH1_R135	0.449	0.447	0.411	-0.007	-0.009	-0.045	-2	-2	-10
PL_UH2_R135	0.443	0.450	0.402	-0.024	-0.017	-0.065	-5	-4	-14
PL_UH0_R540	0.427	0.439	0.384	-0.019	-0.007	-0.062	-4	-2	-14
PL_UH1_R540	0.429	0.435	0.389	-0.024	-0.018	-0.064	-5	-4	-14
PL_UH2_R540	0.425	0.439	0.399	-0.047	-0.033	-0.073	-10	-7	-16
PL_UH0_R135_Tail	0.456	0.433	0.384	0.003	-0.020	-0.069	1	-4	-15
PL_UH0_R135_Tail_3panel	0.449	0.431		-0.004	-0.022		-1	-5	
PL_UH2_R135_Tail	0.465	0.446	0.396	-0.002	-0.021	-0.071	0	-5	-16
PL_UH0_R135_Yaw	0.495	0.488	0.441	0.042	0.035	-0.012	9	8	-3
PL_UH2_R135_Yaw	0.492	0.486	0.454	0.025	0.019	-0.013	6	4	-3

Table D.4: The sum of the total drag and drag reductions of both vehicles in all tested platoons

	Total C_D [-]			ΔC_D [-]			ΔC_D [%]		
	D23	D45	D91	D23	D45	D91	D23	D45	D91
PL_UH0_R135_SV1	0.745	0.822	0.836	-0.154	-0.077	-0.063	-17	-9	-7
PL_UH0_R135_SV2		0.809	0.829		-0.090	-0.070		-10	-8
PL_UH1_R135	0.748	0.814	0.839	-0.154	-0.088	-0.063	-17	-10	-7
PL_UH2_R135	0.745	0.814	0.838	-0.168	-0.099	-0.075	-18	-11	-8
PL_UH0_R540	0.737	0.813	0.818	-0.155	-0.079	-0.074	-17	-9	-8
PL_UH1_R540	0.739	0.805	0.818	-0.160	-0.094	-0.081	-18	-10	-9
PL_UH2_R540	0.730	0.814	0.830	-0.188	-0.104	-0.088	-20	-11	-10
PL_UH0_R135_Tail	0.649	0.720	0.736	-0.250	-0.179	-0.163	-28	-20	-18
PL_UH0_R135_Tail_3panel	0.643	0.720		-0.256	-0.179		-28	-20	
PL_UH2_R135_Tail	0.659	0.730	0.748	-0.254	-0.183	-0.165	-28	-20	-18
PL_UH0_R135_Yaw	0.813	0.862	0.881	-0.086	-0.037	-0.018	-10	-4	-2
PL_UH2_R135_Yaw	0.811	0.873	0.891	-0.102	-0.040	-0.022	-11	-4	-2